Cenozoic tectonic history of the Himachal Himalaya (northwestern India) and its constraints on the formation mechanism of the Himalayan orogen

A. Alexander G. Webb[1,2,*], An Yin[2,3], T. Mark Harrison[2], Julien Célérier[4], George E. Gehrels[5], Craig E. Manning[2], and Marty Grove[2]

[1]*Department of Geology and Geophysics, Louisiana State University, Baton Rouge, Louisiana 70803, USA*
[2]*Department of Earth and Space Sciences and Institute of Geophysics and Planetary Physics, University of California, Los Angeles, California 90095, USA*
[3]*Structural Geology Group, China University of Geosciences Beijing, Beijing 10085, People's Republic of China*
[4]*Research School of Earth Sciences, Australia National University, Canberra, ACT 2601, Australia*
[5]*Department of Geosciences, University of Arizona, Tucson, Arizona 85721, USA*

ABSTRACT

A central debate for the evolution of the Himalayan orogen is how the Greater Himalayan Crystalline complex in its core was emplaced during the Cenozoic Indo-Asian collision. Addressing this problem requires knowledge of the structural relationship between the South Tibet detachment fault (STD) and the Main Central thrust (MCT) that bound these rocks from above and below. The fault relationship is exposed in the Himachal Himalaya of northwestern India, where they merge in their updip direction and form a frontal branch line that has been warped by subsequent top-to-the-southwest shear deformation. To elucidate how the two major crustal-scale faults evolved in the western Himalaya, we conducted integrated geologic research employing field mapping, pressure-temperature (*P-T*) analyses, U-Pb zircon geochronology, trace and rare earth element (REE) geochemistry, and thermochronology. Our field study reveals complex geometric relationships among major thrusts with large-magnitude shortening within each thrust sheet. Three successive stages of top-to-the-southwest thrust development are recognized: (1) imbricate stack development, (2) translation of large thrust sheets along low-angle detachments and backthrusting along the STD, and (3) development of duplex systems via underplating. This kinematic process can be quantified by our new analytical data: (1) *P-T* determinations show 7–9 kbar and 450–630 °C conditions across the STD. The lack of a metamorphic discontinuity across the fault is consistent with a backthrust interpretation. (2) U-Pb zircon geochronology yields ca. 830 Ma and ca. 500 Ma ages of granitoids in the MCT hanging wall, ca. 1.85 Ga ages of granitic gneisses in both the MCT hanging wall and footwall, and 8–6 Ma ages of granitic pegmatites in the MCT footwall. These ages help define regional chronostratigraphy, and the youngest ages reveal a previously unknown intrusion phase. (3) Trace element and REE geochemistry of 1.85 Ga, 830 Ma, and 500 Ma granitoids are characteristic of remelted continental crust, constraining the protolith tectonic setting. (4) U-Pb geochronology of detrital zircon reveals that siliciclastic sedimentary sequences above the STD, below the MCT, and between these two faults have similar age spectra with Neoproterozoic youngest age peaks. This result implies that the STD and MCT each duplicated the same stratigraphic section. (5) Th-Pb geochronology of monazite included in MCT hanging-wall garnet yields Paleozoic and early Tertiary ages, indicating Paleozoic and early Tertiary metamorphism in these rocks. (6) The $^{40}Ar/^{39}Ar$ thermochronology of the K-feldspar from southern MCT hanging-wall rocks evinces cooling below 220–230 °C ca. 13–19 Ma or later, constraining the thrust development history. We use these results to derive a tectonic model of crustal shortening across the Himachal Himalaya involving early thickening, tectonic wedging emplacement of the Greater Himalayan Crystalline complex between the MCT and STD, and continued growth of the Himalayan thrust wedge by accretion of thrust horses from the Indian footwall.

INTRODUCTION

The first-order architecture of the Himalayan orogen is expressed by two major north-dipping faults bounding a high-grade complex in the orogenic core (e.g., Argand, 1924; LeFort, 1996; Yin and Harrison, 2000; DeCelles et al., 2002; Yin, 2006). A central issue with regard to the Cenozoic Himalayan development is how the metamorphic core, the Greater Himalayan Crystalline complex, has been emplaced to its current position (LeFort, 1975; Burchfiel and Royden, 1985; Grujic et al., 1996; Nelson et al., 1996; Webb et al., 2007). Resolving this issue requires knowledge of the kinematic history of each bounding fault, i.e., the Main Central thrust (MCT) below and South Tibet detachment (STD) above, and the structural relationship between these faults.

The regional significance of the MCT as a major Cenozoic shortening structure has been recognized since the classic work of Heim and Gansser (1939) (Fig. 1) (see also Le Fort, 1975; Upreti, 1999; Hodges, 2000; DiPietro and Pogue, 2004). In contrast, the STD was discovered much later (Burg et al., 1984; Burchfiel et al., 1992). The STD is generally north-dipping, features alternating top-to-the-south and top-to-the-north shearing, and juxtaposes the largely low-grade Tethyan Himalayan Sequence on top of the Greater Himalayan Crystalline complex (e.g., Patel et al., 1993; Hodges et al., 1996). Excepting the top-to-the-south

*awebb@lsu.edu.

Geosphere; August 2011; v. 7; no. 4; p. 1013–1061; doi: 10.1130/GES00627.1; 17 figures; 4 tables; 7 supplemental files.

shear indicators, these records are consistent with a normal fault interpretation. The apparent presence of a major normal fault within the contractional orogenic setting of the Himalaya has led to intense debate over the tectonic origin and dynamic role of the STD (e.g., Burg et al., 1984; Burchfiel and Royden, 1985; Yin, 1989; Hodges et al., 1992, 1996; Brown and Nazarchuk, 1993; Patel et al., 1993; Yin et al., 1994, 1999; Lee et al., 2000; Grujic et al., 2002).

Current hypotheses for the emplacement of the Greater Himalayan Crystalline complex offer different solutions to this problem (Fig. 2). Vertical wedge extrusion models show the STD as a normal fault at the crust of a Coulomb orogenic wedge (e.g., Burchfiel and Royden, 1985; Grujic et al., 1996). Models of southward middle-crustal channel flow interpret the STD as a backstop normal fault allowing the extrusion of channel rocks linked to focused denudation along the Himalayan topographic front (e.g., Nelson et al., 1996; Beaumont et al., 2001). In tectonic wedging models, the STD acts largely as a subhorizontal backthrust off of the MCT, with its top-to-the-north shear surfacing as the Great Counter thrust system (Webb et al., 2007). These competing models for the emplacement of the Greater Himalayan Crystalline complex make different predictions (Table 1) (Fig. 2). First, the wedge extrusion model (Burchfiel and Royden, 1985) requires local extension over the highest region of the Himalaya and suggests that slip may be focused along a preexisting lithologic contact (Burg et al., 1984; Burchfiel and Royden, 1985). Second, both wedge extrusion and channel flow models require rapid erosion of the Tethyan Himalayan Sequence and exposure of the Greater Himalayan Crystalline complex during the main motion along the MCT and STD in the Early and Middle Miocene (Nelson et al., 1996; Beaumont et al., 2001; Hodges et al., 2001). In contrast, the tectonic wedging model predicts that the Tethyan Himalayan Sequence was preserved above the Greater Himalayan Crystalline complex during STD motion. Third, the wedge extrusion model predicts the STD and MCT merge downdip to the north, the channel flow model predicts them to be largely subparallel, and the tectonic wedging model predicts them to merge updip to the south.

As the relationship between the STD and MCT is central in differentiating these models, field tests must be conducted in regions where their relationships can be established. This requirement motivates our

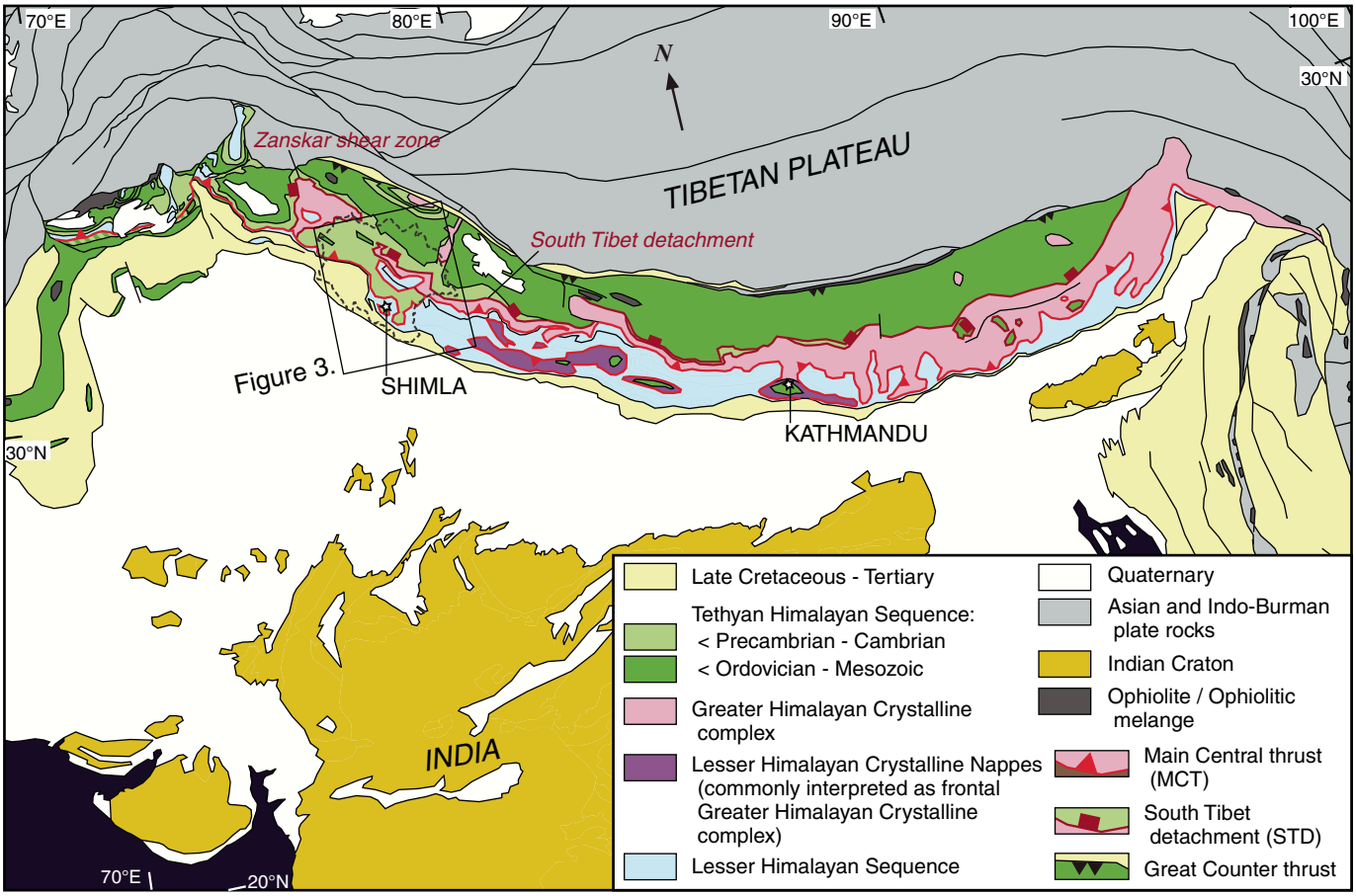

Figure 1. Simplified tectonic map of the Himalayan orogen. The dashed line denotes the Indian state of Himachal Pradesh, the box denotes the boundaries of Figure 3. Based on: Academy of Geological Sciences China (1975), Acharyya et al. (1986), Acharyya (1997), Biju-Sekhar et al. (2003), Buick et al. (2006), Deb et al. (2001), Ding et al. (2001), DiPietro and Pogue (2004), Frank et al. (1973, 1995), Fuchs and Linner (1995), Gilley et al. (2003), Jadoon et al. (1994), Johnson et al. (2001), Kapp et al. (2003), Khan et al. (2004), Leloup et al. (1995), Mitchell (1993), Mitchell et al. (2007), Murphy and Copeland (2005), Pilgrim and West (1928), Rao et al. (2000), Robinson (2005), Robinson et al. (2007), Robinson et al. (2006), Socquet and Pubellier (2005), Srikantia and Sharma (1976), Steck (2003), Thakur (1998), Thiede et al. (2006), Upreti (1999), Valdiya (1980), Vannay and Grasemann (1998), Vannay et al. (2004), Webb et al. (2007), Windley (1988), Yeats and Hussain (1987), Yin and Harrison (2000), Yin (2006); see also references cited in Figure 3.

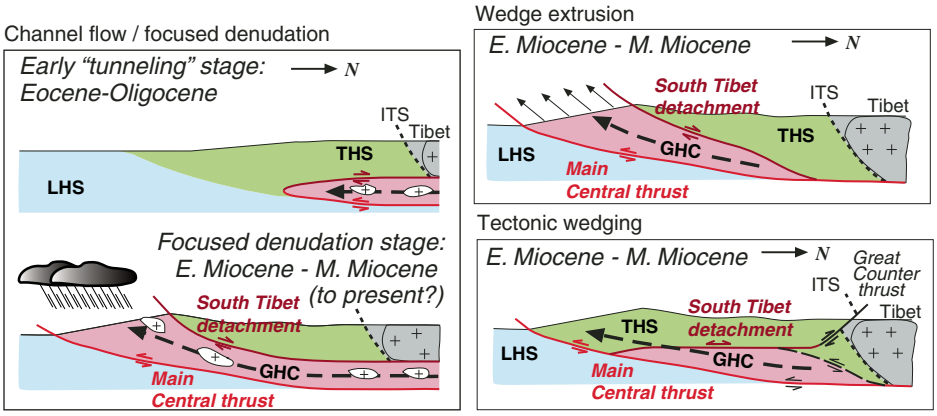

Figure 2. Himalayan tectonic models for the emplacement of the Greater Himalayan Crystalline complex (GHC): channel flow/focused denudation model (e.g., Nelson et al., 1996; Beaumont et al., 2001; Hodges et al., 2001); wedge extrusion model (e.g., Burchfiel and Royden, 1985; Grujic et al., 1996); tectonic wedging model (e.g., Yin, 2006; Webb et al., 2007). THS—Tethyan Himalayan Sequence; LHS—Lesser Himalayan Sequence; ITS—Indus-Tsangpo suture; E.—Early; M—Middle.

geologic investigation of the Himachal Himalaya in northwest India (Fig. 1), where contact relationships between the MCT and STD have been proposed and locally tested (Thakur, 1998; Yin, 2006; Webb et al., 2007). This region loosely marks the transition from the western to the central Himalaya, which are in part distinguished by drastically different preservation of the Tethyan Himalayan Sequence above the STD. In the central Himalaya, the Tethyan Himalayan Sequence has been largely eroded away, leaving the MCT and STD exposed as subparallel structures above and below the Greater Himalayan Crystalline complex (e.g., Hodges et al., 1996; DeCelles et al., 2001). In contrast, the Tethyan Himalayan Sequence is well preserved in the western Himalaya. In the Himachal Himalaya, an along-strike variation of MCT juxtaposition (i.e., from a Greater Himalayan Crystalline complex over Lesser Himalayan Sequence relationship in the east to a Tethyan Himalayan Sequence over Lesser Himalayan Sequence relationship in the west) can be directly observed (Fig. 3) (Thakur, 1998; Steck, 2003; DiPietro and Pogue, 2004). Besides this advantage, the stratigraphic units above and below the MCT are correlative in Himachal (e.g., Miller et al., 2001; Myrow et al., 2003), allowing assessment of the original configuration of the northern Indian margin before the Cenozoic Indo-Asian collision. This correlative stratigraphic relationship across the MCT in the Himachal Himalaya contrasts strongly with the geology of the central Himalaya of Nepal, where rock units across the MCT differ drastically in age and provenance (Parrish and Hodges, 1996; DeCelles et al., 2000).

In this study we compiled a regional geologic map that combines information from existing literature and our new geological and analytical data collected via structural, geochemical, thermobarometric, and U-Th-Pb geochronologic and $^{40}Ar/^{39}Ar$ thermochronologic analyses of key areas and critical samples. We integrate our new results into a tectonic model that shows that the construction of the Himachal Himalaya was mainly accomplished by footwall accretion and vertical thrust stacking of Proterozoic strata of the northern Indian passive margin sequence, consistent with a tectonic wedging emplacement of the Greater Himalayan Crystalline complex.

LITHOLOGIC UNITS

Major lithologic units in the study area include the Cretaceous and Cenozoic Sub-Himalayan Sequence, the Proterozoic and Cambrian Lesser Himalayan Sequence, the high-grade Greater Himalayan Crystalline complex, and the Neoproterozoic to Mesozoic Tethyan Himalayan Sequence (Figs. 3 and 4; Table 2). The Lesser Himalayan Sequence, Greater Himalayan Crystalline complex, and Tethyan Himalayan Sequence are structurally divided as MCT footwall rocks, rocks encased by the MCT below and the STD above, and rocks structurally above the STD, respectively (e.g., Hodges, 2000; Yin, 2006). We describe the lithologic units briefly herein; for an expanded description, see Appendix 1.

The Sub-Himalayan Sequence consists of lower shallow-marine strata and upper continental deposits separated by an Oligocene unconformity (Table 2). Sub-Himalayan Sequence rocks depositionally overlie rocks of the Lesser Himalayan Sequence and correlative rocks at the base of the Himalayan foreland basin (e.g., Powers et al., 1998).

Four subunits are distinguished within the Lesser Himalayan Sequence: (1) the Neoproterozoic–Cambrian Outer Lesser Himalayan Sequence in the hanging walls of the Krol and Tons thrusts, (2) the Paleoproterozoic–Neoproterozoic Damtha and Deoban Groups in the hanging wall of the Bilaspur thrust and the footwalls of the Tons and Berinag thrusts, (3) the Paleoproterozoic Berinag Group in the hanging wall of the Berinag thrust, and (4) the Paleoproterozoic Munsiari Group, dominantly in the hanging wall of the Munsiari thrust (Table 2) (Figs. 3 and 4).

The Greater Himalayan Crystalline complex is ~7–9 km thick and consists of paragneiss, schist, and orthogneiss intruded by minor Tertiary leucogranites concentrated mostly in its upper 2–3 km (Table 2). An inverted metamorphic field gradient is observed across a complete section of these rocks along the Sutlej River, progressing from garnet-staurolite–bearing rocks at the base to migmatitic rocks near the top (Vannay and Grasemann, 1998).

The Tethyan Himalayan Sequence is dominated by the Neoproterozoic–early Cambrian Haimanta Group, early Paleozoic granites, Cambrian Parahio Formation, and overlying Paleozoic–Mesozoic strata (Table 2). Its basement is likely the Paleoproterozoic Baragaon gneiss in the MCT shear zone directly below the unit (Bhanot et al., 1978; Miller et al., 2000; this study). The Haimanta Group is garnet grade across its basal 1–3 km of section, and the grade decreases upsection across the Tethyan Himalayan Sequence.

REGIONAL TECTONIC FRAMEWORK

First-order structures in the Himachal Himalaya are represented by a stack of northern rooted thrusts, many of which are folded (Fig. 3). The main fault zones and fault systems include, from southwest to northeast, (1) the Main Frontal thrust, (2) the Sub-Himalayan thrust zone, (3) the Bilaspur-Palampur thrust system, (4) the Krol-Mandi thrust system, (5) the MCT, (6) the Tons thrust, (7) the Berinag thrust, (8) the Munsiari thrust, (9) the STD, (10) the Tethyan Himalayan fold-and-thrust belt including the Mata nappe, and (11) the Great Counter thrust system (Figs. 3 and

TABLE 1. PREDICTIONS OF HIMALAYAN TECTONIC MODELS

Models	High-grade rock affinity	Fault kinematics	Exhumation history	Spatial distribution of metamorphism	Along-strike structural and/or stratigraphic variation
Wedge extrusion (e.g., Burchfiel and Royden, 1985)	Greater Himalayan Crystalline complex rocks are derived from the India plate	STD top-to-the north	1. Greater Himalayan Crystalline complex exhumed in the Early Miocene, syn-STD motion 2. Paleogene exhumation of Tethyan Himalayan Sequence	1. Exposed metamorphic isograds subparallel to approximately planar MCT, STD, therefore north-dipping 2. Inverted metamorphism dominates lower 5–10 km of MCT hanging wall	Early–Middle Miocene extrusion of the Greater Himalayan Crystalline complex between the MCT and STD at the surface requires continuous exposure of this unit between the Lesser and Tethyan Himalayan Sequences along the length of the orogen.
Channel flow (e.g., Nelson et al., 1996)	Greater Himalayan Crystalline complex rocks are derived from the Asia plate	STD top-to-the north	1. Greater Himalayan Crystalline complex exhumed in the Early Miocene, syn-STD motion 2. Basal Tethyan Himalayan Sequence exhumed prior to the Greater Himalayan Crystalline Complex	1. Exposed metamorphic isograds subparallel to approximately planar MCT, STD, therefore north-dipping 2. Inverted metamorphism dominates lower 5–10 km of MCT hanging wall	Early–Middle Miocene extrusion of the Greater Himalayan Crystalline complex between the MCT and STD at the surface requires continuous exposure of this unit between the Lesser and Tethyan Himalayan Sequences along the length of the orogen.
Modified channel flow (e.g., Beaumont et al., 2004)	Greater Himalayan Crystalline complex rocks are derived from the India plate	STD top-to-the north; asymmetric thrust extrusion model allows alternating top-to-the south and top-to-the north STD shearing (Beaumont et al., 2004)	1. Greater Himalayan Crystalline complex exhumed in the Early Miocene, syn-STD motion 2. Basal Tethyan Himalayan Sequence exhumed prior to or approximately synchronously (with asymmetric thrust extrusion) with the Greater Himalayan Crystalline complex	1. Exposed metamorphic isograds subparallel to approximately planar MCT, STD, therefore north-dipping 2. Inverted metamorphism dominates lower 5–10 km of MCT hanging wall	Early–Middle Miocene extrusion of the Greater Himalayan Crystalline complex between the MCT and STD at the surface requires continuous exposure of this unit between the Lesser and Tethyan Himalayan Sequences along the length of the orogen.
Tectonic wedging (e.g., Yin, 2006; Webb et al., 2007)	Greater Himalayan Crystalline complex rocks are derived from the India plate	Alternating top-to-the south and top-to-the north STD shearing	1. Greater Himalayan Crystalline complex exhumed after the Early Miocene, post-STD motion 2. Basal, hinterland Tethyan Himalayan Sequence exhumed approximately synchronously with the upper Greater Himalayan Crystalline complex	1. Exposed metamorphic isograds subparallel to the folded (open to tightly) MCT, STD, therefore folded 2. Inverted metamorphism south of MCT-STD intersection line dominates only ~1–2 km MCT zone; structurally higher rocks show right-way-up metamorphism	Foreland MCT strands juxtapose Tethyan Himalayan Sequence rocks on top of Lesser Himalayan Sequence rocks; hinterland MCT strands juxtapose Greater Himalayan Crystalline complex rocks atop Lesser Himalayan Sequence rocks. Locally, the leading edge of the Greater Himalayan Crystalline complex remains buried.

Note: STD—South Tibet detachment; MCT—Main Central thrust.

Figure 3. This figure is intended to be viewed at a size of 11 × 17. To view the full-sized PDF file of Figure 3, please visit http://dx.doi.org/10.1130/GES00627.S1. Geological map of the Himachal Himalaya. Lines of cross sections drawn include A-A′ (cross section in Fig. 4A, reconstruction in Fig. 17), A-A′, A″-A‴ (sketch cross section in Fig. 4B), and B-B′ (sketch cross section in Supplemental File 1[1]). Red boxes outline the positions of maps in Fig. 6A, 6B, 6C. Figure 3 is based upon our mapping, analysis of LANDSAT images, discussions with A.K. Jain and S. Singh (2004, personal commun.), and previous work by Agarwal and Kumar (1973), Ahmad et al. (1999), Auden (1934), Bassi (1989), Bhargava (1976, 1980), Bhargava et al. (1991), Bhattacharya et al. (1982), Célérier et al. (2009a), Choudhuri et al. (1992), Das and Rastogi (1988), Dèzes (1999), Dèzes et al. (1999), Epard et al. (1995), Frank et al. (1973, 1995), Fuchs (1982), Grasemann et al. (1999), Gururajan (1990), Gururajan and Virdi (1984), Jäger et al. (1971), Jain (1972), Jain and Anand (1988), Jain et al. (1999), Kumar and Brookfield (1987), Pachauri (1980), Pandey et al. (2003), Pecher and Scaillet (1989), Pilgrim and West (1928), Powers et al. (1998), Raina (1981), Raiverman (2000), Rao and Pati (1980), Rattan (1973), Rautela and Thakur (1992), Robyr et al. (2002), Rupke (1974), Schlup (2003), Schlup et al. (2003), Shanker and Dua (1978), K.K. Sharma (1977), V.P. Sharma (1977), Singh and Jain (1993), Singh and Thakur (2001), Srikantia and Bhargava (1984, 1988), Srikantia and Sharma (1976), Steck (2003), Steck et al. (1998), Tewari et al. (1978), Thakur and Rawat (1992), Thiede et al. (2006), Thöni (1977), Valdiya (1978, 1980), Vannay and Grasemann (1998), Vannay and Steck (1995), Vannay et al. (1999, 2004), Virdi (1979), Wiesmayr and Grasemann (2002), West (1939), Wyss (2000), and Wyss et al. (1999).

[1]Supplemental File 1. PDF file of sketch cross section along profile B-B′; see text Figure 3. The discontinuous graphitic quartzite marker lithology occurs at two levels in the Chandrabhaga River Valley. These occurrences are interpreted as two distinct stratigraphic horizons. Alternatively, these may reflect unrecognized kilometer-scale tight to isoclinal folds. Primary sources for this section are Powers et al. (1998) (sub-Himalayan thrust zone); Srikantia and Sharma (1976) (sedimentary Lesser Himalayan Sequence units); Frank et al. (1995) [Haimanta Group in the Main Central thrust (MCT) hanging wall]; Thakur (1998), Dèzes (1999), Yin (2006), and Webb et al. (2007) (STD, South Tibet detachment). If you are viewing the PDF of this paper or reading it offline, please visit http://dx.doi.org/10.1130/GES00627.S2 or the full-text article on www.gsapubs.org to view Supplemental File 1.

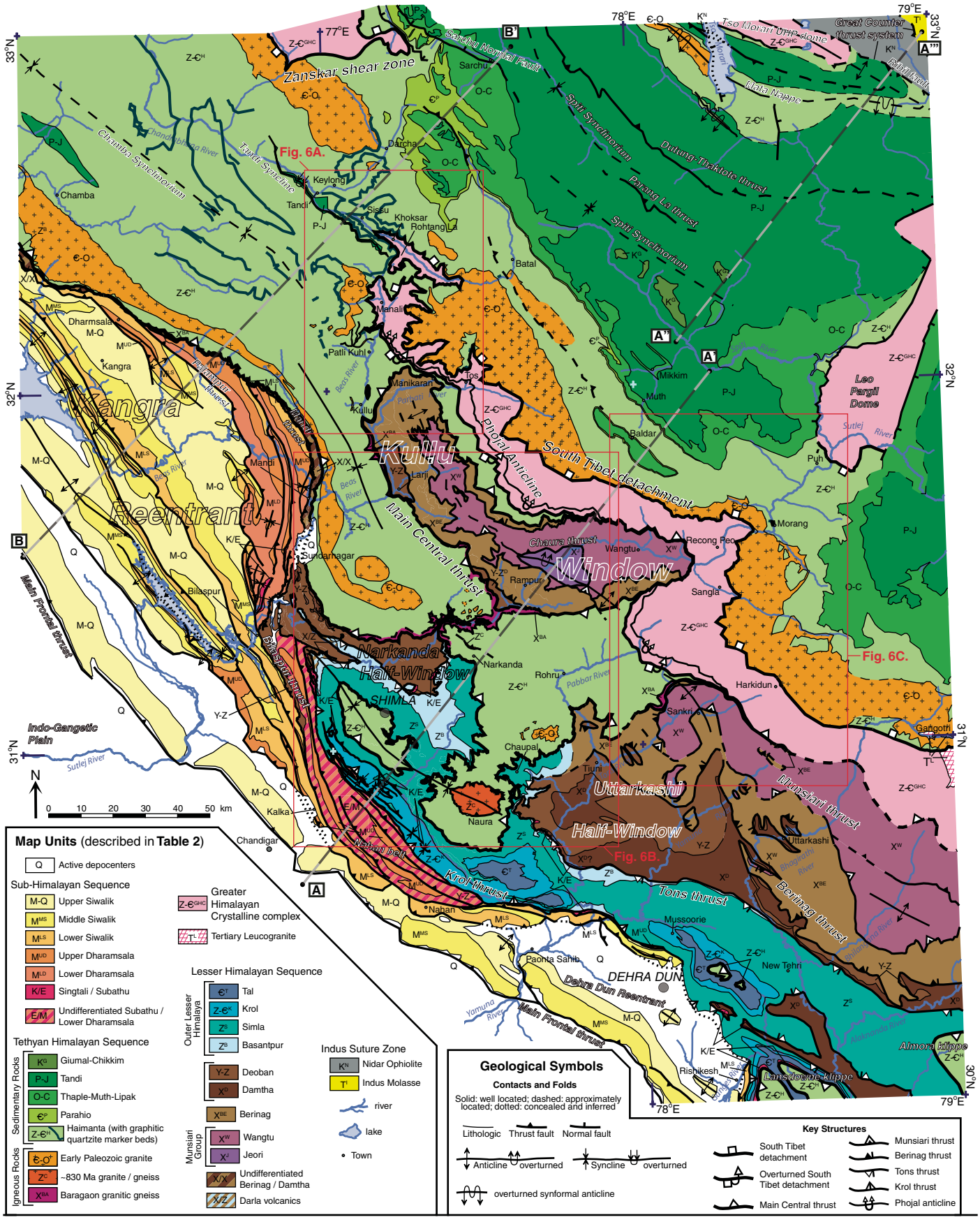

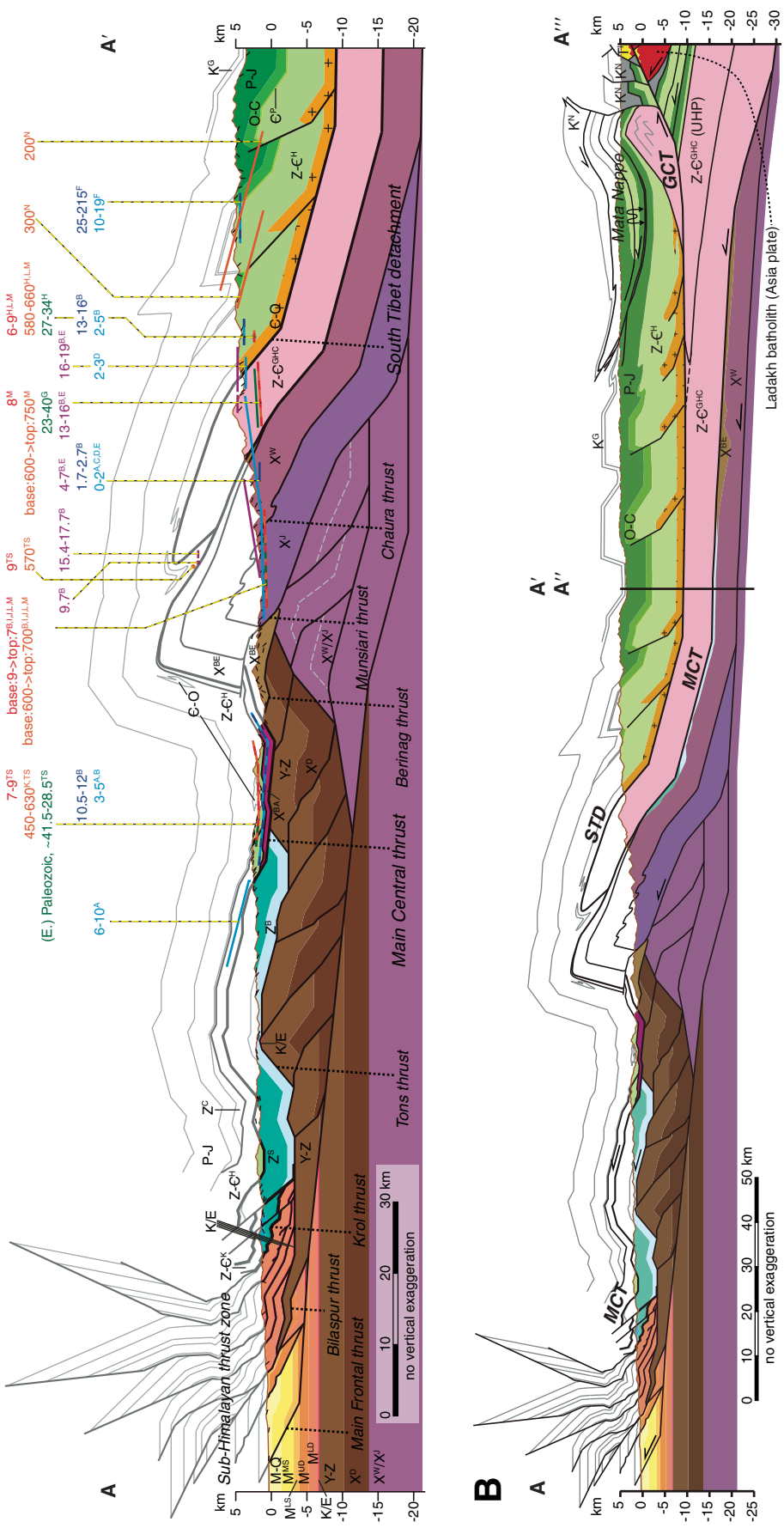

Figure 4. (A) Cross section of the Himachal Himalaya. Section drawn along line A-A′ of Figure 3. Units and symbols are as in Figure 3. Brown curve represents Earth's surface, short black lines along Earth's surface represent bedding and/or foliation attitudes. All faults are top-to-the-southwest with the exception of the South Tibet detachment, which displays records of both top-to-the-southwest and top-to-the-northeast motion. References for analytical data are: [A]Thiede et al., 2009; [B]Vannay et al., 2004; [C]Jain et al., 2000; [D]Thiede et al., 2004; [E]Thiede et al., 2005; [F]Schlup, 2003; [G]E. Catlos, 2004, personal commun.; [H]Chambers et al., 2009; [I]Chambers et al., 2008; [J]Caddick et al., 2007; [K]Gregory, 2004; [L]Vannay and Grasemann, 1998; [M]Vannay et al., 1999; [N]Wiesmayr and Grasemann, 2002; [TS]this study. (B) Sketch cross section of the Himachal and Ladakh Himalaya. MCT—Main Central thrust; STD—South Tibet detachment; GCT—Great Counter thrust system; UHP—ultrahigh pressure. The abbreviations are the same as in the legend in Figure 3.

TABLE 2. TECTONOSTRATIGRAPHY OF THE HIMACHAL HIMALAYA

Unit name (alternative name)	Lithologic description	Thickness (m)	Age constraints	Nd, Sr isotopic constraints*
Himalayan Foreland				
Upper Siwalik Fm†	ss, congl[DD§]	~1700 - 2300[DD]	deposition 7 Ma to Pleistocene: MS[Z#]	N.D.
Middle Siwalik Fm	ss with minor slts, sh, congl[DD]	~1300 - 2000[DD]	deposition 11 to 7 Ma: MS[Z#]	N.D.
Lower Siwalik Fm	slts with minor ss, sh[DD]	~700 - 1300[DD]	deposition 13 to 11 Ma: MS[Z, AA#]	N.D.
Upper Dharamsala Fm (Kasauli)	grey ss, minor sh (fluvial / alluvial)[CC, TT]	~1000 - 1300[DD]	deposition 16.5 to 13 Ma: MS[AA], cf. detrital mica[BB#]	N.D.
Lower Dharamsala Fm (Dagshai)	ss, slts, sh, caliche (fluvial / alluvial)[CC, TT]	up to 1300[DD**]	deposition 20 to 16.5 Ma: MS[AA], cf. detrital mica[BB, UU#]	N.D.
Subathu Fm	ls, sh, minor fine grained ss (shallow marine)[CC, TT]	up to 200[DD**, FF, GG]	latest Paleocene -Middle Eocene: fossils[CC]	N.D.
Singtali Fm	ls, minor quartz arenite (shallow marine)[CC]	~50, discontinuous[CC]	Late Cretaceous - Paleocene: fossils[CC††]	N.D.
Lesser Himalayan Sequence: Outer Lesser Himalaya				
Tal Fm	ss, slts[EEE, S]	~500[S]	Lower Cambrian: trilobites[A, EEE], Re-Os isochron[B]	≤ L Pt[C*]
Krol Gp	dl, ls with minor sh, slts[R, FFF]	~1500 - 2200[HH, S, FFF]	~590-543 Ma: fossils[GGG, R, EEE], ^{13}C shift[HHH]	≤ LPt[M]
Shimla Gp (Chandpur + Nagthat + Blaini)	sh (minor slate), slts, ss, with minor gw, tillite, congl[CCC, FF, BBB, DDD]	~3800 - 4100[II], cf. ~3300[FF]	<~620 Ma: detrital U-Pb zrc[TS]; stratigraphically below Krol Gp[S]	≤ L Pt[E, M, Y]
Basantpur Fm (Mandhali)	interbedded ls, slts, sh (minor slate)[FF, BBB]	>~300-640[S, JJ], cf.>~1360[FF]	839±138 Ma: Re-Os isochron[B], Neo-Pt: strom[O, YY]	≤ L Pt[E, M]
Lesser Himalayan Sequence: Parautochthon				
Deoban Gp (Shali)	dl, ls with minor sh, chert, ss[S]	>~3000[HH, II]	≥ 2 levels, lower: (latest Paleo?-)Meso-Pt, upper: Neo-Pt. strom and other fossils[S, N, O, P, Q, WW, XX, YY, ZZ]	≥ M Pt[M, Y*]
Damtha Gp (Sundarnagar; Chakrata [lower member], Rautgara [upper])	gw, slts, slate succeeded by qtzt, sl, basic sills and dikes[S]	>~2900[HH]	≥ Paleo-Pt, stratigraphically below Deoban Gp[S]	N.D.
Lesser Himalayan Sequence: Berinag thrust hanging wall rocks				
Berinag Gp (Rampur, Manikaran)	greenschist-facies sericitic quartz-arenite, metabasalt (sills, dikes, flows), minor sl[S, J]	>~1000[KK]	~1.85 - 1.8 Ga: detrital U-Pb zrc[M, TS], U-Pb zrc from metabasalt[J]	qtzt: ≥ M Pt[M, Y], meta-basalt: ≤ L Pt[J, JJJ, VV]
Lesser Himalayan Sequence: Munsiari Group				
Wangtu gneiss (Bandal)	dominantly granitic augen gneiss[LL]	>~2000[LL]	~1.85 Ga: Rb-Sr whole rock[K, J], U-Pb zrc[J, L, M]	≥ M Pt[J, M]
Jeori metasedimentary rocks	paragneiss, mica schist, minor metabasite, qtzt, granitic gneiss[LL]	unknown	some layers <~1.9 Ga, other layers >~2068 Ma: detrital U-Pb zrc[M, TS], igneous U-Pb zrc[III]	≥ M Pt[J, M]
Felsic pegmatite (cross-cuts Wangtu gneiss foliation)		up to ~4 m thick dikes	~8-6 Ma: U-Pb zrc, Th-Pb monazite[TS]	N.D.
Greater Himalayan Crystalline complex				
	paragneiss, schist, orthogneiss	~4500-8000[LL]	some layers younger than ~850 Ma: detrital zrc[M, TS], 495 Ma orthogneiss: Rb/Sr[K]	≤ L Pt[M, Y]
Leucogranite		up to ~100's m thick	~27-20 Ma: U-Pb monazite, uraninite[H], Th-Pb monazite[TS]	N.D.
Tethyan Himalayan Sequence: sedimentary rocks				
Giumal-Chikkim succession	ss, black sh, ls[EE]	~350[RR]	Cretaceous: fossils[RR]	N.D.
Tandi Gp	carbonate, sh, slts, qtzt[MM]	>~1920[MM]	Permian - Jurassic: fossils[T, U, V]	N.D.
Thaple-Muth-Lipak succession	sh, slts, qtzt, quartz-arenite, carbonate, congl[MM]	~1650[MM], cf. ~1100[NN]	Ordovician - Carboniferous: fossils[V]	N.D.
Parahio Fm	ss, sh (siliciclastic deltaic)[AAA]	~700[NN], cf. >1350[AAA]	uppermost Lower Cambrian-middle Middle Cambrian: fossils[A, W, AAA]	N.D.
Haimanta Gp	phyllite, schist, garnet schist, graphitic schist, psammitic schist, minor carbonate, minor metabasalt	>~6250[MM], cf. ~2000-3500[NN]	<~550 Ma - Early Cambrian: trilobites[X], cross-cutting igneous ages[E, K], detrital U-Pb zrc[TS]	≤ L Pt[E, M, Y]

(*continued*)

TABLE 2. TECTONOSTRATIGRAPHY OF THE HIMACHAL HIMALAYA (*continued*)

Unit name (alternative name)	Lithologic description	Thickness (m)	Age constraints	Nd, Sr isotopic constraints*
Tethyan Himalayan Sequence: igneous rocks				
Early Paleozoic granitoids	granite, minor mafic enclaves, minor aplite, locally gneissic	up to at least ~2000[OO]	Cambro-Ordovician: Rb-Sr whole rock[D], U-Pb zrc[E, F, TS]	≤ L Pt[E]
~830 Ma (Chaur-Black Mtn) granite	granite, granitic gneiss	up to ~3000[QQ]	~830 Ma: U-Pb zrc[G, TS]	N.D.
Baragaon granitic gneiss	mylonitic granitiod gneiss	up to ~1100[PP]	~1.85 Ga: Rb-Sr whole rock[I, J], U-Pb zrc[TS]	≥ M Pt[J, M]
Indus Suture Zone				
Nidar Ophiolite	ultramafics, gabbros, pillow basalts[SS]	~2100-2700[SS]	140.5±5.3 Ma: Sm-Nd (plagioclase-clinopyroxene)[SS]	N.D.
Indus Molasse	sh, slts, ss, congl[EE]	unknown	early Eocene[EE]	N.D.

*Himalayan pre-Cenozoic rocks plot in two largely distinct groups in Nd and Sr isotopic space (see Supplemental File 2[2]). These groups can be distinguished by age: Middle Proterozoic and older rocks yield $\varepsilon_{Nd}(500) < \sim -14$ and a broad range of $^{87}Sr/^{86}Sr(500)$ values (this group is abbreviated as "≥ M Pt" in the table), whereas Late Proterozoic and younger rocks yield $\varepsilon_{Nd}(500) > \sim -14$ and a narrow range of $^{87}Sr/^{86}Sr(500)$ values (this group is abbreviated as "≤ L Pt" in the table).

†Additional abbreviations in this table are: Fm = Formation, Gp = Group, congl = conglomerate, ss = sandstone, slts = siltstone, sh = shale, gw = greywacke, ls = limestone, dl = dolomite, qtzt = quartzite, N.D. = not determined, MS = magnetostratigraphy, zrc = zircon, strom = stromatolites, Pt = Proterozoic.

§Capitalized, superscript letters refer to sources: [A]Hughes and Jell, 1999; [B]Singh et al., 1999; [C]Myrow et al., 2003; [D]Jäger et al., 1971; [E]Miller et al., 2001; [F]Marquer et al., 2000; [G]Singh et al., 2002; [H]Walker et al., 1999; [I]Trivedi et al., 1984; [J]Miller et al., 2000; [K]Frank et al., 1977; [L]Singh et al., 1994; [M]Richards et al., 2005; [N]Valdiya, 1969; [O]Raha and Sastry, 1982; [P]Srivastava and Kumar, 2003; [Q]Tewari, 2003; [R]Singh and Rai, 1983; [S]Valdiya, 1980; [T]Powell and Conaghan, 1973; [U]Srikantia and Bhargava, 1979; [V]Srikantia and Bhargava, 1998; [W]Garzanti et al., 1986; [X]Hughes and Droser, 1992; [Y]Ahmad et al., 2000; [Z]Meigs et al., 1995; [AA]White et al., 2001; [BB]Najman et al., 1997; [CC]Najman et al., 1993; [DD]Powers et al., 1998; [EE]Steck, 2003; [FF]Srikantia and Sharma, 1976; [GG]Raiverman, 2000; [HH]Rupke, 1974; [II]Srivastava and Mitra, 1994; [JJ]Bhargava, 1976; [KK]V.P. Sharma, 1977; [LL]Vannay and Grasemann, 1998; [MM]Wiesmayr and Grasemann, 2002; [NN]Vannay and Steck, 1995; [OO]Wyss et al., 1999; [PP]Grasemann et al., 1999; [QQ]Srikantia and Bhargava, 1988; [RR]Steck et al., 1998; [SS]Linner et al., 2001; [TT]Najman and Garzanti, 2000; [UU]White et al., 2002; [VV]Bhat and LeFort, 1993; [WW]Venkatachala and Kumar, 1998; [XX]Srivastava and Kumar, 1997; [YY]Sinha, 1975; [ZZ]Raha, 1980; [AAA]Myrow et al., 2006; [BBB]Kumar and Brookfield, 1987; [CCC]Pilgrim and West, 1928; [DDD]Valdiya, 1970; [EEE]Hughes et al., 2005; [FFF]Jaing et al., 2003; [GGG]Jaing et al., 2002; [HHH]Aharon et al., 1987; [III]Singh et al., 2006; [JJJ]Bhat and LeFort, 1992; [TS]This study.

#The age estimates for the Miocene and younger SH rocks largely depend on magnetostratigraphic correlation. However, the youngest $^{40}Ar/^{39}Ar$ age of detrital white micas, which record the time at which the mica cooled below ~370 °C, provide a maximum age of deposition. Detrital mica ages of ~22 Ma at the base of the Lower Dharamsala, and ~16 Ma in the Upper Dharamsala (BB,UU) are only consistent with the proposed magnetostratigraphic ages if extraordinary cooling rates are invoked (see Yin (2006)). The youngest white mica ages obtained from Himalyan bedrock are >4 Ma (Celerier et al., 2009b), so using ~4 m.y. as a minimum lag time between the cooling age and depositional age suggests that the magnetostratigraphic ages for the Lower and Upper Dharamsala are at least ~2 m.y. too old. Adjusting the ages of these units may also affect interpreted ages of the Siwalik strata.

**According to the [DD]Powers et al. (1998) model, the Main Himalayan Detachment reactivates the onlapping depositional contact of the Tertiary foreland basin over the Vindhyan Group. In this scheme, the Lower Dharmsala and Subathu pinch out along the reactivated portion of the contact, and thus have 0 thickness at the pinch out. The exposed sections of these units have thicknesses tending toward the upper thickness values given in the table.

††[S]Valdiya (1980) notes that the "lower Singtali" may be equivalent to the Gondwanas (i.e., late Paleozoic-Early Mesozoic).

4). Excepting the STD and the Great Counter thrust system, all major structures are southwest-directed thrusts. Several large structural culminations are also exposed in the map area due to folding of major thrusts and the development of low-angle detachment faults. We refer to these structures as (1) the Narkanda half-window, (2) the Uttarkashi half-window, (3) the Kullu window, (4) the Leo Pargil dome, and (5) the Tso Morari gneiss dome (Fig. 3). We briefly describe this regional tectonic framework herein; for an expanded description, see Appendix 2.

MCT Footwall Structures

The Sub-Himalayan thrust zone is bounded by the Main Frontal thrust below and the Krol and Mandi thrusts above (Fig. 3). The Main Frontal thrust places Neogene–Quaternary strata over the modern Indo-Gangetic Plain deposits; the Mandi and Krol thrusts place Lesser Himalayan Sequence rocks over Paleogene–Quaternary strata of the Sub-Himalayan Sequence (Kumar et al., 2006; Srikantia and Sharma, 1976; Powers et al., 1998; Raiverman, 2000).

The Tons thrust, exposed along the Sutlej River near Shimla and across the southern margin of the Uttarkashi half-window, places the Outer Lesser Himalayan Sequence over the Deoban and Damtha Groups (Fig. 3) (e.g., Valdiya, 1980; Célérier et al., 2009a). The Munsiari thrust can be traced along most of the central Himalayan orogen (e.g., Upreti, 1999; Yin, 2006; Searle et al., 2008; see discussions in Célérier et al., 2009a, 2009b), and is referred to as the MCT I in Nepal (Bordet et al., 1972; Arita, 1981; Harrison et al., 1998). The thrust crops out in the Kullu window and the Uttarkashi half-window, where it places the Munsiari Group (Wangtu and Jeori gneiss) over the Berinag Group (Figs. 3, 4, 6B, and 6C) (e.g., V.P. Sharma, 1977; Valdiya, 1980; Vannay et al., 2004). The Berinag thrust appears in both the hanging wall and footwall of the Munsiari thrust, where it juxtaposes Berinag Group rocks over the Wangtu gneiss and the Damtha Group, respectively (Fig. 3) (e.g., V.P. Sharma, 1977; Valdiya, 1980; Vannay et al., 2004; Célérier et al., 2009a).

[2]Supplemental File 2. PDF file of $^{87}Sr/^{86}Sr$ (500 Ma) vs. ε_{Nd} (500 Ma) plots for the western and central Himalaya. In the Nepal Himalaya, Nd and Sr isotopic compositions and detrital zircon age distributions are different in the Lesser Himalayan Sequence (LHS), Greater Himalayan Crystalline complex (GHC), and Tethyan Himalayan Sequence (THS). It has been proposed that such data can be used to identify the structural setting of Himalayan strata (e.g., Parrish and Hodges, 1996). However, rocks of the same age in the Lesser Himalayan Sequence, Greater Himalayan Crystalline complex, and Tethyan Himalayan Sequence have the same isotopic compositions and detrital zircon patterns (e.g., Myrow et al., 2003; Richards et al., 2005). This suggests that distinctions from isotopic and detrital zircon signatures in Himalayan rocks cannot be used directly to infer structural setting. Such distinctions are nonetheless valuable for constraining age ranges of Himalayan strata and thus for making stratigraphic comparisons. Neoproterozoic and younger rocks are generally distinguishable from Mesoproterozoic and older rocks in $^{87}Sr/^{86}Sr$ (500 Ma) vs. ε_{Nd} (500 Ma) space. (A) $^{87}Sr/^{86}Sr$ (500 Ma) vs. ε_{Nd} (500 Ma) plot for western and central Himalaya rocks. Data for this plot are divided into three plots to ease tracking of data for individual units. (B) $^{87}Sr/^{86}Sr$ (500 Ma) vs. ε_{Nd} (500 Ma) plot for Himachal Himalaya rocks. Data from Bhat and Le Fort (1992, 1993), Miller et al. (2000, 2001), and Richards et al. (2005). (C) $^{87}Sr/^{86}Sr$ (500 Ma) vs. ε_{Nd} (500 Ma) plot for Kumaun and Nepal Himalaya rocks (Kumaun Himalaya—northwest India Himalaya to the east of Himachal Pradesh). Data from Ahmad et al. (2000), Deniel et al. (1987), France-Lanord et al. (1993), Inger and Harris (1993), and Prince (1999). (D) $^{87}Sr/^{86}Sr$ (500 Ma) vs. ε_{Nd} (500 Ma) plot for western Himalayan (Nanga Parbat) syntaxis rocks. Data from Argles et al. (2003), Foster et al. (2000, 2002), Gazis et al. (1998), George et al. (1993), and Whittington et al. (1999). If you are viewing the PDF of this paper or reading it offline, please visit http://dx.doi.org/10.1130/GES00627.S3 or the full-text article on www.gsapubs.org to view Supplemental File 2.

MCT

The MCT is classically defined as the tectonic boundary between the Greater Himalayan Crystalline complex above and the Lesser Himalayan Sequence below (e.g., Heim and Gansser, 1939; Le Fort, 1996; Hodges, 2000; Yin, 2006). This definition is uncertain because of debates over which local lithological units should be attributed to which tectonic unit, and it is circular, since the Greater Himalayan Crystalline complex and Lesser Himalayan Sequence are defined by their bounding structures (see discussion by Upreti, 1999). Nonetheless, for the Himachal Himalaya most workers share a consensus interpretation of the MCT as a continuous, folded, southwest-directed thrust shear zone as much as 2 km thick that was active in the Early and Middle Miocene and has a largely established map trace (as shown in Fig. 3) (e.g., Thakur and Rawat, 1992; Frank et al., 1995; Steck, 2003; Vannay et al., 2004). This interpretation is based on congruent lithology, strain concentration, metamorphic grade, and thermochronologic ages along the mapped shear zone (e.g., Frank et al., 1995; Grasemann et al., 1999; Vannay et al., 2004; Thiede et al., 2005). The MCT hanging-wall rocks show variation; at its northeasternmost trace along the Sutlej River, the MCT underlies a well-established inverted metamorphic sequence that is universally acknowledged as Greater Himalayan Crystalline complex rocks (Fig. 3) (e.g., Vannay and Grasemann, 1998; Hodges, 2000; Steck, 2003; DiPietro and Pogue, 2004; Yin, 2006). Conversely, it has long been recognized that the MCT hanging-wall rocks to the west of Mandi (i.e., west of ~31°50′N, 77°E) display a right-way-up metamorphic field gradient to chlorite zone conditions and are structurally continuous with the Tethyan Himalayan Sequence to the northeast (Fig. 3) (Frank et al., 1995; Fuchs and Linner, 1995; Thakur, 1998; Steck, 2003; DiPietro and Pogue, 2004; Yin, 2006). Therefore the Himachal region requires a relaxation of the MCT definition as the boundary between the Greater Himalayan Crystalline complex and the Lesser Himalayan Sequence.

Based on the change in hanging-wall rocks, we divide the MCT into northern and southern segments. The northern MCT juxtaposes the Greater Himalayan Crystalline complex over the Lesser Himalayan Sequence; the southern MCT places the Tethyan Himalayan Sequence and the Baragaon gneiss over the Lesser Himalayan Sequence (Fig. 3). The intersection line of the STD and the MCT marks the boundary between the two segments of the MCT to the north and south (Thakur, 1998; Yin, 2006; Webb et al., 2007). In subsequent text, we refer to the "MCT zone" if the ~2 km thickness of the shear zone is relevant.

In the map area the MCT is folded and displays large full and half-windows and isolated klippes (Fig. 3). Cutoff relationships in the MCT footwall suggest that the thrust cuts upsection to the southwest in its transport direction. However, the presence of a large footwall ramp along the MCT in the map area raises the question of whether the Lesser Himalayan Sequence strata in the footwall ramp were horizontal when the MCT was initially cutting across them. As Cretaceous–Eocene beds overlie the Shimla Group and Tal Formation of the younger Outer Lesser Himalayan Sequence units in the south and the Deoban-Damtha strata in the north (Srikantia and Sharma, 1976; Valdiya, 1980) (Fig. 3), the Proterozoic–Cambrian sequence of the northern Indian passive margin must have been tilted to the south prior to the emplacement of the MCT hanging wall in the region.

Minimum displacement along the MCT in the map area is ~115 km, determined from the northernmost and southernmost exposures of the fault. Early to Late Miocene activity on the northern segment of the MCT has been inferred from U-Th monazite-inclusion dating, $^{40}Ar/^{39}Ar$ muscovite cooling ages, and zircon fission track ages from the Greater Himalayan Crystalline complex hanging-wall rocks (Fig. 4A) (Walker et al., 1999; Schlup, 2003; Vannay et al., 2004; Thiede et al., 2005). The portion of the MCT across the Kullu and Uttarkashi windows must have ceased

motion in the Late Miocene when these windows were developed and caused folding of the MCT, as indicated by cooling ages (Vannay et al., 2004; Thiede et al., 2005; Caddick et al., 2007; Chambers et al., 2008). However, the relationship does not preclude the southernmost MCT linking younger thrusts in the Lesser Himalayan Sequence to continue its motion after the Middle Miocene.

STD

The STD juxtaposing the Tethyan Himalayan Sequence over the Greater Himalayan Crystalline complex can be traced continuously from the central Himalaya to the northern end of the Kullu window (Figs. 1 and 3) (Burg et al., 1984; Burchfiel et al., 1992; Choudhuri et al., 1992; Thakur, 1998; Dèzes et al., 1999è; Jain et al., 1999; Wyss et al., 1999; Steck, 2003; DiPietro and Pogue, 2004; Yin, 2006). Here the STD is folded and overturned within the southwest-verging Phojal anticline, and the overturned fault trace extends back to the southeast and intersects the MCT on the north and south sides of the eastern Kullu window and at the northwestern rim of the Uttarkashi window (Fig. 3) (Thakur, 1998; Webb et al., 2007). The MCT-STD branch line trends to the northwest, parallel to the strike of the orogen. It is largely buried to the northwest and eroded to the southeast. In the Himachal Himalaya the fault features both top-to-the-northeast and top-to-the-southwest structures, including S-C fabric, normal drag shear bands, σ-type porphyroclasts, and asymmetric isoclinal to tight folds, across a 300–600-m-thick shear zone (Choudhuri et al., 1992; Jain et al., 1999; Vannay et al., 2004; our observations).

The Zanskar shear zone represents a possible northwestern extension of the STD (Figs. 1 and 3) (e.g., Searle, 1986; Herren, 1987; Patel et al., 1993; Dèzes et al., 1999; Epard and Steck, 2004). The northwest-trending, northeastern segment of this shear zone has been interpreted as (1) an along-strike continuation of the STD, connected in map view to the right-way-up STD across the Himachal Himalaya (e.g., Searle et al., 1988; Jain et al., 1999), or (2) as part of an STD window (Thakur, 1998; Dèzes, 1999; Yin, 2006). We follow the second interpretation because of the established continuity of the Tethyan Himalayan Sequence from Chamba to the Tso Morari, i.e., weakly deformed rocks cross the path of the proposed STD–Zanskar shear zone map-view connection (e.g., Frank et al., 1995; Fuchs and Linner, 1995). Because the Zanskar STD window is warped but not overturned, it follows that the Phojal anticline is a local structure along the northern margin of the Kullu and Uttarkashi windows that does not extend to the Zanskar region.

The amount of displacement along the STD is difficult to determine because rocks above and below the fault share the same protoliths in this region. Also, there is no pronounced metamorphic offset across the fault: metamorphic isograds are subparallel to the STD (Fig. 5). Therefore, despite the significant evidence for shear deformation across the STD

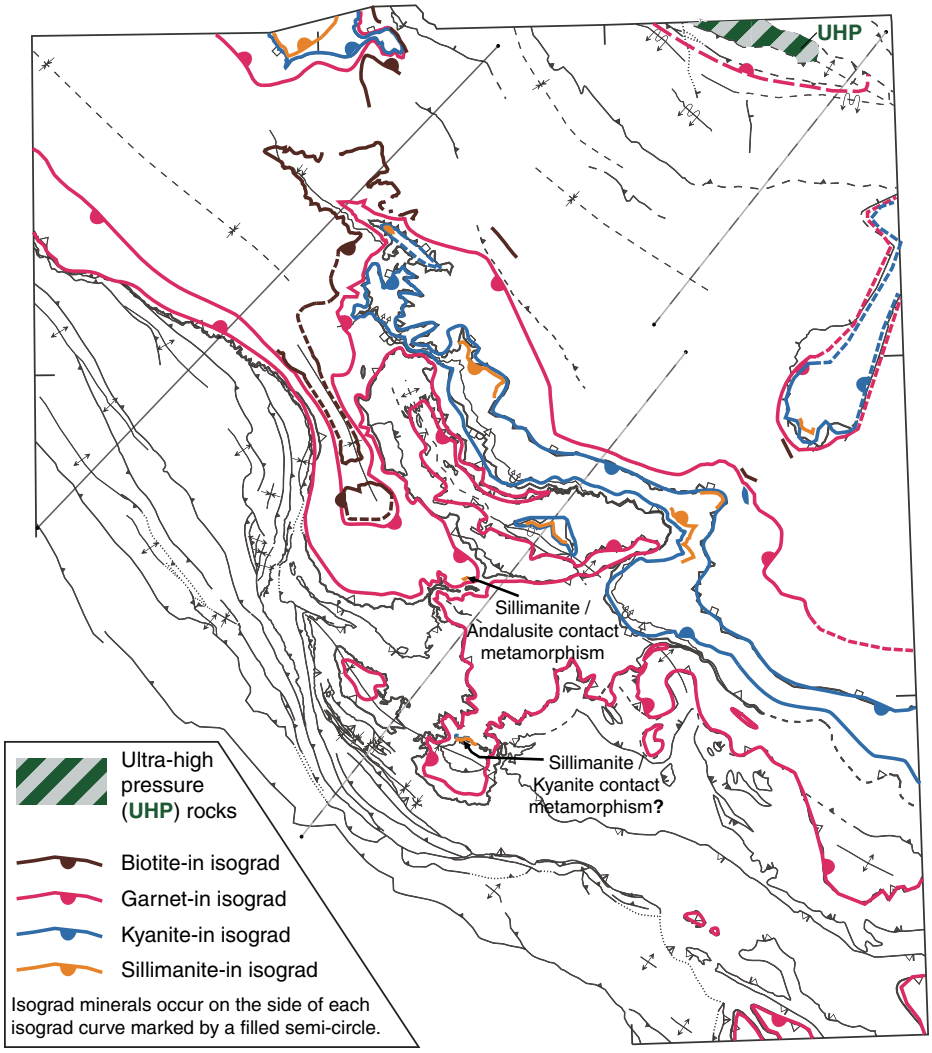

Figure 5. Metamorphic isograd map of the Himachal Himalaya, with (1) largely continuous garnet-in and kyanite-in isograds and (2) discontinuous biotite-in and sillimanite-in isograds (due to incomplete metamorphic mapping). Main references are Frank et al. (1973), Epard et al. (1995), and Vannay and Grasemann (1998); see Appendix 1 for additional references.

zone, local lithologic and petrologic information do not constrain the magnitude of fault offset. The fault may have initiated in the Eocene as a basal décollement of the Tethyan Himalayan fold-thrust belt (Wiesmayr and Grasemann, 2002). Early to Middle Miocene $^{40}Ar/^{39}Ar$ muscovite ages in the immediate STD hanging wall and footwall suggest that plastic deformation along the STD ceased in that period (Walker et al., 1999; Vannay et al., 2004; Thiede et al., 2005).

Most Tethyan Himalayan Sequence strata northeast of the right-way-up STD are involved in the dominantly top-to-the-southwest Tethyan Himalayan fold-thrust belt within the Spiti Synclinorium (Figs. 3 and 4B) (e.g., Frank et al., 1995; Fuchs and Linner, 1995; Vannay and Steck, 1995; Steck et al., 1998; Wiesmayr and Grasemann, 2002). Similar relationships also occur across the Chamba Synclinorium in the northwest of our map area (e.g., Frank et al., 1995; Fuchs and Linner, 1995). To the north, Tethyan Himalayan Sequence rocks and suture zone rocks are thrust northeastward over the Indus molasse along strands of the latest Oligocene–Miocene Great Counter thrust system (e.g., Schlup et al., 2003; de Sigoyer et al., 2004). The Great Counter thrust system may represent the northern extension of the STD (e.g., Yin et al., 1994, 1999).

STRUCTURAL GEOLOGY

Thrusting is the dominant expression of contractional deformation in the footwall of the MCT. Although many of these thrusts are well defined locally, the relationships among the structures and deformation in individual thrust systems have not been studied in detail. Further issues include: (1) MCT-STD geometric relationships, (2) internal deformation of units to address the assumption of constant bed thickness in line-length balancing, and (3) variable deformation style and strain as functions of both lithology and structural positions relative to nearby faults. To address these issues, we conducted detailed geologic mapping and outcrop-scale observations across the Himachal Himalaya. We summarize the main results of our structural observations in the following.

Mandi-Bilaspur Thrust System Hanging-Wall Structures

Bedding in the Deoban and Damtha Groups is deformed by brittle structures, including dominantly southwest-verging parallel folds and dominantly southwest-directed brittle faults (Figs. 6B, 6D [stereoplots L3, L4, L6, L7], 7A, and 7B). Fold amplitudes range from <1 m to ~100 m, with interlimb angles from 40° to 140°. Deoban rocks commonly contain as much as 3% carbonate veins generated from pressure solution during the development of axial cleavage, best displayed in the fold hinge zones. Carbonate rocks of the Deoban Group are deformed in a southwest-directed thrust duplex with the roof fault at the base of the Baragaon gneiss in the MCT shear zone (Fig. 7B). We also observed folded quartz veins in southwest-verging similar folds in Deoban carbonaceous phyllites, located within the 50-m-thick basal section of the Baragaon gneiss (Fig. 7C). The extensive thrusting and folding in the Narkanda and Uttarkashi half-windows suggest that the contractional deformation here is penetrative at the kilometer scale.

Tons Thrust System and Hanging-Wall Structures

The Tons thrust hanging wall displays large and distributed internal deformation. The bedding and phyllitic fabric in the Shimla Group in a zone of ~500 m above the Tons thrust is pervasively folded in the Narkanda and Uttarkashi half-windows (Figs. 6B and 6D; stereoplots L7, L8). They are typically expressed by the formation of southwest-verging tight folds with wavelengths ranging from a few millimeters to a few meters (Fig. 7D). The fold development is spatially associated with slatey cleavage (Fig. 7E). Horizontal shortening of the highly folded strata locally exceeds 70% (Fig. 7E). Above this zone, deformation intensity increases upward toward the MCT zone, with bedding planes progressively transposed by slaty cleavage first and then schitosity near the MCT. Rocks at the highest structural levels of the Tons hanging wall exhibit greenschist facies metamorphism, expressed by the presence of pelitic phyllite, graphitic phyllite, and chlorite-pyrite schists. Tight to isoclinal southwest-verging folds, slaty cleavage, and phyllitic fabric with northeast-trending stretching lineations occur and are increasingly dominant upsection (Fig. 6B and 6D).

Berinag Thrust and Hanging-Wall Structures

Similar to the Bilaspur and Tons thrust hanging walls, internal deformation of the Berinag thrust sheet is penetrative. The Berinag thrust is expressed by a southwest-directed brittle structure in the southwestern Kullu window and Uttarkashi half-window to a top-to-the-southwest shear zone in the northeastern portions of the windows (Fig. 6; stereoplots L1, L2, L3, L6). Hanging-wall quartzites of the Berinag Group are partially recrystallized at the southwestern limits of the exposed thrust sheet, where preserved sedimentary structures include cross-bedding (Fig. 7F). Here the Berinag thrust hanging wall shows large-magnitude internal shortening, with tight and/or isoclinal meter-scale folds of quartzite cross-bedding indicating ~64% horizontal shortening (Fig. 7G). The bulk of the Berinag thrust sheet within the Kullu window is schistose with north-northeast–trending stretching lineations defined by white mica (Fig. 6). Folds of schistosity are dominantly southwest verging and tight to isoclinal in cross-section view. At the eastern end of the Kullu window an ~30-m-thick band of Berinag quartzite occurs between concordant contacts with Wangtu orthogneiss below and Greater Himalayan Crystalline complex paragneiss above. The quartzite here is completely recrystallized, with grain sizes as large as 5 mm; all three units display moderately northeast-plunging stretching lineations and top-to-the-southwest mylonitic fabric. Therefore deformation intensity within the Berinag thrust sheet increases to the northeast.

Munsiari Thrust and Hanging-Wall Structures

Penetrative deformation occurs throughout the Munsiari thrust hanging wall, with the exception of late crosscutting undeformed granites (Figs. 6B–6D; stereoplots L2, L5). The Munsiari thrust juxtaposes orthogneiss atop Berinag Group quartzites along a 1–2-km-thick top-to-the-south to top-to-the-south-southwest ductile shear zone containing S-C mylonitic fabrics. South-southwest–directed brittle structures overprint the ductile structures. These structures include Riedel shears, cataclasite, slickenfibers, and (in the Uttarkashi half-window) a >50-m-thick schuppen zone comprising 2–15-m-thick horses of quartzite, granitic schist, and granitic gneiss. Gneissic fabric across the Munsiari Group is characterized by a dominantly north-northeast–trending stretching lineation (Figs. 6B–6D). Gneissic foliation in the Jeori gneiss unit exposed in the Sutlej River Valley (~15 km northeast of Rampur) is penetratively deformed by kink folds with centimeter- to meter-scale wavelengths and ~90° interlimb angles (Fig. 7H). Along a 10 km stretch of the Sutlej River in the eastern Kullu window (centered on the town of Wangtu), unfoliated pegmatitic granites crosscut the foliation of the Wangtu granitic gneiss (Fig. 7I). The Late Miocene ages of these granites provide a lower limit for the development of the gneissic fabric (see following Geochronology discussion). These granites are the only unit within the Munsiari thrust hanging wall, and indeed within the Lesser Himalayan Sequence, for which we did not observe outcrop-scale deformation.

MCT and Hanging-Wall Structures

We divide the MCT into northern and southern portions based on Greater Himalayan Crystalline complex and Tethyan Himalayan Sequence hanging-wall lithologies, respectively. This division is structurally defined by the overturned South Tibet detachment, which is folded with the southwest-verging Phojal anticline. In this interpretation, the southern MCT hanging wall is continuous with the STD hanging wall. Therefore determining the deformation style and strain of the southern MCT hanging wall, the northern MCT hanging wall, and the STD hanging wall provides key tests of the interpretation. We review our main structural observations from each area in the following.

Southern MCT and Hanging-Wall Structures

Observations of deformation in the MCT hanging wall south of the Kullu window are limited because (1) most preserved rocks are near the base of the thrust sheet, with structurally high rocks largely eroded away, and (2) despite this knowledge, the undulatory folding of the thrust sheet limits our ability to tightly constrain structural elevation above the MCT base across much of the thrust sheet. This portion of the MCT is defined by a 1–2 km top-to-the-southwest shear zone featuring S-C fabrics with northeast-trending stretching lineations defined by biotite and feldspar, normal drag shear bands, ultramylonites, σ-type porphyroclasts of feldspar, brittle-ductile synthetic and antithetic microfaulting of feldspar, and tight to isoclinal folds [Figs. 6A, 6B, 6D (stereoplots TG1, T5, T6, T7, T8), 8A, and 8B]. The base of the shear zone is largely coincident with the garnet isograd within an inverted metamorphic field gradient (Fig. 5). Where the MCT juxtaposes Haimanta rocks directly above Outer Lesser Himalaya rocks (at Narkanda and along the Shimla klippe), mylonitic garnet schist of the MCT zone concordantly overlies pelitic phyllite, chlorite-pyrite schists, and graphitic phyllite, and graphitic schist. Here shear bands and isoclinal folds persist across ~400 m structurally below

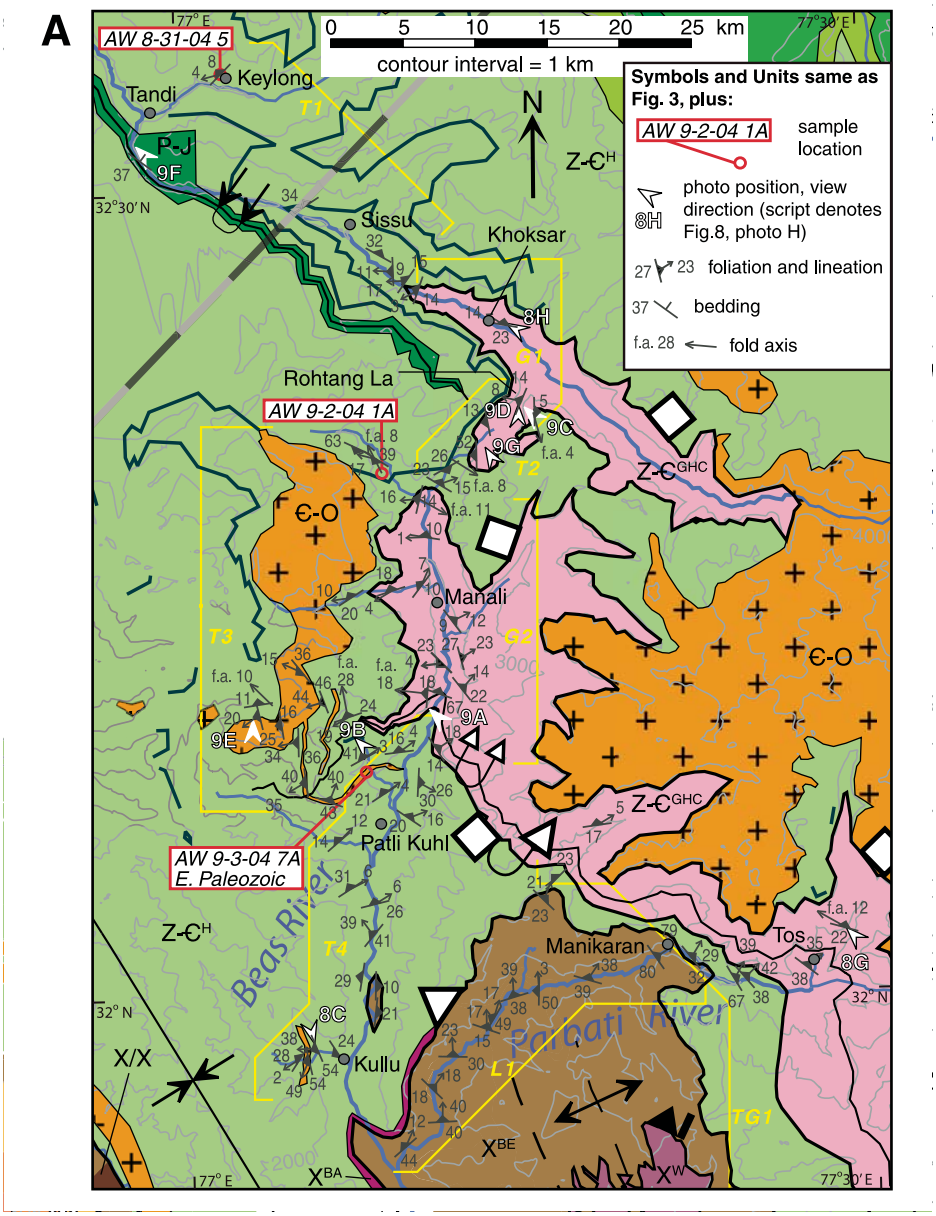

Figure 6 (*continued on following pages*). (A) Geological map of the Upper Beas Valley region. (B) Geological map of the central Sutlej River region. Gray structural data are from this study; blue structural data are taken from the literature and were used for cross section construction. (C) Geological map of the northeastern Sutlej River region. Topographic contours in A, B, and C are from the Shuttle Radar Topography Mission; in some areas these data are distorted (e.g., at 32°25′N, 76°50′E). (D) Equal area stereoplots for regions labeled in A, B, and C. The regions were selected on the basis of shared and/or similar structural setting and geographic proximity. The regions and stereoplots are labeled with letters and numbers in order to denote different regions (numbers) within different tectonic units (denoted by letters) (e.g., L1—Lesser Himalayan Sequence, area 1; G2—Greater Himalayan Crystalline complex, area 2; T4—Tethyan Himalayan Sequence, area 3). The abbreviations are the same as in the legend in Figure 3.

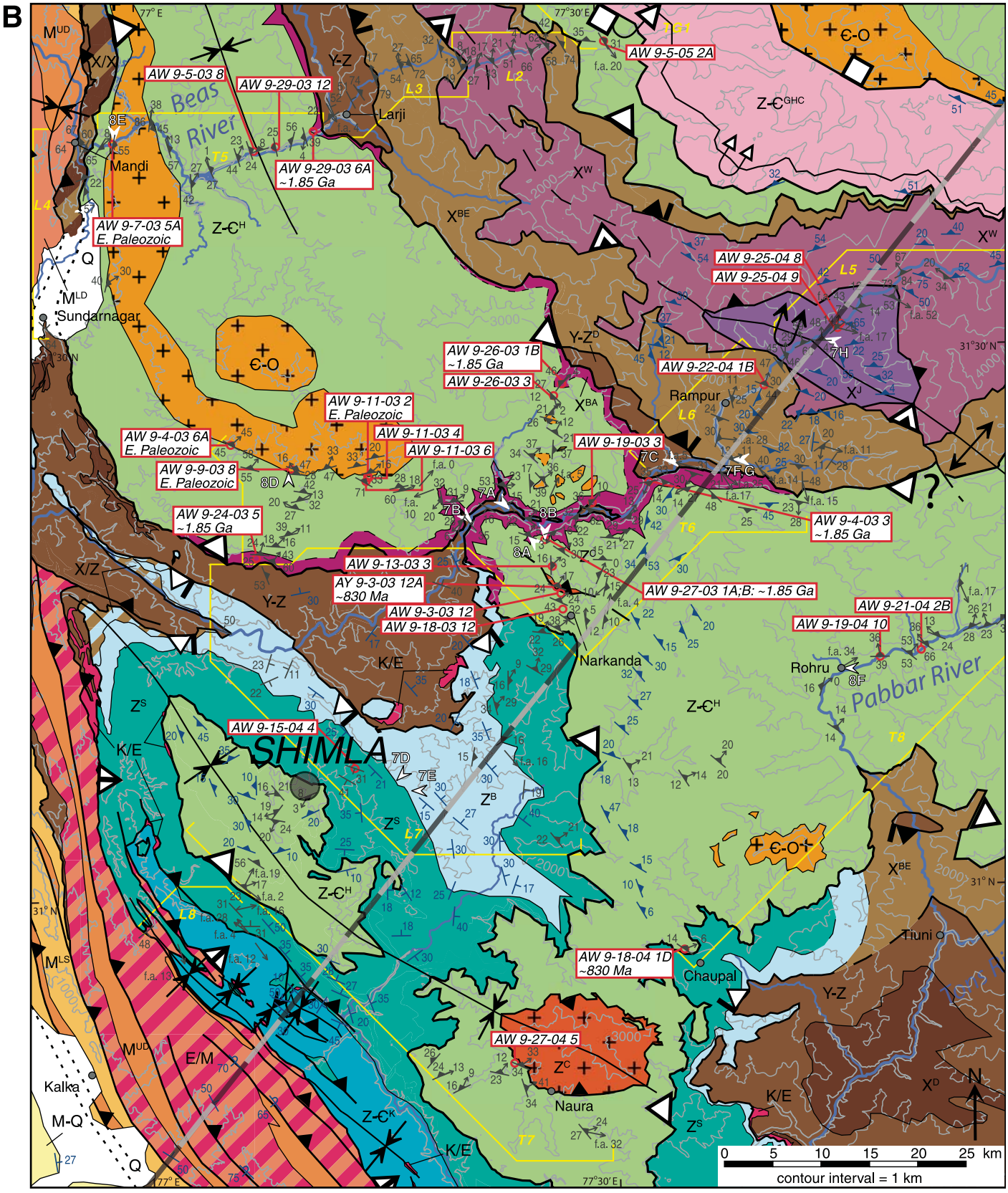

Figure 6 (*continued*).

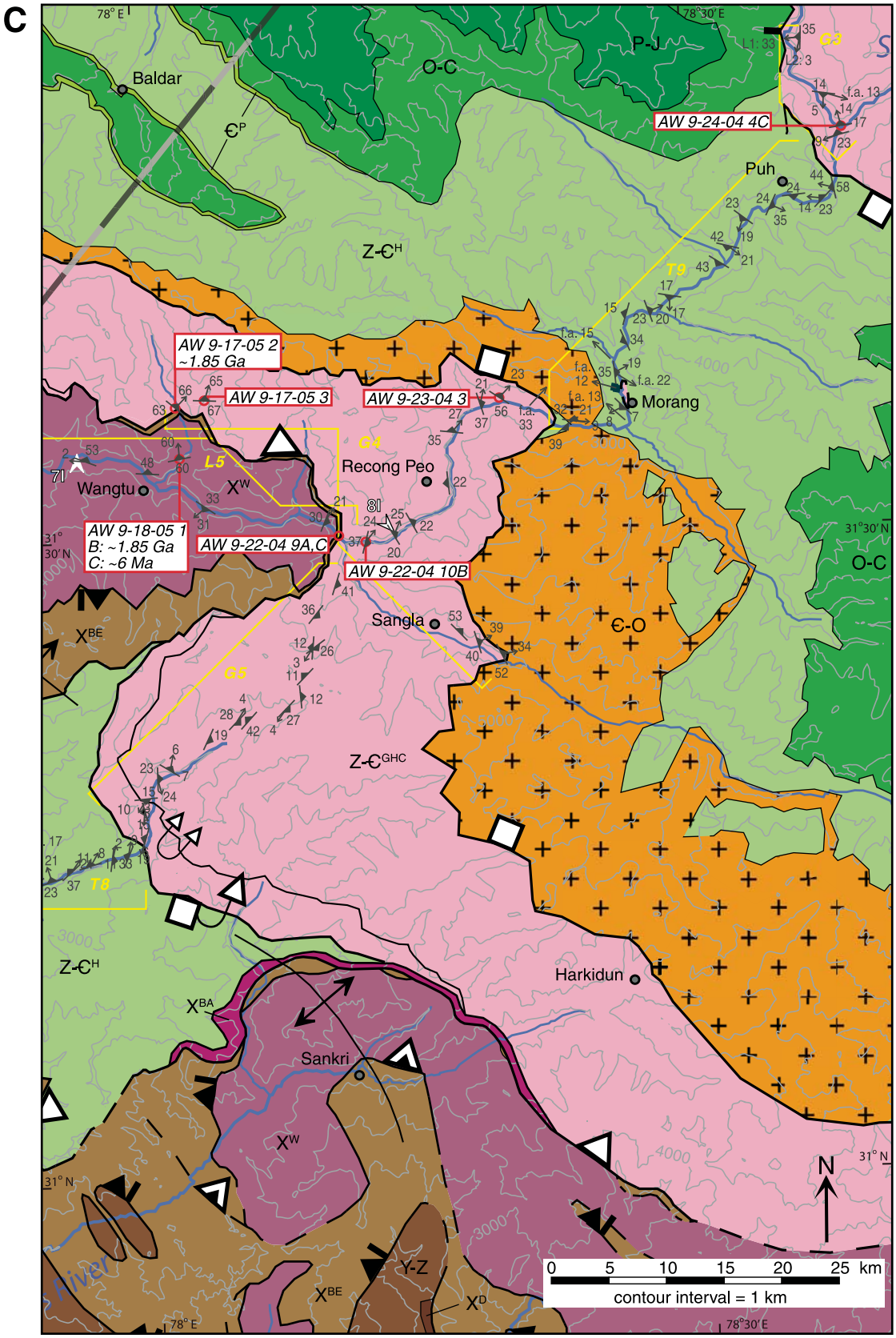

Figure 6 (*continued*).

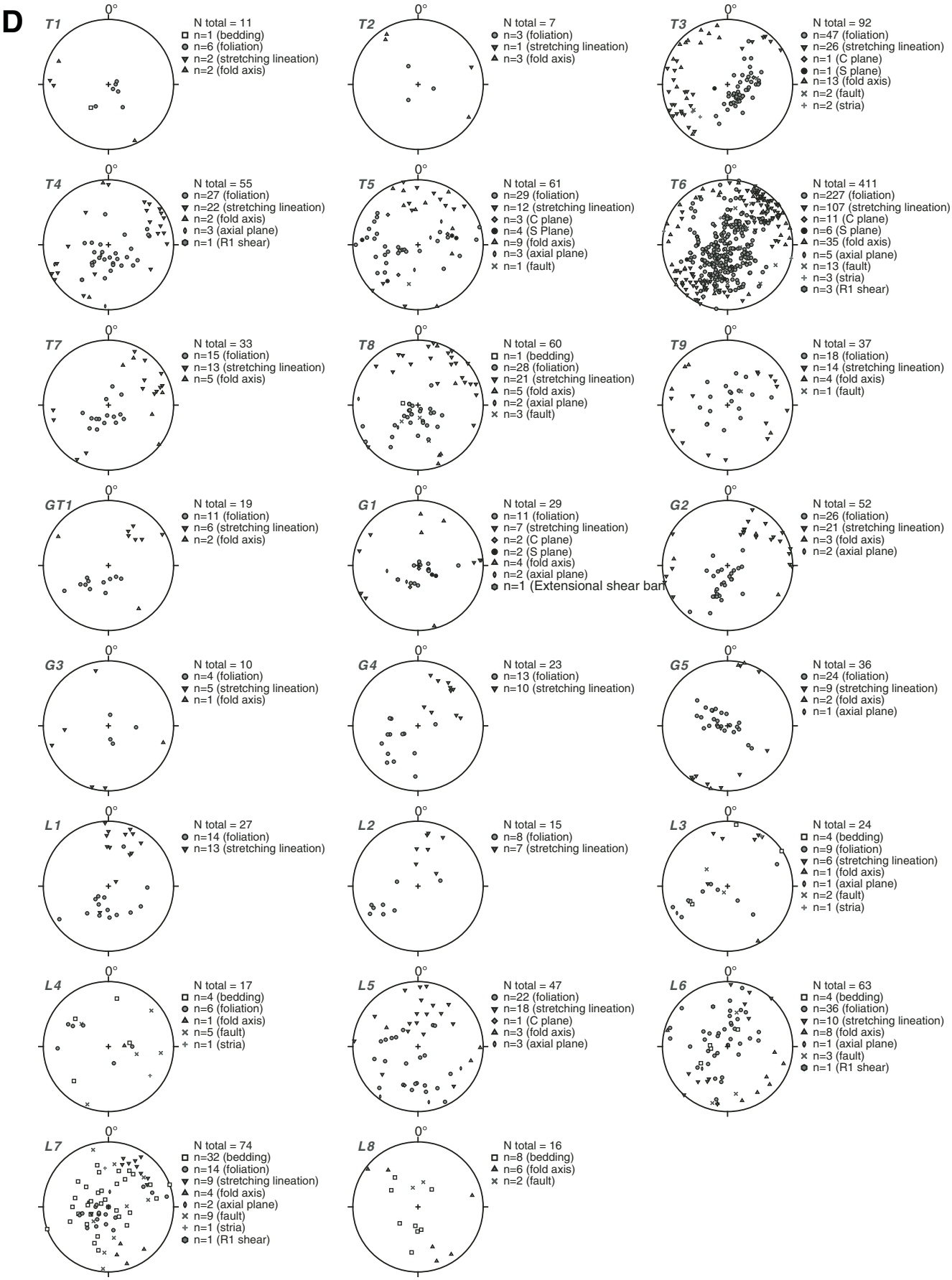

Figure 6 (*continued*).

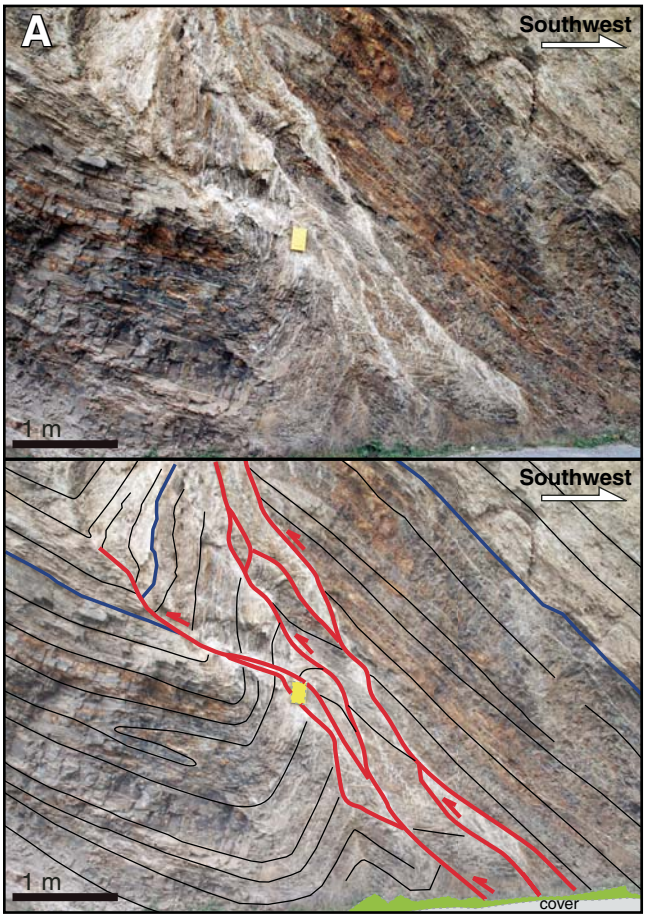

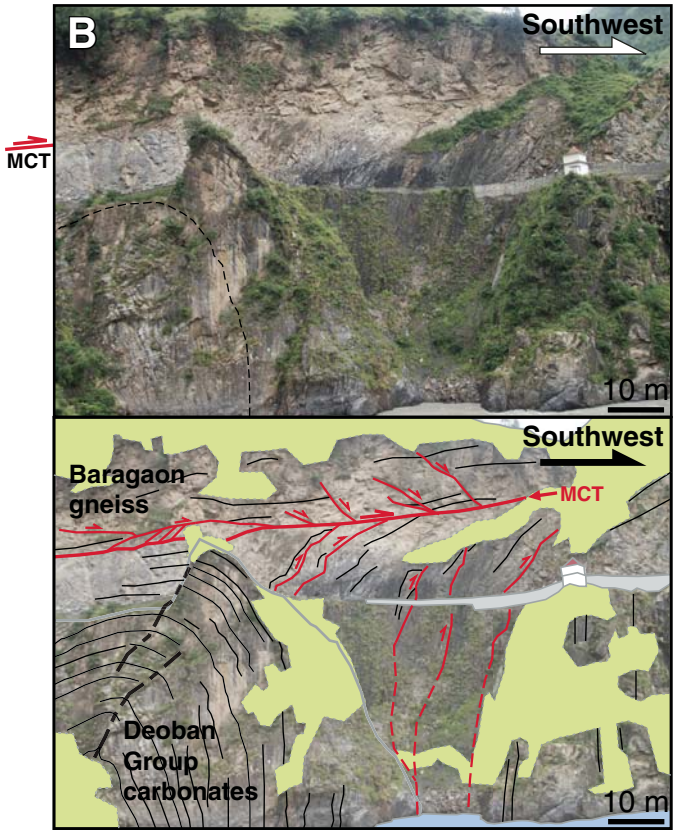

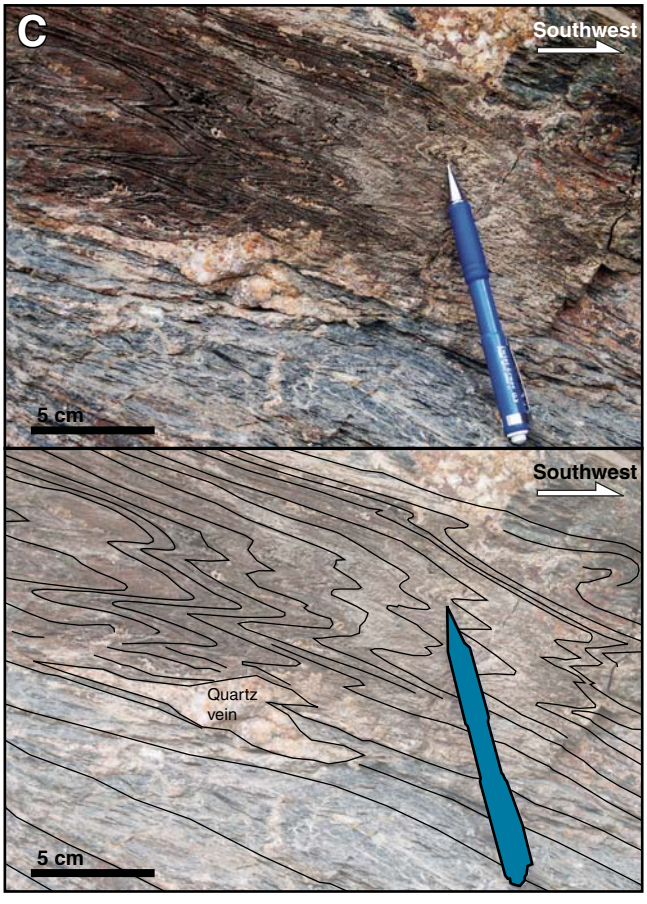

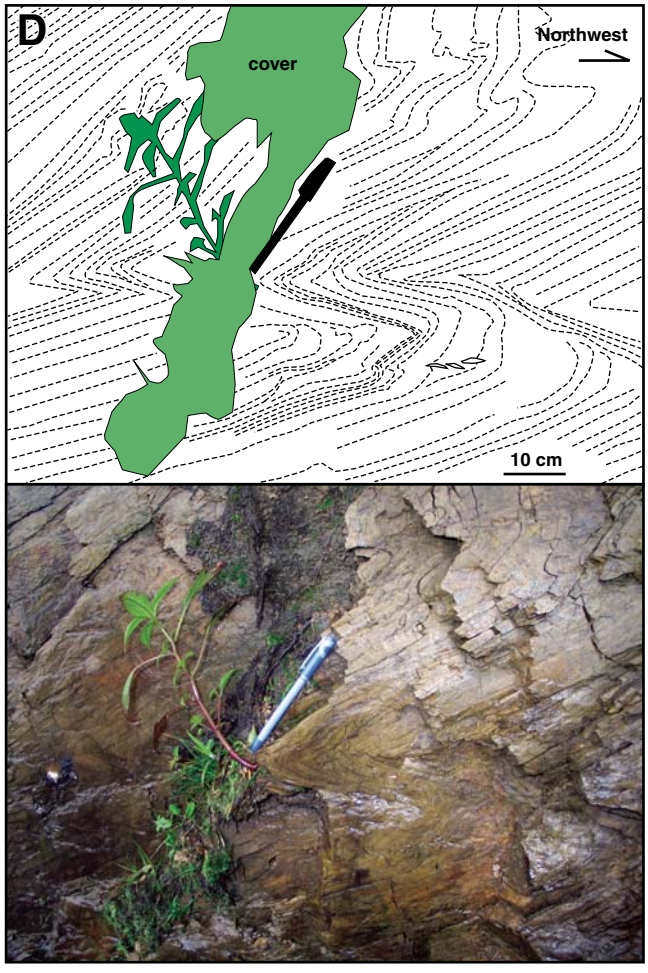

Figure 7 (*continued on following pages*). Field photographs of the Main Central thrust (MCT) footwall (locations marked in Figs. 6A, 6B, 6C). All photographs were taken in the Sutlej River Valley except for 6D, which was taken along the Shimla-Narkanda Road. (A) Thrust fault system within the Deoban Group with associated folds. (B) Folding and duplexing of Deoban carbonates beneath the MCT. Here the base of the MCT is a brittle fault, with fractures interpreted as Riedel shears. (C) Tight similar folds in Deoban carbonaceous schist within the MCT zone. (D) Tight folding of Shimla Group rocks. (E) Folding of Shimla Formation rocks with preserved S_0, shortening estimate. (F) Cross-bedding preserved in Berinag Group quartzites. (G) Tight to isoclinal folds in Berinag Group quartzites, same site as F. (H) Kink folds of Jeori paragneiss. (I) Wangtu gneiss foliation crosscut by undeformed granitic pegmatite.

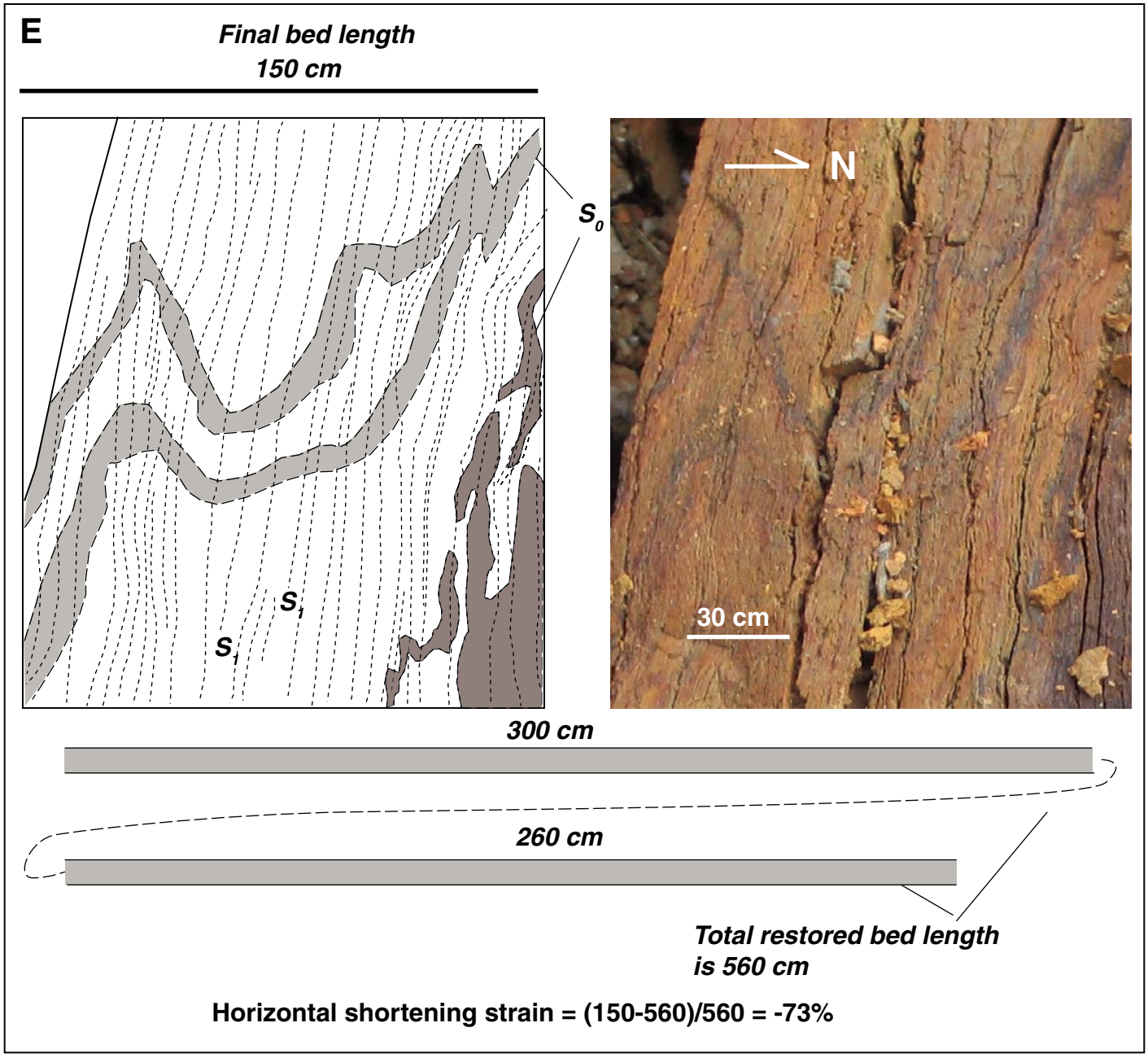

Figure 7 (*continued*).

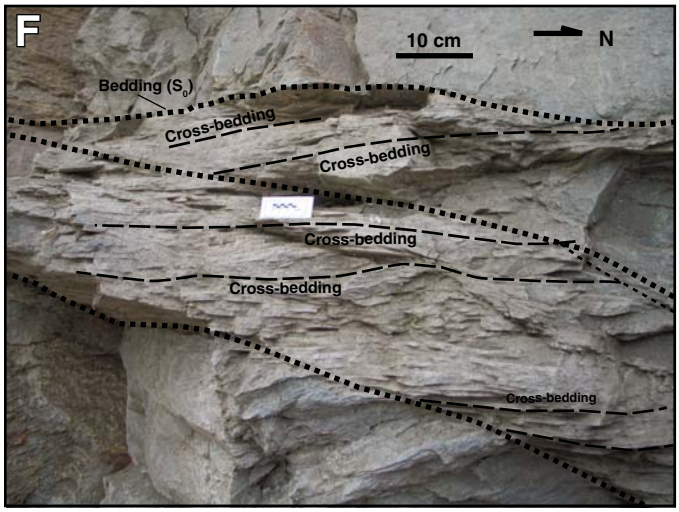

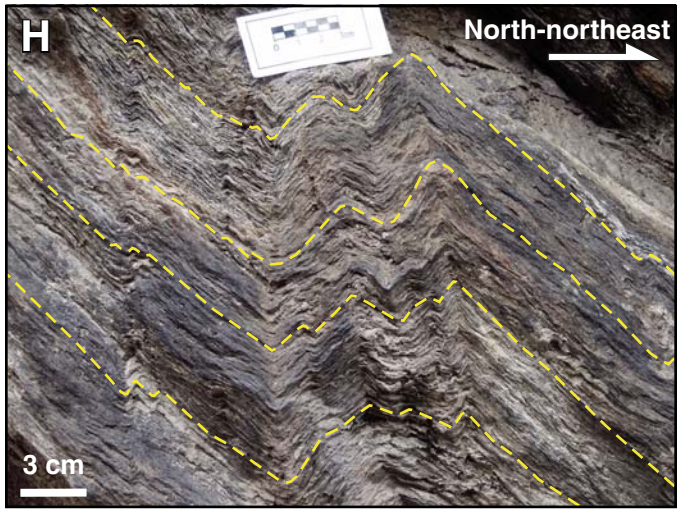

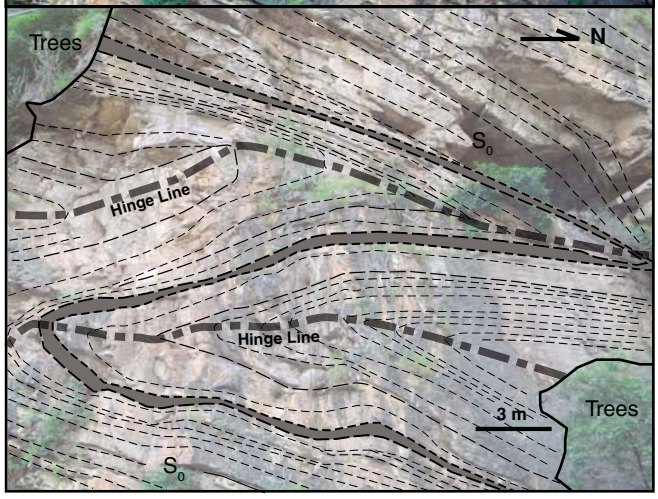

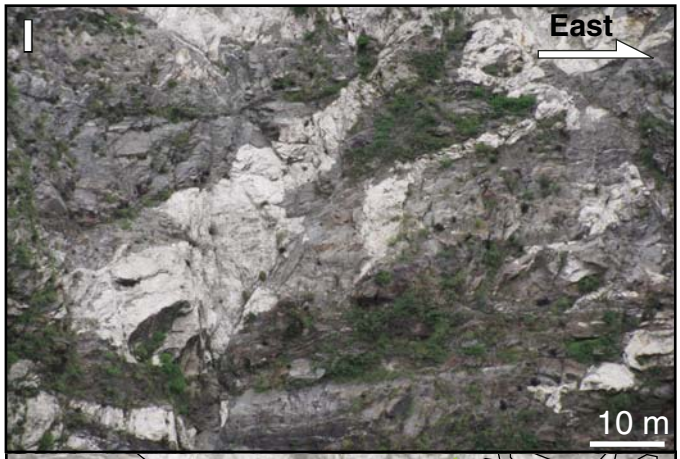

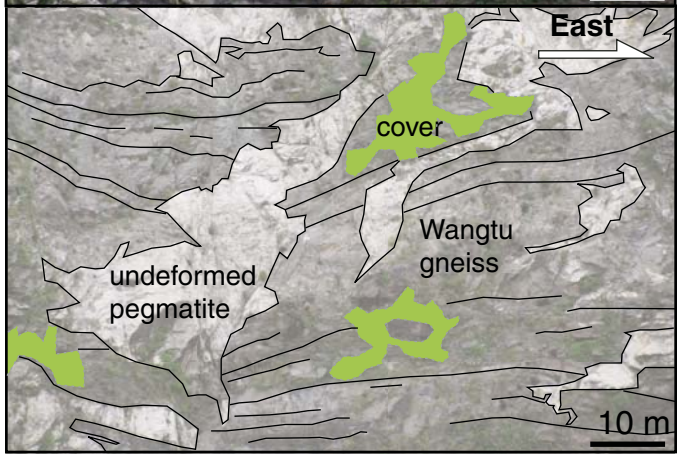

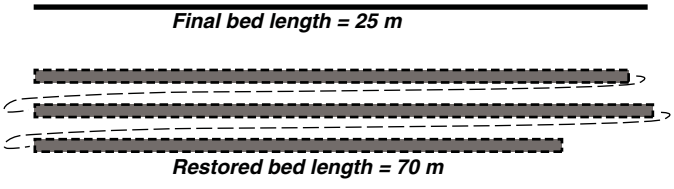

Horizontal shortening strain = (25-70)/70 = -64%

Figure 7 (*continued*).

the MCT zone. As previously noted, a brittle fault juxtaposes Baragaon gneiss over Deoban strata at the base of the MCT zone. The geometry of R1 shears and meter-scale duplexing along the brittle fault support a top-to-the-southwest sense of motion along this fault (Fig. 7B). The contact between the Baragaon gneiss and the overlying Haimanta Group is concordant and locally folded (Fig. 8B). In summary, the southern MCT is dominated by top-to-the-southwest ductile fabrics, with southwest-directed brittle deformation occurring along the MCT contact between the Baragaon gneiss and the Deoban Group.

The southern MCT hanging wall is dominated by ductile fabrics, with minor brittle deformation. The dominant structural fabrics are shallow to moderate foliations defined by micas and subparallel to locally preserved bedding, northeast-trending stretching lineations, crenulation cleavage, and largely southwest-verging tight to isoclinal folds of schistosity [Figs. 6 (stereoplots TG1, T5, T6, T7, T8) and 8C]. These fabrics are not entirely penetrative: they are ubiquitous in Haimanta metasedimentary rocks and Baragaon gneiss, but not throughout early Paleozoic granites. The early Paleozoic granite-Haimanta contacts are concordant, and the granite is foliated, lineated, and even locally mylonitized ~5–30 m from the contact (Fig. 8D). However the internal fabric of the granite ranges from weakly foliated to unfoliated (Fig. 8E). A top-to-the-southwest shear zone developed across an ~50-m-thick layer of ca. 830 Ma (see Geochronology discussion) mylonitic granitic gneiss exposed ~4 km north of Narkanda. We named this the Audi shear zone, based on a local village, and interpret it as continuous with shear fabrics developed at the base of ca. 830 Ma rocks near Naura (Figs. 3, 4, and 6B). For purposes of comparison with the northern MCT hanging wall and the STD hanging wall, the key observation is that the penetrative nature of deformation in the southern MCT hanging wall is not complete: early Paleozoic granites are largely undeformed. We also observed top-to-the-southwest, 0.2–1-m-thick, brittle fault zones (Fig. 8F). In Haimanta rocks, the faults are developed along graphite-rich layers and display a steel blue color. Limited exposure prevented us from tracing such faults farther than ~50 m.

The transect of the thrust sheet along the Beas River from Mandi to Larji presents the best opportunity to observe the structurally high portions of the southern MCT hanging wall, because the sheet is here folded in a single syncline and the preserved core of this syncline preserves rocks that are ~4.5 km above the MCT base (Figs. 3, 4, and 6B). The northeastern flank has ultramylonitized Baragaon granite at the MCT base. To the southwest, overlying rocks ~1.5 km thick, are garnet schists with

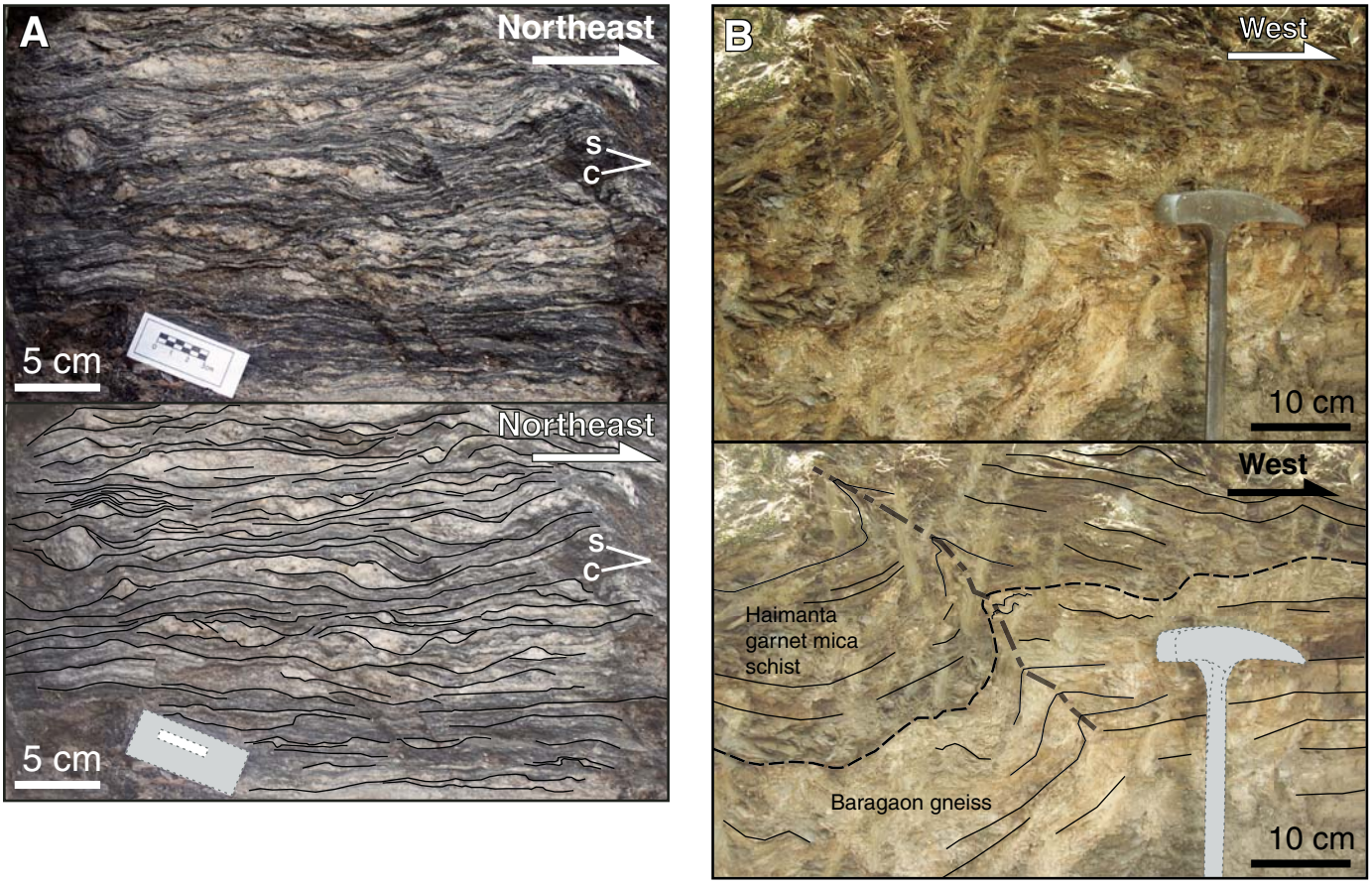

Figure 8 (*continued on following pages*). Field photographs of the Main Central thrust (MCT) zone and its hanging wall (locations marked in Figs. 6A–6C). (A) Baragaon gneiss, mylonitized in the MCT zone along the Sutlej River. (B) Folded concordant contact of Baragaon gneiss with Haimanta schist, Sutlej River Valley. (C) Isoclinal folds of Haimanta quartzite and phyllite; foliation is preferentially developed in the pelitic layers, Beas River Valley. (D) Mylonitization of the base of the Mandi granite, near Karsog. (E) Bulk of the Mandi granite is weakly deformed to undeformed; photo from near Mandi. (F) Brittle faulting and folding near Rohru. (G) Isoclinal folding of the Greater Himalayan Crystalline complex in Tos Valley. (H) Tight folds in the Greater Himalayan Crystalline complex, Chandra Valley. (I) Shear bands in the Greater Himalayan Crystalline complex, Sutlej Valley.

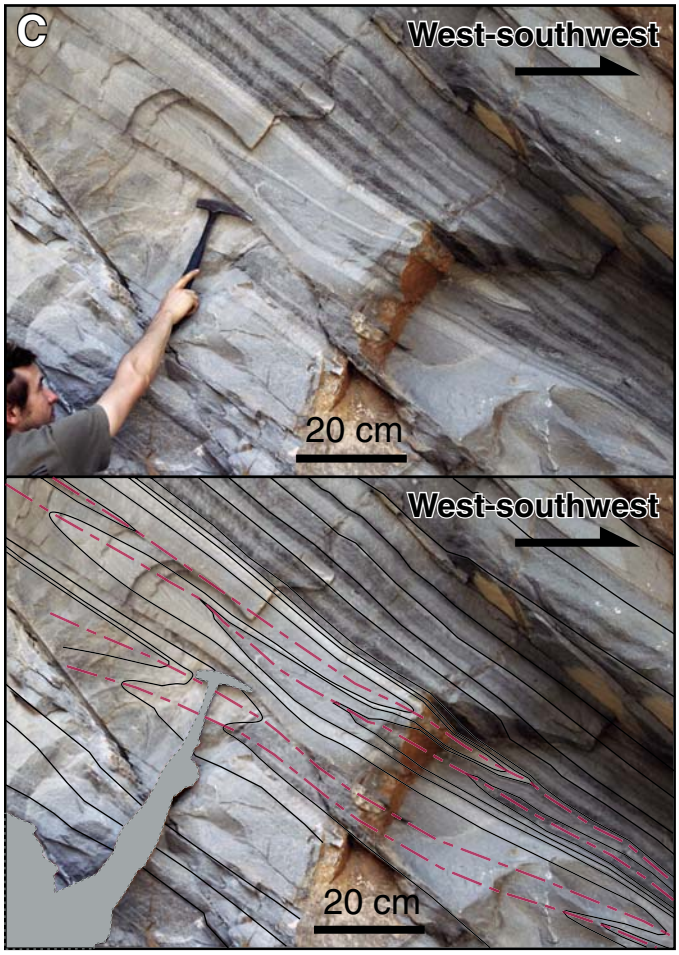

Figure 8 (*continued*).

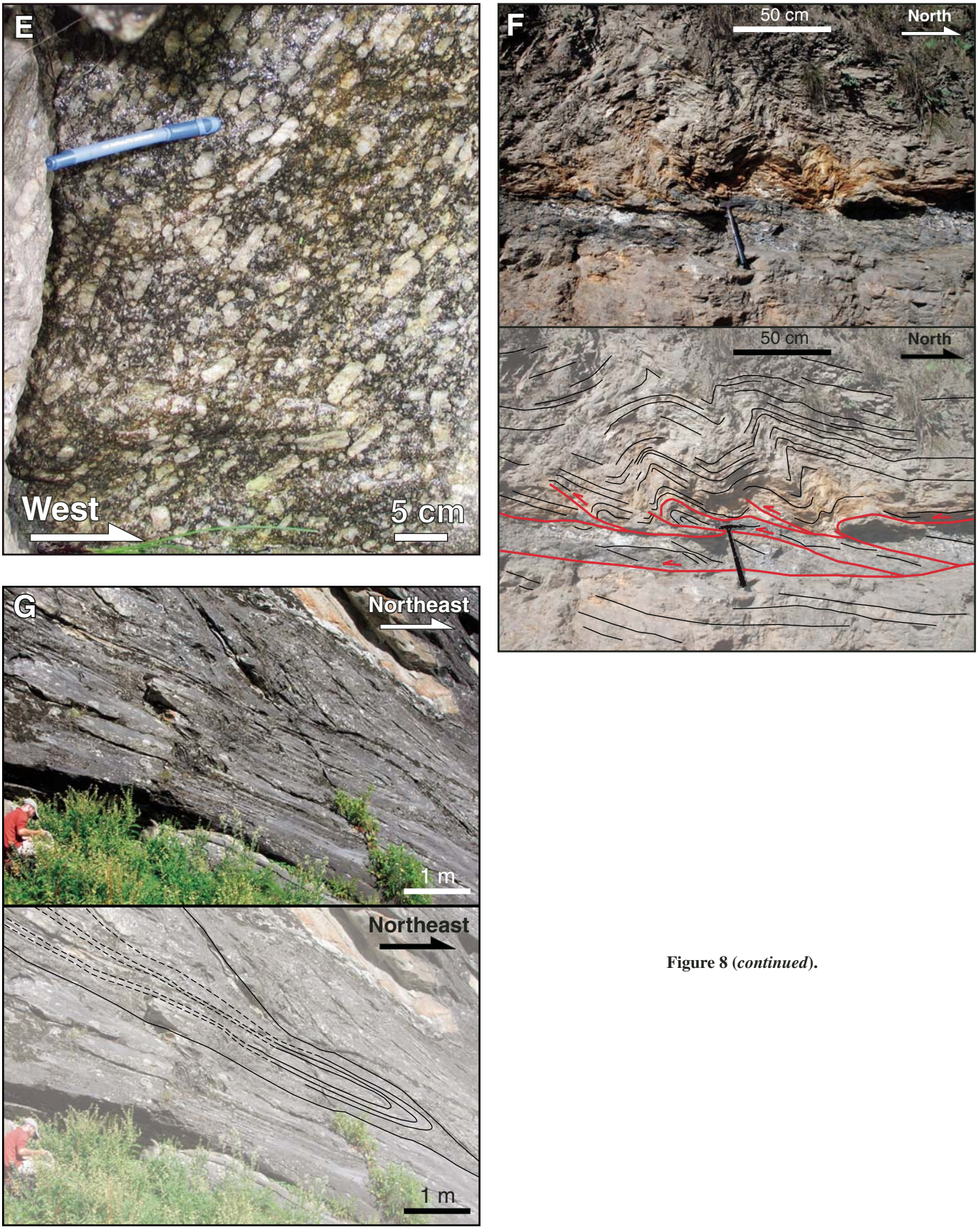

Figure 8 (*continued*).

top-to-the-southwest S-C fabrics, northeast-trending stretching lineations, tight to isoclinal southwest-verging folds, and 1%–5% quartz veins that are folded consistently with the schist. At higher structural levels, rocks show decreases in deformation intensity and metamorphic grade. The next ~1.5 km farther up structural section has <1% quartz veins, poorly developed stretching lineations, and tight folding, and the top of this portion marks the right-way-up garnet isograd. At the core of the syncline, folds are tight to open, stretching lineations are rare, and foliations defined by micas are parallel to original bedding. The southwestern flank of the syncline shows similar patterns and includes a large early Paleozoic granite body that is partially undeformed. The overall structural pattern of the southern Beas transect across the MCT hanging wall reveals a decrease in deformation intensity concomitant with a decrease in metamorphic grade from the bottom to the preserved top of the thrust sheet.

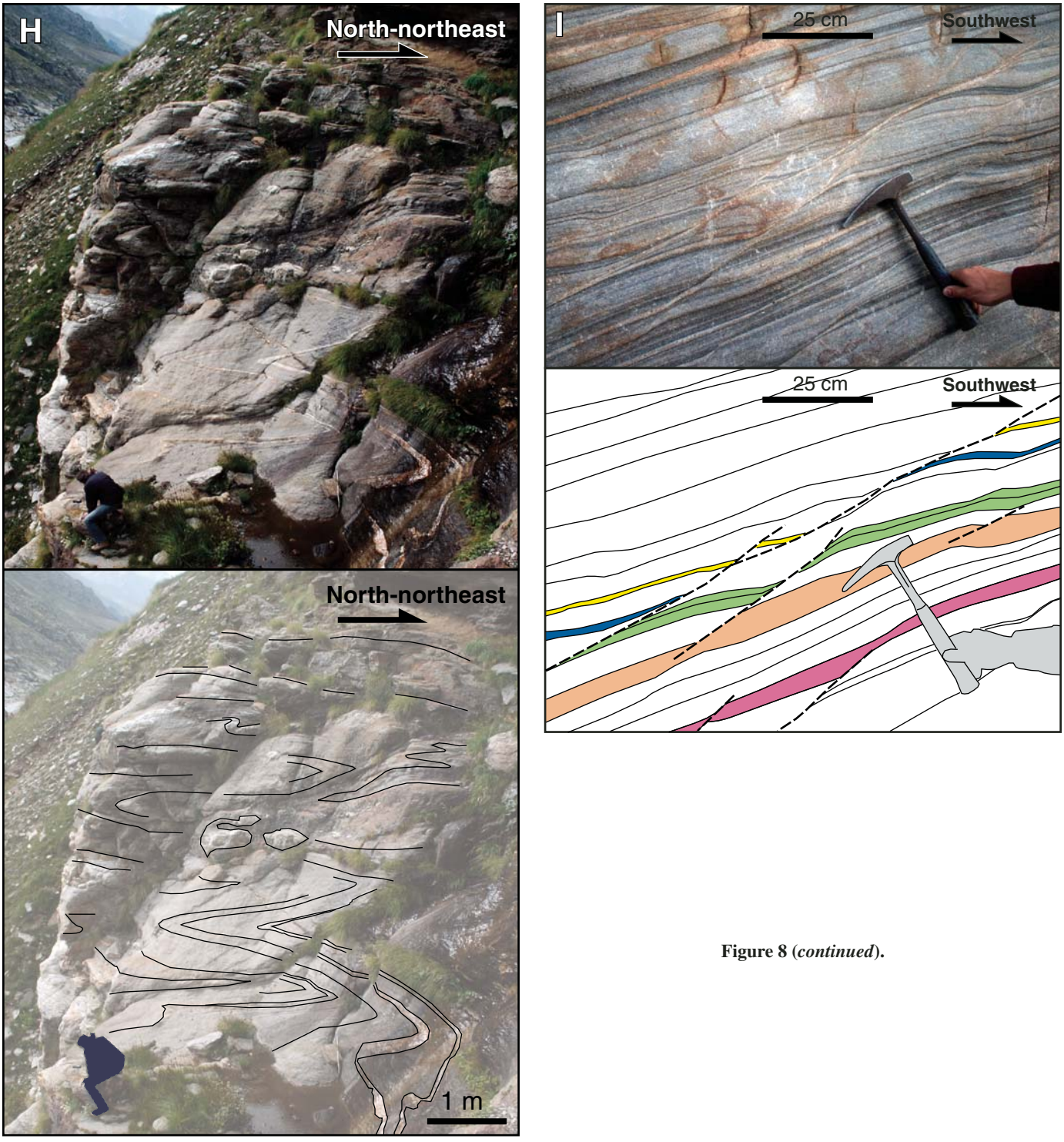

Figure 8 (*continued*).

Northern MCT and Hanging-Wall Structures

In contrast to the southern MCT hanging wall, the northern MCT hanging wall is penetratively deformed at all observed outcrops (Figs. 6A–6D; stereoplots G1, G2, TG1, G4, G5). The northern exposure of the MCT at the eastern end of the Kullu window is defined by an ~2-km-thick, east-northeast–dipping, top-to-the-southwest ductile shear zone with S-C fabric and normal drag shear bands. The lithologic contact of Greater Himalayan Crystalline complex and underlying Lesser Himalayan Sequence lithologies is concordant, and the shear zone extends ~0.5 km below the contact. The Greater Himalayan Crystalline complex here and across the entire Himachal Himalaya displays mica-defined foliation, northeast-trending stretching lineation, tight to isoclinal folds (which are largely southwest and west verging) of schistosity, S-C fabric, and normal drag shear bands ranging from centimeter to meter scale in length (Figs. 6 and 8G–8I). Folds in southern Greater Himalayan Crystalline complex sections along the Beas and Pabbar Rivers commonly mirror characteristics associated with the large-scale Phojal anticline: southwest vergence, ~20°–40° interlimb angles, folding of existing foliation, and development of a new moderately northeast-dipping axial planar cleavage overprinting shallow, dominantly northeast-dipping foliation.

STD and Hanging-Wall Structures

The STD occurs in two primary geometries across the Himachal Himalaya: subhorizontal to shallowly northeast-dipping right-way-up fault strands in the right-way-up limb of the Phojal anticline, and moderately northeast-dipping overturned fault strands in the overturned limb of the Phojal anticline (Figs. 3, 4, and 6). As described in our early work (Webb et al., 2007), the key evidence for the Phojal folding and concomitant overturning of the STD comprises (1) overturned top-to-the-northeast shear structures including extensional shear bands and σ-type porphyroclasts (Fig. 9A), (2) folded lithologies and contacts including the Haimanta schist–Greater Himalayan Crystalline complex gneiss contact and Haimanta marker lithologies of graphitic quartzite and garnet-hornblende calc-silicate schist (Figs. 9B, 9C), and (3) folding of metamorphic isograds, which could cross structures but appear to parallel the STD across the Himalaya (Fig. 5). By extrapolation discussed in our early work, we interpret that the Phojal anticline hinge plane and the overturned strand of the STD must both intersect the MCT across the eastern Kullu window, pass across the Pabbar River northwest of Rohru, and intersect the MCT again along the Uttarkashi half-window. The only readily accessible transect across such structures is along the Pabbar River (Figs. 6B–6D; stereoplots T8, G5). Our mapped position of the STD in this valley was determined on the basis of lithology, metamorphic grade, and folding consistent with the Phojal anticline and STD. We identified top-to-the-southwest shear structures, but not top-to-the-northeast shear structures, in the mapped position of the STD. However, exposure here is so spotty that such evidence of the 300–600-m-thick shear zone may well be covered. From south to north, rocks change from graphitic and garnet schist with garnet-hornblende calc-silicate schist marker layers to leucosome-bearing paragneiss, consistent with a Haimanta to Greater Himalayan Crystalline complex change. Along the mapped hinge zone of the Phojal anticline, west- and southwest-verging tight to isoclinal overturned folds with 10–50 m amplitudes are exposed on cliff sides; these folds may reflect the larger scale Phojal anticline.

The right-way-up STD shear zone across the region has both top-to-the-southwest and top-to-the-northeast shear structures [Figs. 6A–6D (stereoplots T1, T2, T3, T9) and 9D]. Above the shear zone, Haimanta metasedimentary rocks are foliated (foliation defined by micas and subparallel to commonly preserved bedding), commonly lineated, and foliation is folded within southwest- and northeast-verging tight to isoclinal outcrop-scale folds (Figs. 6A–6D; stereoplots T1, T2, T3, T9). Early Paleozoic granites are strongly deformed within the STD shear zone, but above it these are weakly deformed and undeformed where observed (~15 km southwest of Manali, ~5 km southwest of Morang along the Sutlej River, and ~7 km east of Sangla). Apophyses extend from these granites, crosscut foliation, and are locally warped (Fig. 9E). These relationships demonstrate that some foliation developed in the Haimanta above the STD prior to early Paleozoic granitic crystallization, but at least some internal deformation of these rocks outlasted this intrusion. The largest fold in the STD hanging wall is the Tandi syncline, a northeast-verging overturned syncline with an ~2 km amplitude defined by the contact of the Haimanta Group and the Tandi Group and by sedimentary layering, which is particularly well preserved within the Tandi Group (Figs. 9F, 9G). This may represent a large drag fold consistent with top-to-the-northeast deformation in the STD thrust sheet. The section of the STD hanging wall exposed along the upper Sutlej contains folds from outcrop scale (generally isoclinal to tight) to ~100 m amplitude scale (generally tight to open); the entire region from near Morang to the Spiti-Sutlej confluence forms a broad synclinorium (Figs. 3, 4A, and 6C). At the north end of this synclinorium (near Puh), a southwest-dipping sequence has pelitic schist overlying fine-grained psammitic paragneiss, which overlies kyanite- and sillimanite-bearing migmatitic paragneiss of the Leo Pargil dome. The paragneiss may represent the Greater Himalayan Crystalline complex, but the southern transition to lower grade Haimanta metasedimentary rocks is uncertain. Our reconnaissance observations reveal C′ cleavage indicating a top-to-the-southwest sense of shear within the fine-grained paragneiss; we speculate that this zone may contain the STD.

In summary, the overall deformation pattern within the STD hanging wall matches that of the southern MCT hanging wall: above the respective shear zones, deformation intensity decreases with increasing structural levels, and early Paleozoic granites are partially undeformed.

GEOCHEMISTRY

Major and trace element geochemistry data were obtained for felsic plutonic rocks of different crystallization ages in order to characterize their sources, evolution, and tectonic settings. Five samples of the ca. 1.85 Ga Baragaon granitic gneiss (AW 9–4-03 3, AW 9–24–03 5, AW 9–26–03 1B, AW 9–27–03 1B, AW 9–29–03 6A), one sample of ca. 830 Ma granitic gneiss (AY 9–3-03 12A), and two samples from early Paleozoic granite (AW 9–4-03 6A, AW 9–7-03 5A) were analyzed at Actlabs using X-ray fluorescence and inductively coupled plasma– mass spectrometry (ICP-MS) (Figs. 6B and 10; Supplemental File 3[3]; for age constraints, see Geochronology discussion). The analyzed samples are (1) granite (excepting sample AW 9–26–03 1B, a granodiorite) (Supplemental File 3A [see footnote 3]) and (2) calc-alkaline (excepting sample AW 9–29–03 6A, which

[3]Supplemental File 3. PDF file of geochemistry of granitoid samples. (A) QAP (quartz–alkali feldspar–plagioclase feldspar) diagram for granitoid samples generated using whole-rock major element data. CIPW norms were calculated for each sample and projected on the diagram. All samples plot within (or on the edge of) the granite field, with the exception of one Baragaon sample that plots within the granodiorite field. (B) AFM diagram for granitic samples; A = K_2O + Na_2O; F = Fe_2O_3 + FeO; M = MgO. Curve for calc-alkaline and thoeliitic division is from Kuno (1968). (C) Geochemical discrimination diagrams for granites after Pearce et al. (1984). VAG—volcanic arc granite; syn-COLG—syncollisional granite; ORG—ocean ridge granite; WPG—within-plate granite. (D) Table of geochemical data for granitoid samples. If you are viewing the PDF of this paper or reading it offline, please visit http://dx.doi.org/10.1130/GES00627.S4 or the full-text article on www.gsapubs.org to view Supplemental File 3.

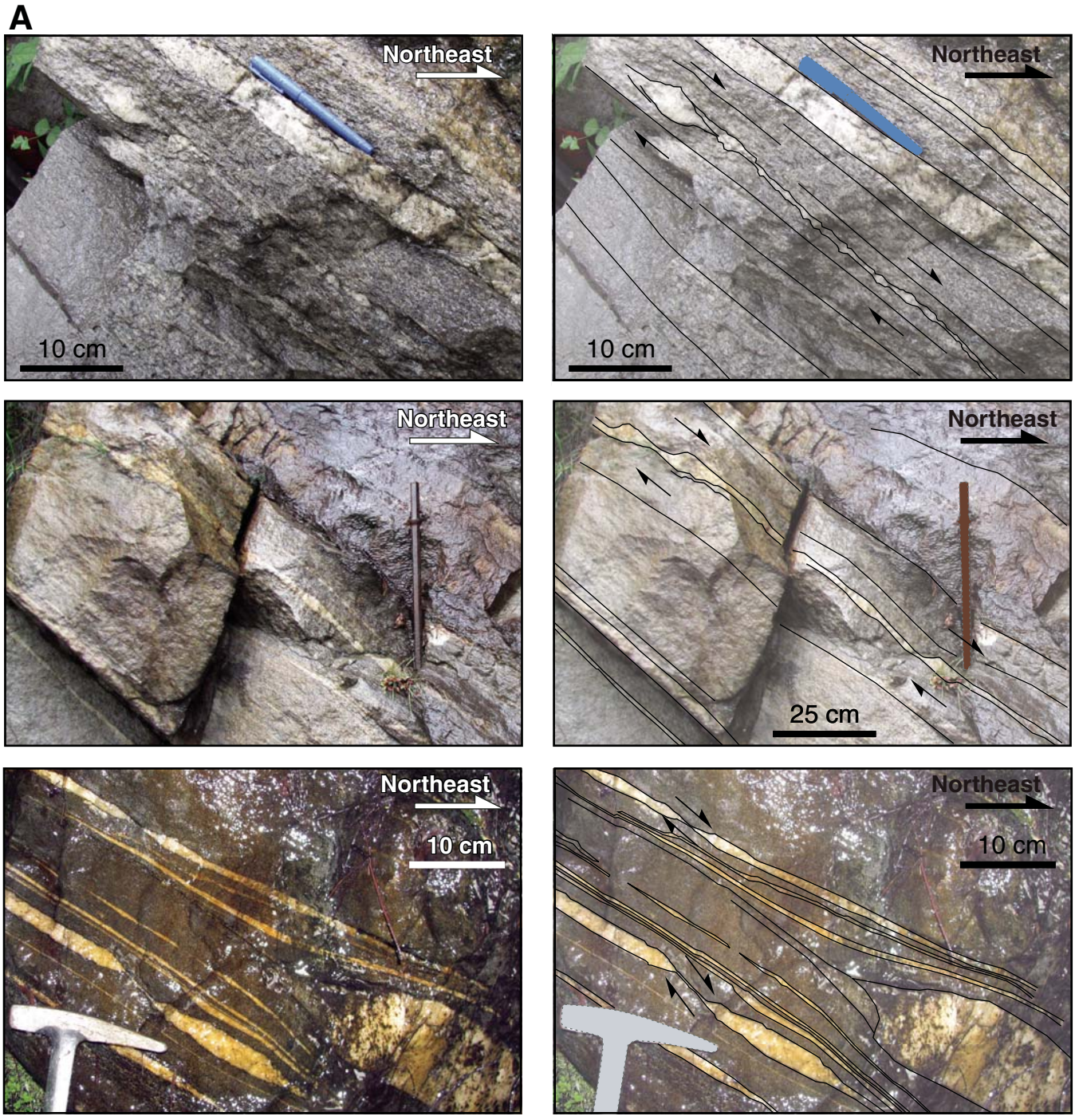

Figure 9 (*continued on following pages*). Field photographs of the South Tibet detachment (STD) zone and its right-way-up hanging wall (locations are marked in Figs. 6A–6C). (A) Top-to-the-northeast shear fabrics observed in the overturned STD zone, Beas River Valley. (B) Graphitic quartzite south of the STD, Beas River Valley. (C) Rohtang STD section, with orange-black weathering graphitic quartzite layer cropping out near the ridge crest. THS—Tethyan Himalayan Sequence; GHC—Greater Himalayan Crystalline complex. (D) Rohtang STD top-to-the-east-northeast shear indicators including C′ shears and σ-type porphyroclasts. (E) Top of the Hannuman Tibba granite, intruding across foliation in overlying Haimanta metasedimentary rocks, western Beas River Valley. Some shearing appears to post-date cross-cutting relationship, as the cross-cutting dikes are locally folded. (F) Tandi Syncline as viewed from the Chandra Valley. Asymmetric parasitic structures help define the axis of the syncline. (G) Tandi Syncline as viewed from the upper Beas River Valley.

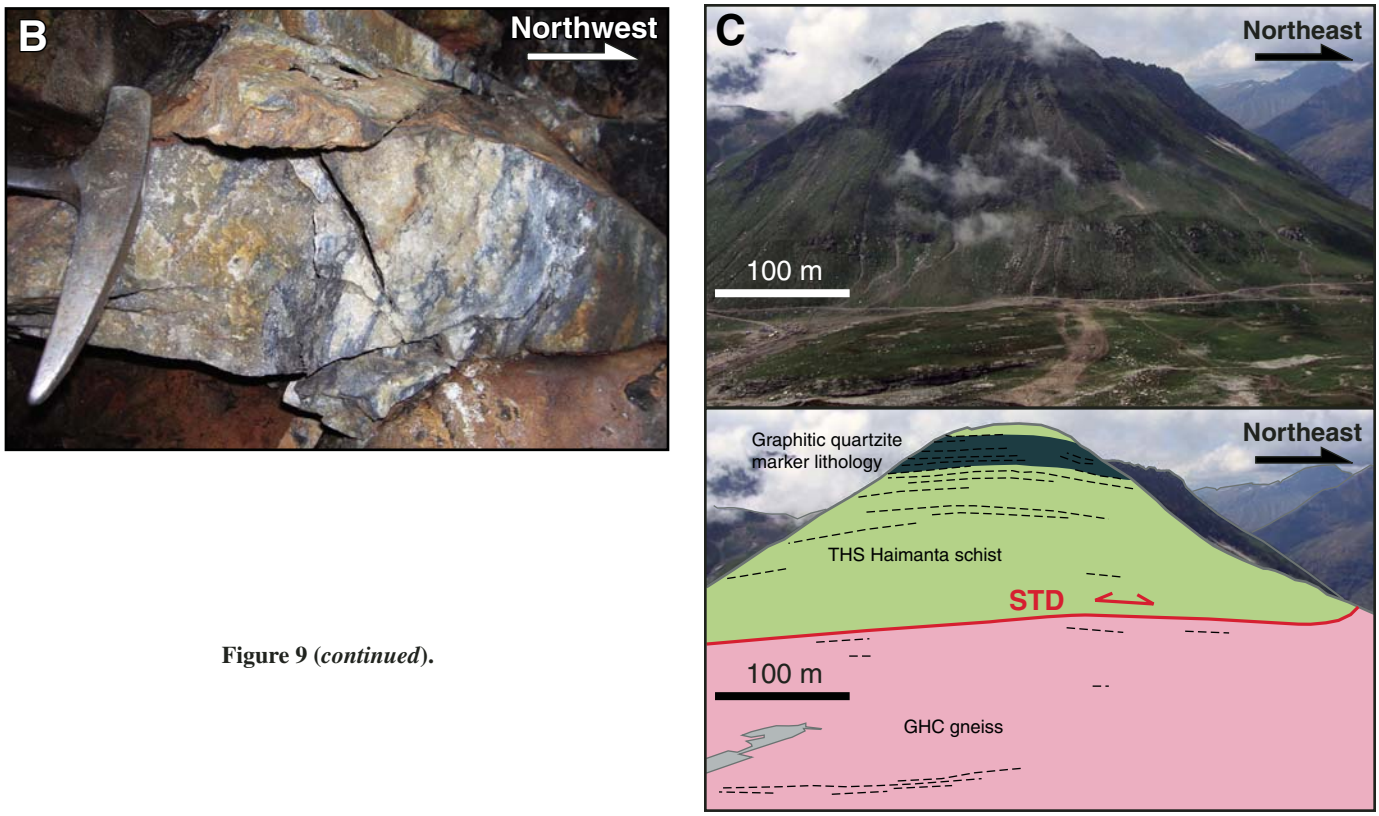

Figure 9 (*continued*).

is tholeiitic) (Supplemental File 3B [see footnote 3]). Percent SiO_2 ranges from 65.3 to 73.1 and molar $Al_2O_3/(Na_2O + CaO + K_2O)$ values between 1.38 and 2.04 show that the rocks are highly peraluminous (Supplemental File 3D [see footnote 3]). Chondrite-normalized rare earth element (REE) data show relative enrichment in light REEs (La_N/Yb_N 7.47–31.29). The observed strong enrichment in lighter trace elements and REEs is indicative of a dominant continental crust source (Fig. 10). The samples are characterized by negative Eu anomalies (Eu_N/Eu^*_N 0.15–0.55) and negative Ta, Nb, P, and Ti anomalies. The negative Eu anomalies show the involvement of plagioclase in fractional melting. Negative Ta, Nb, P, and Ti anomalies suggest an arc setting for the original melts that gave rise to these rocks and/or the remelted continental crust component of these rocks. Elemental data plotted on granite discrimination diagrams (after Pearce et al., 1984) overlap the boundary between the syncollisional and within-plate granite fields and plot near the volcanic arc field (Supplemental File 3C [see footnote 3]). The two early Paleozoic samples plot exclusively within the syncollisional field, but data from similar granites across the northwest India Himalaya (15 samples from Miller et al., 2001) show more variation, overlapping the boundary between the syncollisional and within-plate granite fields, near the volcanic arc field. In summary, the results demonstrate that granitic rocks of distinct ages (i.e., ca. 1.85 Ga, ca. 830 Ma, and early Paleozoic) are all dominantly sourced from remelted continental crust and may reflect an arc setting here during or prior to granitic magma generation.

THERMOBAROMETRY

The presence of pelitic bulk compositions allowed us to acquire pressure and temperature estimates of metamorphic conditions in the basal section of the Tethyan Himalayan Sequence Haimanta Group in the southern MCT hanging wall, i.e., southwest of the overturned STD (Table 3; Supplemental File 4[4]). This work is required for comparison of this section with the Greater Himalayan Crystalline complex and with the Tethyan Himalayan Sequence section above the STD; thermobarometric studies of both have been done (Epard et al., 1995; Vannay and Grasemann, 1998; Vannay et al., 1999; Jain et al., 1999; Walker et al., 1999; Chambers et al., 2009). We analyzed six garnet-bearing mica schists using the University of California, Los Angeles (UCLA) JEOL 8200 electron microprobe. Mineral compositions were measured for thermobarometric calculations and X-ray composition maps of garnet crystals were obtained to assess zoning patterns. For individual mineral analyses we used a 4 µm spot size (<1 µm spot size for garnet), a 15 kV accelerating voltage, and a current of 15 nA; for X-ray maps we used a current of 100 nA with 1–5 µm pixels and a dwell time of 30–50 ms per pixel. Programs AX and THERMOCALC 3.21 (Holland and Powell, 1998) were employed to calculate the activities of phases and the equilibrium Clapeyron slopes of exchange (garnet-biotite) and net transfer (garnet-biotite-muscovite-plagioclase) reactions.

Samples AW 9–21–04 2B and AW 9–5-05 2A were collected from schist with garnet, muscovite, biotite, and plagioclase with average compositions of An_{15} and An_{21}, respectively (Table 3). Garnet in these samples preserves dominantly growth zoning, with decreasing Mn and increasing Fe and Mg from core to rim (Supplemental File 4A [see footnote 4]). Minor retrograde reactions may be recorded by thin (<15 µm) outermost

[4]Supplemental File 4. PDF file. (A) Mn zoning maps of garnet crystals from thermobarometry analyses. (B) Electron microprobe analyses for thermobarometry results. If you are viewing the PDF of this paper or reading it offline, please visit http://dx.doi.org/10.1130/GES00627.S5 or the full-text article on www.gsapubs.org to view Supplemental File 4.

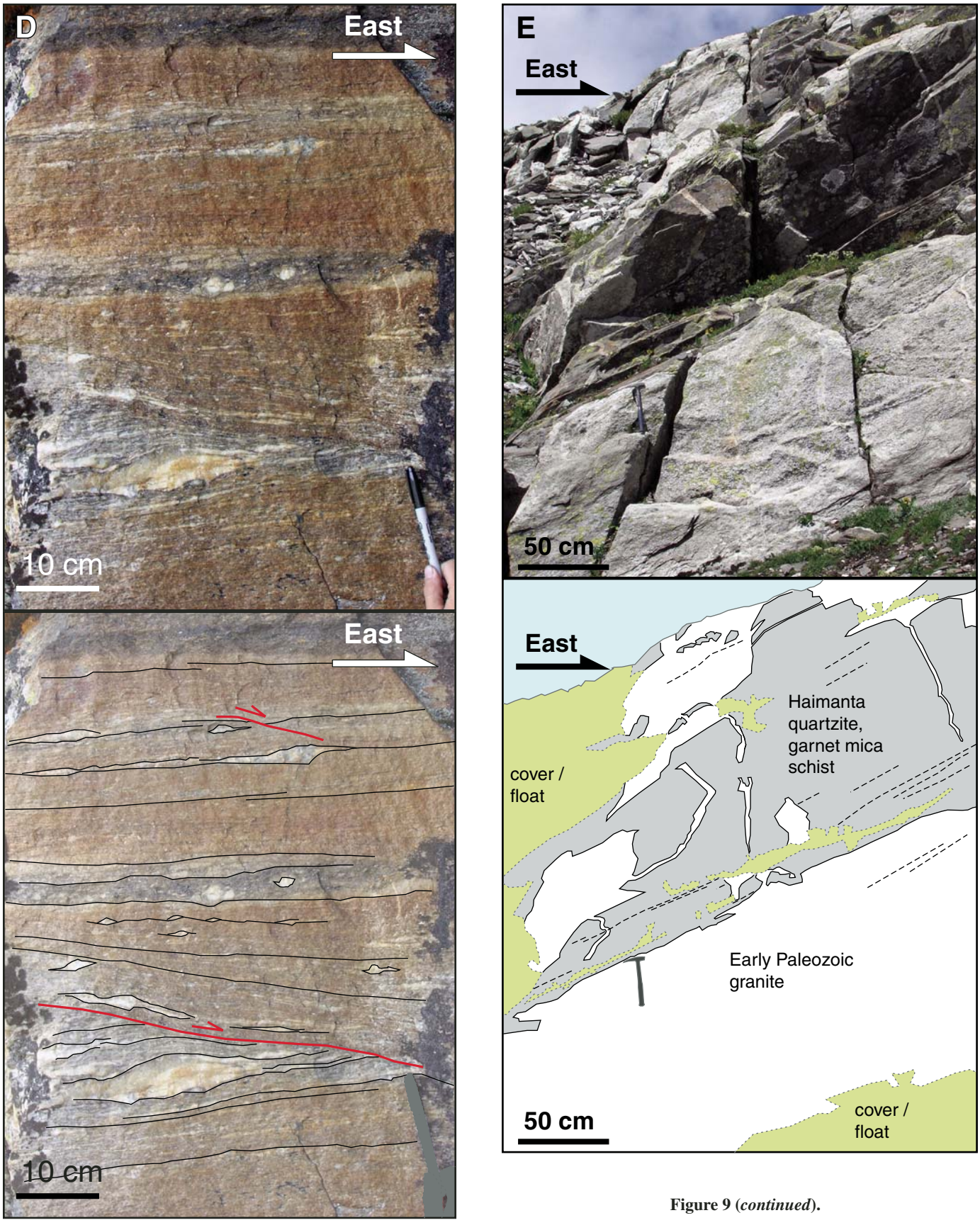

Figure 9 (*continued*).

rims of high Mn. All quartz is recrystallized. Data from the low-Mn inner rims of garnet crystals were used in thermobarometric calculations to retrieve pressure-temperature (*P-T*) conditions of 8.5 ± 2.0 kbar and 629 ± 127 °C and 8.8 ± 2.0 kbar and 617 ± 124 °C for two thin section areas of sample AW 9–21–04 2B, and 9.3 ± 2.0 kbar and 566 ± 120 °C for sample AW 9–5-05 2A (Table 3; Supplemental File 4B [see footnote 4]).

Samples AW 9–11–03 6 and AW 9–13–03 3 were collected from schist with garnet, muscovite, biotite, and plagioclase with average compositions of An_{12} and An_{4}, respectively (Table 3). Garnet in these samples preserves growth zoning, with decreasing Mn and increasing Fe and Mg from core to rim (Supplemental File 4A [see footnote 4]). All quartz is recrystallized. Data from the low-Mn rims of garnet crystals were used in thermobarometric calculations to retrieve *P-T* conditions of 6.9 ± 1.7 kbar and 446 ± 97 °C for sample AW 9–11–03 6, and 9.6 ± 2.3 kbar and 535 ± 116 °C for sample AW 9–13–03 3 (Table 3; Supplemental File 4B [see footnote 4]). These results are consistent with expectations based upon the pelitic petrogenetic grid (Spear and Cheney, 1989). However, the low An plagioclase of sample AW 9–13–03 3 is not in the range of the barometer, which is not well calibrated below An_{9} (Ghent and Stout, 1981). Comparison with other results in this region suggests that retrieved pressure conditions for this sample likely overestimate pressure by <3 kbar, which would also result in a modest (<30 °C) overestimate of maximum temperature.

Sample AW 9–3-03 12 was collected from schist with garnet, muscovite, biotite, and plagioclase with an average composition of An_{24} (Table 3). Garnet in this sample is unzoned in Fe, Mg, and Mn (Supplemental File 4A [see footnote 4]). All quartz is recrystallized. Garnet rim

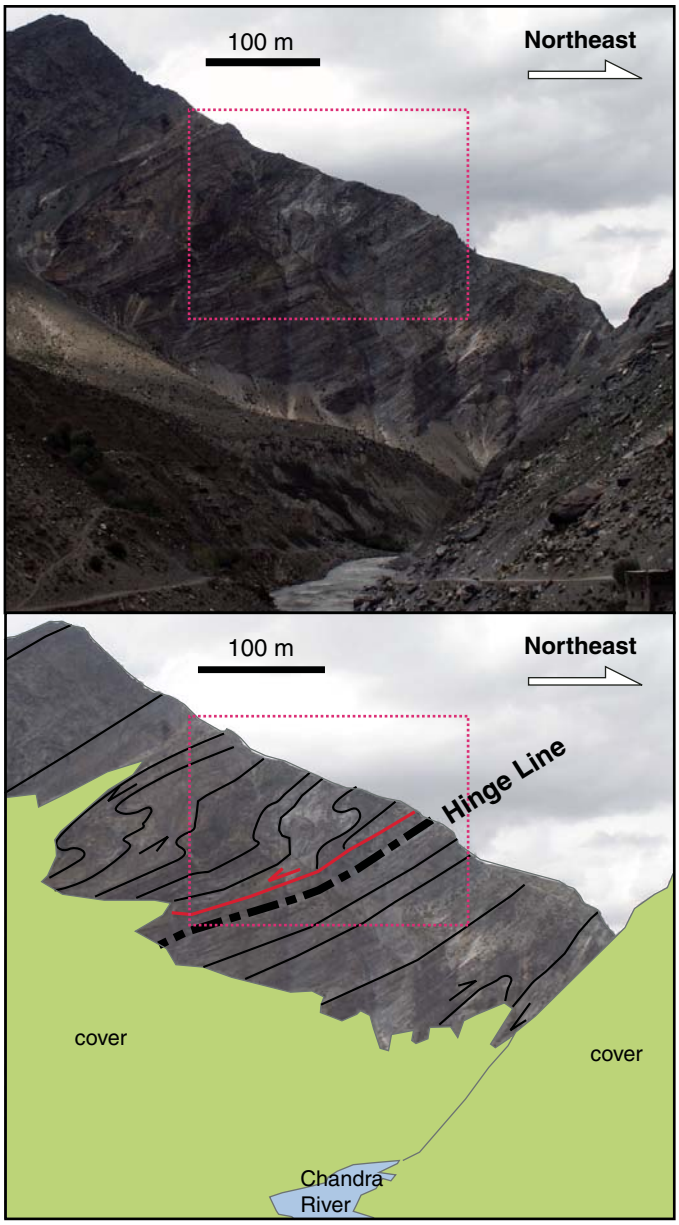

F

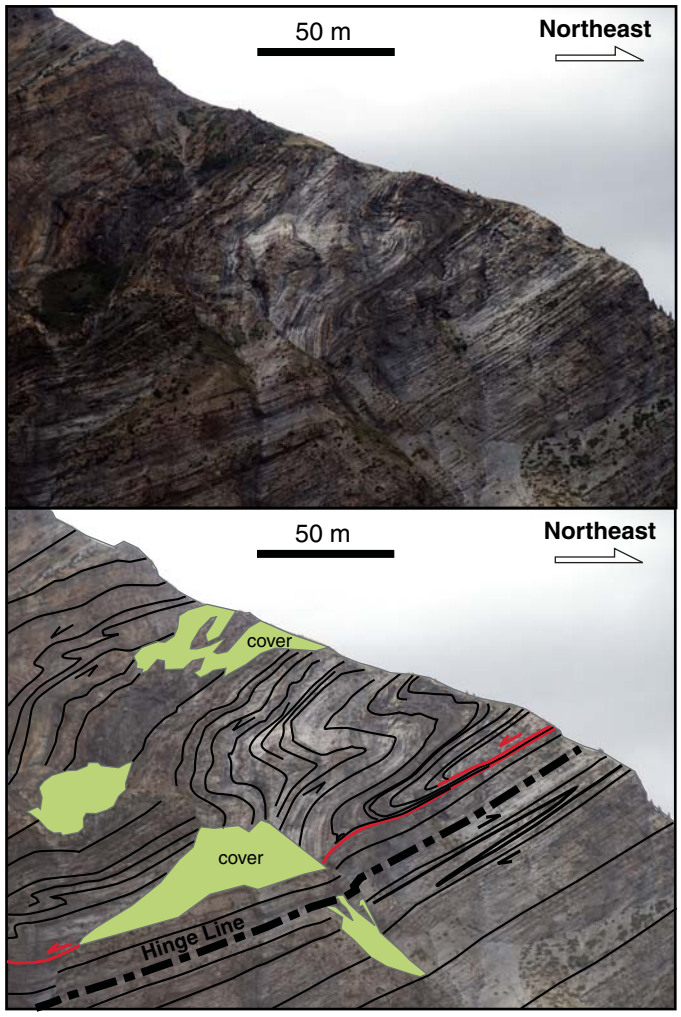

Figure 9 (*continued*).

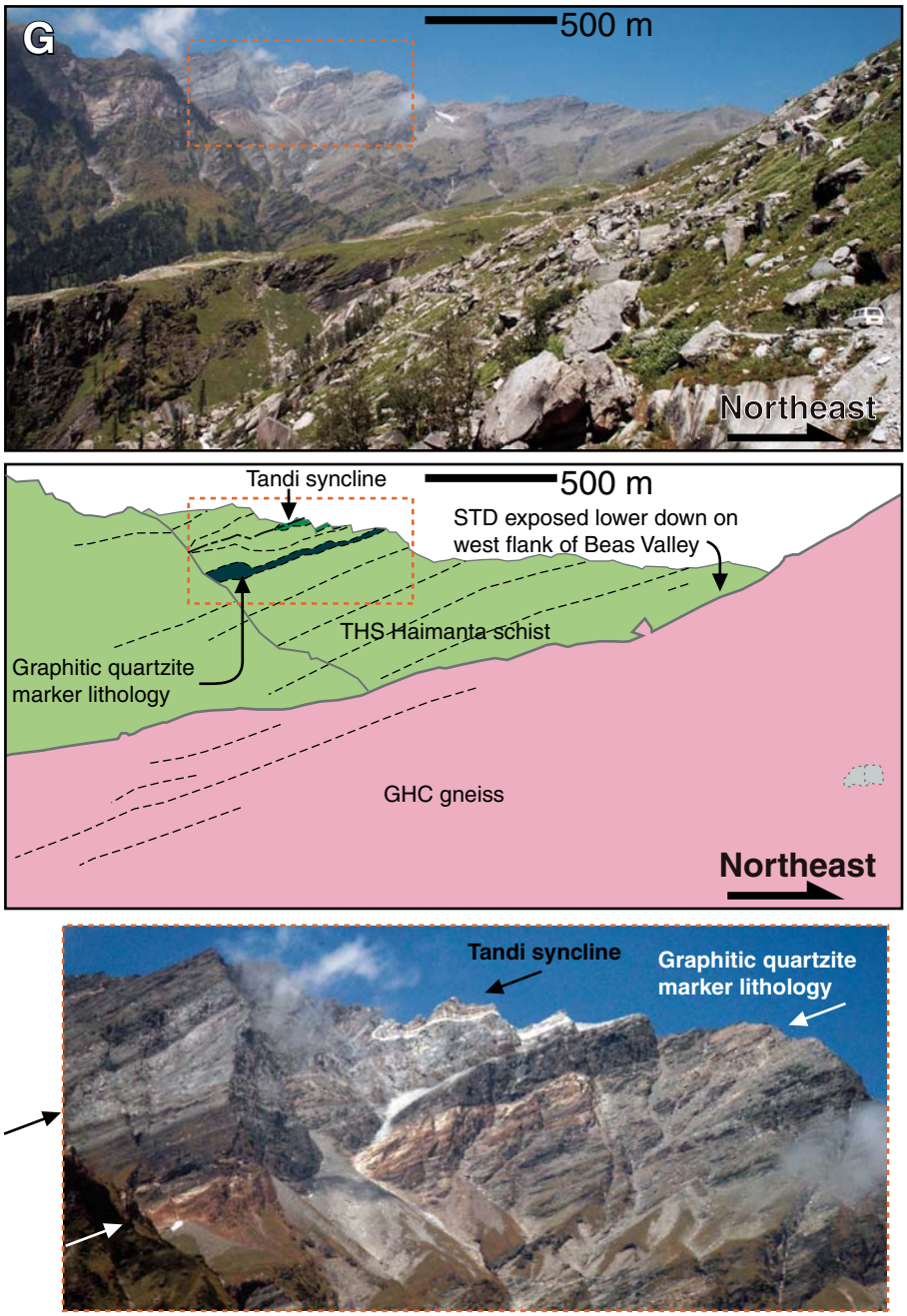

Figure 9 (*continued*).

compositions were used to determine *P-T* conditions of 7.2 ± 1.6 kbar and 494 ± 101 °C (Table 3; Supplemental File 4B [see footnote 4]).

The collection site of sample AW 9–29–03 12 is at the top of the garnet zone in the right-way-up metamorphic sequence observed along the Beas River (Figs. 5 and 6B) (see also Epard et al., 1995); this sample is therefore expected to yield the lowest maximum *P-T* conditions of this sample suite. It was collected from schist with garnet, muscovite, biotite, and plagioclase with an average composition of An_1 (Table 3). Garnet in this sample is unzoned in Fe, Mg, and Mn (Supplemental File 4A; see footnote 4). Most quartz is recrystallized, but ≤1 mm relict quartz grains occur as porphyroclasts wrapped around by the dominant quartz-mica fabric. Retrieved *P-T* conditions are 13.1 ± 2.9 kbar and 480 ± 105 °C (Table 3; Supplemental File 4B [see footnote 4]). These results are consistent with expectations based upon the pelitic petrogenetic grid (Spear and Cheney, 1989), but the very low An plagioclase is outside the calibrated range of the barometer (Ghent and Stout, 1981). Comparison with other regional results suggest that retrieved pressure conditions for this sample likely overestimate maximum pressure by ~5–7 kbar, which would also result in a modest (<50 °C) overestimate of maximum temperature.

The new temperature and pressure determinations are consistent with metamorphic conditions of the structurally lowest levels of (1) the Lesser Himalayan Sequence Jeori crystalline rocks, (2) the Greater Himalayan Crystalline complex, and (3) the Tethyan Himalayan Sequence Haimanta Group to the north of the STD (e.g., Epard et al., 1995; Vannay and Grasemann, 1998; Vannay et al., 1999; Caddick et al., 2007; Chambers et al., 2008, 2009). The decrease in metamorphic grade at increasing structural

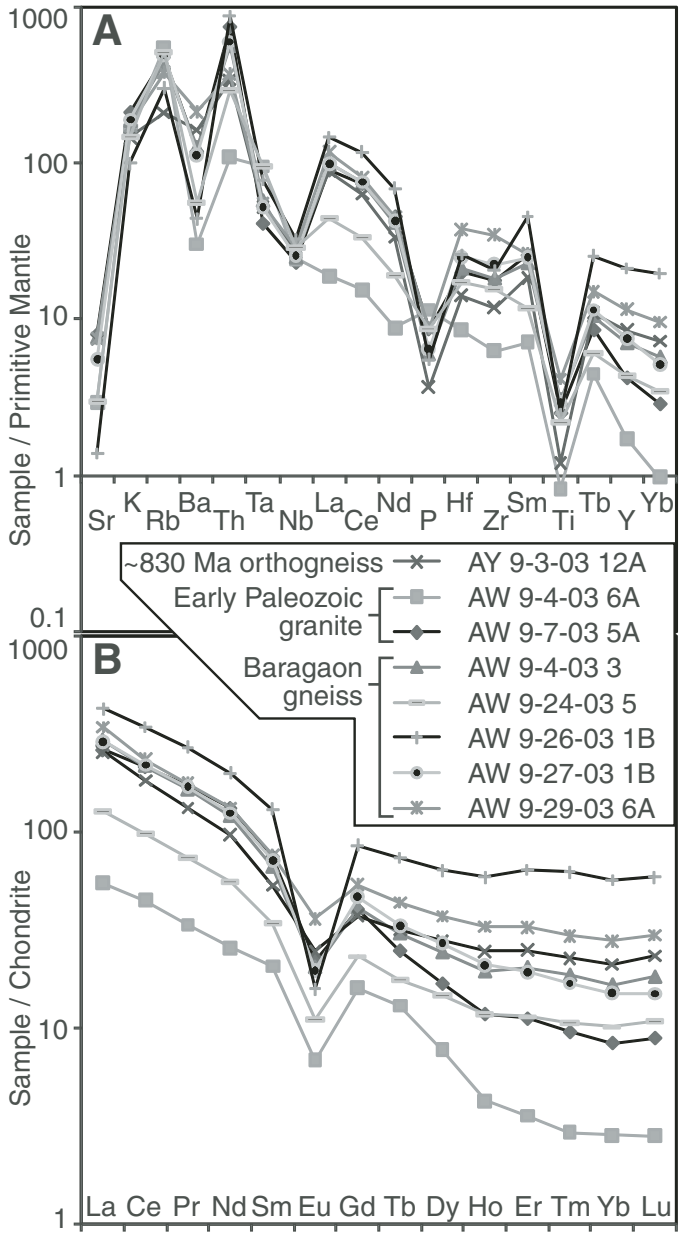

Figure 10. Trace element geochemistry of granitoid samples. (A) Trace element (spider) diagram. (B) Rare earth element plot.

levels is inconsistent with the famous inverted metamorphic field gradient of the Greater Himalayan Crystalline complex (Vannay and Grasemann, 1998; Vannay et al., 1999).

GEOCHRONOLOGY

U-Th-Pb Zircon Geochronology: Granitic Rocks

We conducted U-(Th)-Pb spot dating of zircon from granitoid and leucogranite samples using the Cameca 1270 ion microprobe at UCLA to constrain the lithostratigraphy and timing of deformation above, below, and within the MCT shear zone. We briefly describe our results here; Appendix 3 contains a description of our methods and an expanded report

TABLE 3. THERMOBAROMETRY RESULTS

Sample number		Pressure (kbar)			Temperature (°C)			Cor
AW 9-3-03 12		7.2	±	1.6	494	±	101	0.90
AW 9-11-03 6		6.9	±	1.7	446	±	97	0.87
AW 9-13-03 3*		9.6	±	2.3*	535	±	116*	0.89
AW 9-29-03 12*		13.1	±	2.9*	480	±	105*	0.89
AW 9-21-04 2B†	(i)	8.5	±	2.0	629	±	127	0.85
	(ii)	8.8	±	2.0	617	±	124	0.86
AW 9-5-05 2A		9.3	±	2.0	566	±	120	0.93

Note: Calculations of garnet-biotite-muscovite-plagioclase (P) barometer and garnet-biotite (T) thermometer made with THERMOCALC v3.21 with May 2001 database (Holland and Powell, 1998). Mineral formulas and activities were calculated with the program A-X by Tim Holland and Roger Powell. Uncertainties are ±1σ for each analysis. "Cor" is correlation coefficient from THERMOCALC.

*Samples AW 9-13-03 3 and AW 9-29-03 12 feature low An-content plagioclase (Ca/[Ca+Na] < 0.06), with values below the range of activity models for the barometer (e.g., Ghent and Stout, 1981). This results in large pressure over-estimates (likely by ~2 to ~7 kbar) and corresponding small temperature over-estimates (by < 50 °C).

†For sample AW 9-21-04 2B, data was collected in two areas of a thin section: areas i and ii, encompassing two different garnet crystals. Results for the areas are given separately.

of our results. Granitoid ages generally increase with structural depth: the MCT hanging wall features early Paleozoic and ca. 830 Ma granites and granitic gneiss, the MCT zone contains ca. 830 Ma and ca. 1.85 Ga granitic gneiss, and the MCT footwall has ca. 1.85 Ga granitic gneiss. Dates of leucogranite crosscutting foliation in the Leo Pargil dome and pegmatite crosscutting foliation of the Wangtu gneiss provide minimum ages for these fabrics and age information on the thermal conditions represented by their crystallization.

To characterize the age and affinities of granitic rocks in the MCT hanging wall, we analyzed 53 spots on 38 zircon crystals from 5 samples (Fig. 11); 2 granitic samples yield early Paleozoic dates: AW 9–7-03 5A, from granite with 5 cm feldspars ~5 km east of Mandi (Figs. 6B and 10F), and AW 9–3-04 7A, collected from an ~1-m-thick mylonitic granite sill ~20 km north of Kullu in the overturned limb of the Phojal anticline (Fig. 6A). Calculated weighted mean ages of $^{238}U/^{206}Pb$ dates from concordant data of these two samples are 470.6 ± 5.3 Ma (AW 9–7-03 5A; 2σ, mean square of weighted deviates, MSWD = 1.9) and 473 ± 26 Ma (AW 9–3-04 7A; 2σ, MSWD = 0.73). We interpret the weighted mean ages as the granite crystallization ages. Sample AY 9–3-03 12A was collected from mylonitic augen gneiss of the Audi shear zone. Results for this sample are reversely discordant and interpreted to record the protolith crystallization ca. 830 Ma (see Appendix 3). Sample AW 9–4-03 6A was collected from mylonitic augen gneiss ~1 m structurally above a sheared top-to-the-southwest basal contact with Haimanta Group metasedimentary rocks (Fig. 6B). Results with a range of dates spanning the Paleoproterozoic to the early Paleozoic and variable concordance and/or discordance are interpreted to reflect zircon inheritance ca. 840 Ma or earlier, a granitic crystallization event between ca. 840 Ma and the early Paleozoic, and early Paleozoic metamorphic overgrowth of zircon rims. Sample AW 9–24–04 4C represents tourmaline-bearing leucogranite that crosscuts bedding preserved in amphibolite-grade metasedimentary rocks of the Leo Pargil dome (Fig. 6C). Acquired dates are variable, discordant, and extend from the Precambrian to the Tertiary. The youngest ($^{238}U/^{206}Pb$) date is 50.4 ± 2.4 Ma (1σ). These data likely reflect the ages of inherited zircon prior to Tertiary leucogranite crystallization.

We analyzed 71 spots on 51 zircon crystals from 7 samples to characterize the age and affinities of mylonitic augen gneiss within the MCT shear zone (Fig. 11). Analyses of six of these samples are consistent with protolith crystallization ca. 1.85 Ga (samples AW 9–4-03 3, AW 9–24–03 5, AW 9–26–03 1B, AW 9–27–03 1B, AW 9–29–03 6A, AW 9–17–05 2;

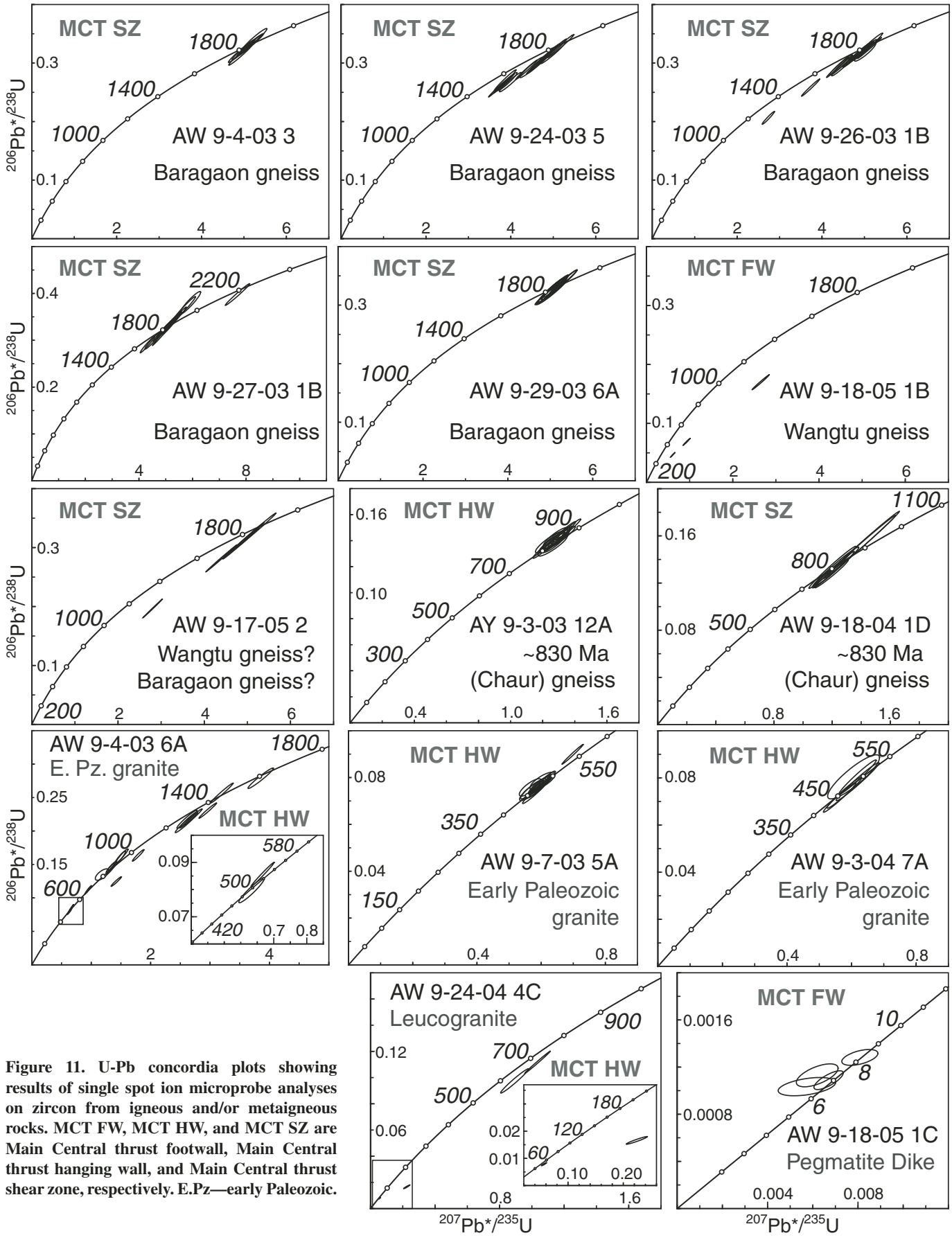

Figure 11. U-Pb concordia plots showing results of single spot ion microprobe analyses on zircon from igneous and/or metaigneous rocks. MCT FW, MCT HW, and MCT SZ are Main Central thrust footwall, Main Central thrust hanging wall, and Main Central thrust shear zone, respectively. E.Pz—early Paleozoic.

Figs. 6B, 6C). These results help define the age and spatial extent of the ca. 1.85 Ga Baragaon gneiss within the MCT shear zone (although the affinity of sample AW 9–17–05 2 is ambiguous; see Appendix 3). Analyses of sample AW 9–18–04 1D (Fig. 6B) yield a $^{207}Pb/^{206}Pb$ weighted mean age of 831 ± 19 Ma (2σ, MSWD = 0.69), which we interpret as the protolith crystallization age. This is the southernmost MCT shear zone sample, and it provides a geometric limit on the Baragaon gneiss.

We analyzed two samples from a single site in the MCT footwall: AW 9–18–05 1B and AW 9–18–05 1C were collected from Wangtu gneiss and an undeformed pegmatitic felsic dike that crosscuts foliation of the Wangtu gneiss, respectively (Figs. 6C and 11). Discordant results for sample AW 9–18–05 1B are consistent with previous dates of ca. 1.85 Ga for the crystallization of the granitic protolith of the Wangtu gneiss (Table 2). Four spot analyses on different zircon crystals from sample AW 9–18–05 1C yield Late Miocene $^{238}U/^{206}Pb$ ages, with a weighted mean age 7.4 ± 1.2 Ma (2σ, MSWD = 5.1) (Supplemental File 5[5]). Late Miocene $^{232}Th/^{208}Pb$ monazite ages were also obtained for this sample (see Th-Pb Monazite Geochronology discussion). We interpret the Late Miocene dates from the undeformed dike as crystallization ages. Therefore the dikes result from partial melting and recrystallization during the concluding phases of the Late Miocene deformation and metamorphism of the Munsiari Group.

U-Th-Pb Zircon Geochronology: Detrital Zircon

We conducted U-Th-Pb geochronology of detrital zircon grains from 16 samples to test models for the composition and correlation of sequences carried by major thrust faults. All ages are spot ages collected using the laser ablation multicollector (LA-MC) ICP-MS facility at the University of Arizona (Tucson) and the UCLA ion microprobe. Appendix 4 contains a description of our methods. Results from the Lesser Himalayan Sequence Shimla Group, the Greater Himalayan Crystalline complex, and the Tethyan Himalayan Sequence Haimanta Group all span the Proterozoic. In contrast, results from the Lesser Himalayan Sequence Berinag and Jeori Groups are dominantly Paleoproterozoic and older.

MCT Footwall

Because the Shimla Group of the Outer Lesser Himalayan Sequence has been alternately considered Paleoproterozoic and Neoproterozoic (see preceding), zircon grains from a siltstone sample of this unit (AW 9–15–04 4) were analyzed to constrain the depositional age (Fig. 12M). Sparse data (only 23 suitable analyses) show a concentration of 11 dates ranging from 600 Ma to 850 Ma, indicating a late Neoproterozoic maximum depositional age for the sampled layer.

Berinag Group quartzites were investigated to constrain their depositional age and examine along-strike and regional map correlations. Previous workers have alternately correlated quartzites between the Wangtu gneiss and the Greater Himalayan Crystalline complex on the northeastern flank of the Kullu window as Berinag Group or Greater Himalayan Crystalline complex rocks (cf. K.K. Sharma, 1977; Vannay and Grasemann, 1998). Therefore we analyzed detrital zircon from this setting and from the thick Berinag Group quartzites southwest of the Munsiari thrust. Samples AW 9–22–04 9A and AW 9–22–04 9C are from an ~50-m-thick, highly recrystallized quartzite layer between Wangtu orthogneiss and Greater Himalayan Crystalline complex paragneiss at the eastern end of the Kullu window, whereas sample AW 9–22–04 1B is a quartzite from the Berinag Group near Rampur. These three samples all yield youngest age peaks between ca. 1.88 Ga and ca. 1.94 Ga and are dominated by Paleoproterozoic ages, consistent with late Paleoproterozoic maximum depositional ages. The two Berinag samples from just below the Greater Himalayan Crystalline complex paragneiss have distinct age distributions, one with substantial population of dates as old as ca. 3.0 Ga and the other showing a single, dominant ca. 1.88 Ga age peak. Similarly, our Berinag sample from south of the Munsiari thrust has a range of ages from ca. 1.9 to 3.0 Ga, whereas 6 of 7 ages from a similarly located sample from Richards et al. (2005) have ca. 1.87 Ga dates. The similar age populations obtained from quartzites of the northeastern and southwestern Kullu window support grouping these rocks into the Berinag Group. The two age patterns obtained in both regions suggest that the Berinag Group may contain layers with distinct sources.

Sparse younger dates were obtained from the Berinag samples from the eastern end of the Kullu window: AW 9–22–04 9C yields 5 scattered younger ages, with $^{238}U/^{206}Pb$ ages of 969 ± 26 Ma, 846 ± 8 Ma, 572 ± 39 Ma, 513 ± 14 Ma, and 469 ± 3 Ma, and AW 9–22–04 9A likewise yields $^{238}U/^{206}Pb$ ages as young as the Phanerozoic. The concordia plot of sample AW 9–22–04 9A shows that the young ages define a clear discordia line from ca. 1.85 to 1.9 Ga to the Cenozoic (Supplemental File 5B [see footnote 5]), and a single discordant approximately Cenozoic age has a high U/Th ratio. These results are consistent with minor zircon growth and Pb loss during Cenozoic metamorphism, so these young dates are not considered detrital ages. AW 9–22–04 9C data with Paleoproterozoic $^{207}Pb/^{206}Pb$ ages also show discordia lines trending toward the late Phanerozoic, but the five Neoproterozoic–early Paleozoic analyses listed above plot near or on the concordia curve. Our preferred interpretation is that the five young dates reflect Pb loss and not detrital ages, but if these represent real detrital ages then sample 9C could represent Paleoproterozoic to Cenozoic Himalayan strata. In summary, we interpret the data for the Berinag samples to indicate a maximum depositional age of ca. 1850 Ma and Pb loss related to Cenozoic metamorphism. Deposition soon after ca. 1850 Ma is consistent with the ca. 1.8 Ga age of interlayered and crosscutting metabasalt (Miller et al., 2000).

We performed detrital zircon geochronology of the Jeori gneiss in order to test a proposed correlation of these rocks with the MCT hanging-wall rocks to the south of the Kullu window (i.e., the Jutogh thrust hanging wall of Richards et al., 2005). The age patterns obtained for Jeori paragneiss samples (AW 9–25–04 8 and AW 9–25–04 9) span ca. 1.9 to 3.0 Ga. Age distributions of the Jeori samples and Berinag samples, excepting only Berinag sample AW 9–22–04 9A, are indistinguishable at the 95% confidence level according to the Kolmogorov-Smirnov statistic (Fig. 13; Supplemental File 5b [see footnote 5]). However, the minimum age peaks of the two Berinag samples and the Jeori rocks are distinct: the Berinag samples show younger minimum age peaks ca. 1.92 Ga and scattered ca. 1.8 to 1.94 Ga ages for the Berinag versus ca. 1.94 Ga and ca. 1.96 Ga for the Jeori). These data suggest a maximum depositional age of ca. 1.94 Ga for the protoliths of the Jeori metasedimentary samples. The lack of a ca. 1.85 Ga signal suggests that the Jeori rocks were deposited prior to crystallization of the Wangtu granitic protolith. The proposed correlation of Jeori gneiss with the MCT hanging-wall rocks south of the

[5]Supplemental File 5. PDF file. (A) Ion microprobe U-(Th)-Pb zircon data table. (B) U-Pb concordia plots showing results of single spot analyses on zircon from metasedimentary and/or sedimentary rocks. Most data were acquired via laser ablation–inductively coupled plasma–mass spectrometry (LA-ICP-MS) at the University of Arizona Laserchron Center; analyses labeled "ion microprobe" were acquired via the University of California Los Angeles ion microprobe. (C) LA-ICP U-(Th)-Pb zircon data. (D) Kolmogorov-Smirnov (K-S) statistic applied to the probability density functions of detrital zircon samples. If you are viewing the PDF of this paper or reading it offline, please visit http://dx.doi.org/10.1130/GES00627.S6 or the full-text article on www.gsapubs.org to view Supplemental File 5.

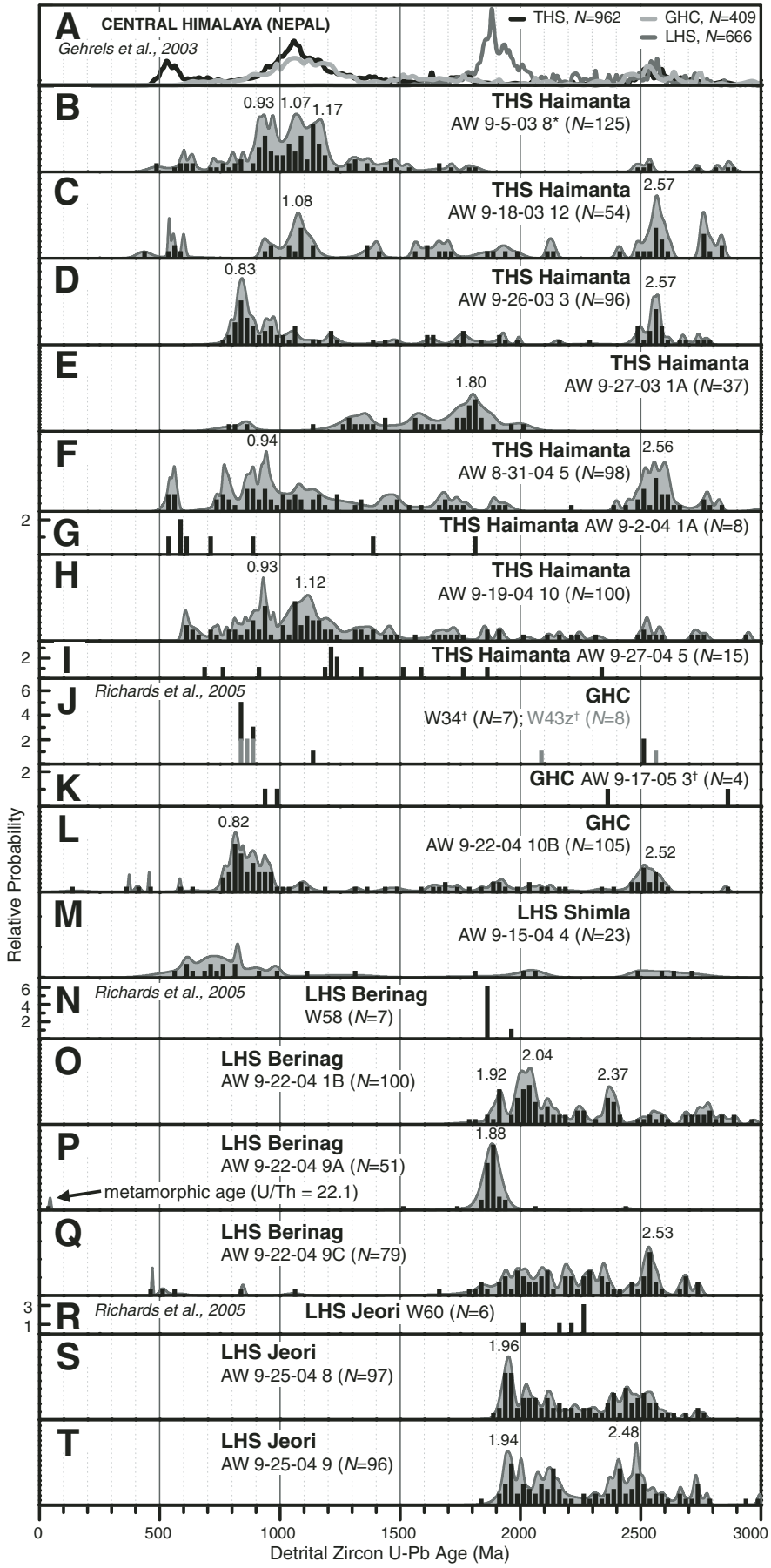

Figure 12. Age histograms and relative probability plots of zircon U-Pb age populations for metasedimentary and sedimentary rocks. THS—Tethyan Himalayan Sequence; GHC—Greater Himalayan Crystalline complex; LHS—Lesser Himalayan Sequence. Published data from the central Himalaya (Gehrels et al., 2003) are plotted in A, and data from the Himachal Himalaya (Richards et al., 2005) are plotted in J, N, and R. Data bins are 25 m.y. For most samples $^{238}U/^{206}Pb$ ages and $^{207}Pb/^{206}Pb$ ages are plotted according to a simple best age algorithm: if the average of the $^{238}U/^{206}Pb$ age and the $^{207}Pb/^{206}Pb$ age is greater than 1000 Ma, the $^{207}Pb/^{206}Pb$ age is plotted, otherwise the $^{238}U/^{206}Pb$ age is plotted. The following exceptions occur. *Data for sample AW 9–5-03 8 (B) consist of 33 ion microprobe analyses and 92 laser ablation–inductively coupled plasma–mass spectrometry (LA-ICP-MS) analyses. The ion microprobe analyses are all plotted as $^{207}Pb/^{206}Pb$ ages and LA-ICP-MS analyses are plotted via the best age algorithm. †For samples AW 9–17–05 3, W34, and W43z, all data are plotted as $^{207}Pb/^{206}Pb$ ages. Concordia plots and tables for detrital zircon data are presented in Supplemental File 4 (see footnote 4).

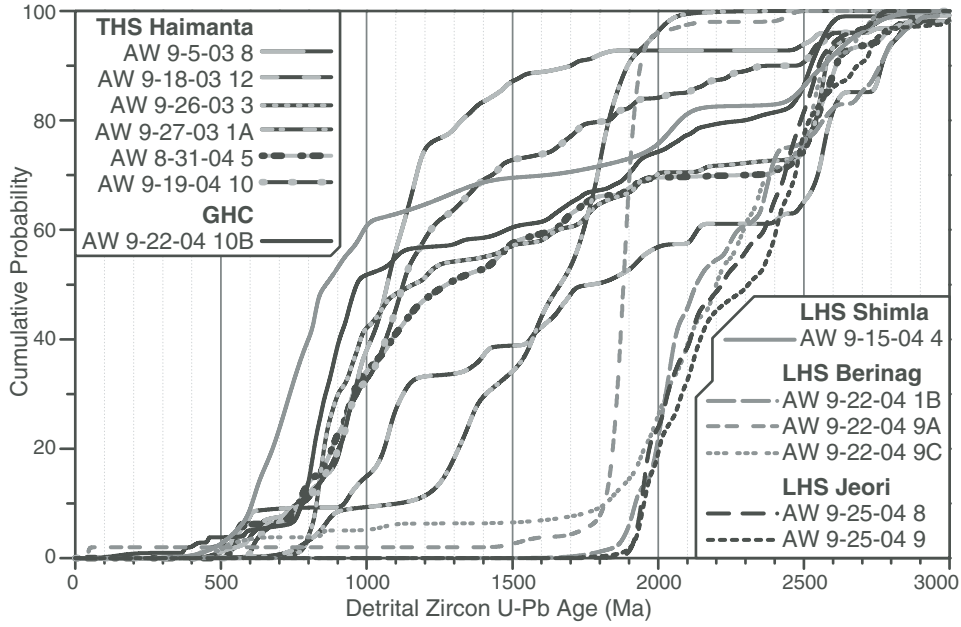

Figure 13. Cumulative probability diagram of detrital zircon U-Pb age results. THS—Tethyan Himalayan Sequence; GHC—Greater Himalayan Crystalline complex; LHS—Lesser Himalayan Sequence.

Kullu window is not supported by these data, because as detailed herein, these latter rocks yield Neoproterozoic detrital zircon age peaks.

MCT Hanging Wall

We analyzed zircon grains from the MCT hanging wall, focusing on the metasedimentary rocks of the southern MCT hanging wall (Figs. 12 and 13; Supplemental File 5 [see footnote 5]). Our mapping suggests that these are Tethyan Himalayan Sequence Haimanta Group rocks, but alternative models show these as Greater Himalayan Crystalline complex rocks, a combination of Tethyan Himalayan Sequence and Greater Himalayan Crystalline complex rocks, or divided into multiple Greater Himalayan Crystalline complex and Lesser Himalayan Sequence thrust sheets (e.g., Bhargava et al., 1991; Thakur and Rawat, 1992; Frank et al., 1995; DiPietro and Pogue, 2004; Richards et al., 2005).

Analyses of MCT footwall rocks (described above), a Tethyan Himalayan Sequence Haimanta Group sample from a site widely acknowledged to be in the Tethyan Himalayan Sequence Haimanta Group strata above the STD (e.g., Thakur and Rawat, 1992; Frank et al., 1995; Vannay and Steck, 1995; Jain et al., 1999), and a Greater Himalayan Crystalline complex sample provide bases of comparison for proposed correlations of the southern MCT hanging wall with the other thrust sheets. The Tethyan Himalayan Sequence Haimanta sample, AW 8–31–04 5, was collected from a quartz-mica phyllite in Keylong (Fig. 6A). We obtained 98 zircon dates from this sample, yielding well-constrained dates ranging from ca. 550 Ma to ca.3000 Ma (Figs. 12 and 13; Supplemental File 5 [see footnote 5]). There is no dominant age probability peak, but the largest are ca.940 Ma and a broad peak ca. 2560 Ma, with additional peaks ca.560, ca.770, and ca. 890 Ma (Fig. 12F). The Greater Himalayan Crystalline complex sample, AW 9–22–04 10B, was collected from Sutlej River section to the east of the Kullu window (Fig. 6C). Spot ages on 105 zircon grains yield well-constrained dates ranging from ca. 770 Ma to ca. 2600 Ma, with broad peaks ca. 820 Ma and ca. 2520 Ma (Fig. 12L). Detrital zircon results for the metasedimentary rocks of the southern MCT hanging wall (AW 9–5-03 8, AW 9–18–03 12, AW 9–26–03 3, AW 9–27–03 1A, AW 9–19–04 10, AW 9–27–04 5) have broadly similar age ranges and dominant age peaks to these two samples, with well-constrained ages ranging from ca. 550 Ma to ca. 3500 Ma.

The broadly shared detrital age pattern of the Haimanta, Greater Himalayan Crystalline complex, and southern MCT hanging-wall samples includes a Neoarchean through Proterozoic span of ages with two dominant age peak zones, one from ca. 2600–2500 Ma and the other across the Neoproterozoic. One sample, AW 9–27–03 1A, does not prominently show either age peak zone. It is a sample of phyllonite with microscopic garnet that occurs <1 m above the (sharp, mylonitic, folded) contact with ca. 1.85 Ga Baragaon gneiss in the southern MCT hanging wall (Figs. 6B and 8B). The 37 ages for this sample span the Proterozoic, but the only significant age peak is a diffuse ca. 1.8 Ga peak, suggesting that the Baragaon rocks were a dominant source for these zircon grains. The original contact may have been sedimentary; an unconformity between correlative lithologies is observed in the Pakistan Himalaya (DiPietro and Isachsen, 2001).

The consistent age populations of southern MCT hanging-wall metasedimentary samples support hypotheses that group these rocks in a single unit. As the age populations match results for a recognized Tethyan Haimanta Group sample (AW 8–31–04 5), these data support field evidence suggesting that all of these rocks are Tethyan Himalayan Sequence Haimanta Group. Similar age ranges for the Greater Himalayan Crystalline complex mean that these data alone cannot distinguish between the Haimanta Group and the Greater Himalayan Crystalline complex. The detrital age patterns and protoliths of the Greater Himalayan Crystalline complex, Haimanta Group, and Shimla Group of the Outer Lesser Himalayan Sequence are all similar, suggesting that these sequences may restore as a single stratigraphic layer prior to Phanerozoic tectonism.

Th-Pb Monazite Geochronology

Because monazite commonly crystallizes during metamorphism, Th-Pb monazite geochronology can be used to date metamorphic events (e.g., Harrison et al., 1997; Catlos et al., 2001); monazite is also commonly used to date igneous rocks (e.g., Harrison et al., 1995). Th-Pb analyses of monazite grains were obtained via the Cameca 1270 ion microprobe at UCLA using a beam current of 10–15 nA focused to a size of 15–30 μm

in diameter. Th-Pb ratios were determined using a calibration curve based primarily on ThO_2/Th versus Pb/Th from monazite standard 554 (45 ± 1 Ma; Harrison et al., 1995). Monazite grains in metamorphic rocks were dated in situ, allowing direct examination of the textural relationships between monazite grains and metamorphic fabrics. These monazite grains were commonly very small (<15 μm in diameter) and were identified using the scanning electron microscope in backscatter mode.

Despite examining thin sections of ~40 garnet schist samples of the MCT hanging wall southwest of the Kullu window, only 4 samples contained sufficient monazite to warrant analysis: AW 9–3-03 12, AW 9–11–03 4, AW 9–11–03 6, and AW 9–13–03 3 (Fig. 6B; Table 4). The first three samples yielded 13 latest Proterozoic to early Mesozoic dates from monazite grains included in garnet, and in the matrix. For these samples, ages range from ca. 600 Ma to ca. 200 Ma, with 1σ analytical errors of as much as ~33 m.y. Dates do not all overlap within 2σ for any one sample, even after matrix monazite dates are excluded. The range of ages may result from remaining difficulties in dating of pre-Cenozoic monazite (Peterman et al., 2006). Sample AW 9–13–03 3 yielded Cenozoic dates. The only monazite grain included in garnet yielded the oldest spot date, 41.5 ± 7.2 Ma (1σ), while younger spot ages from matrix monazite grains range from 39.9 ± 6.5 to 28.4 ± 2.3 Ma (1σ).

Monazite grains were analyzed from a leucogranite intruding the upper levels of the Greater Himalayan Crystalline complex (AW 9–23–04 3) and an undeformed pegmatite intruding the Wangtu (described above, AW

TABLE 4. Th-Pb MONAZITE GEOCHRONOLOGY

Sample / setting Grain setting	$^{208}Pb^*/^{232}Th^{\dagger}$	± 1 s.e.	$^{208}Pb/^{204}Pb$	$^{208}Pb^*$ (%)	ThO_2/Th	$^{208}Pb^*/^{232}Th$ age (Ma ± 1 s.e.)
AW 9-3-03 12 / Tethyan Haimanta Group garnet schist						
Matrix	2.95E-02	1.67E-03	9048.1	99.59	2.57	587.7 ± 32.7§
Included in garnet	2.49E-02	6.11E-04	14313.0	99.74	2.91	497.9 ± 12.0§
Included in garnet	2.46E-02	5.32E-04	3100.4	98.82	2.89	490.7 ± 10.5§
Matrix	2.42E-02	6.70E-04	2498.9	98.53	2.83	483.2 ± 13.2§
Included in garnet	2.11E-02	3.55E-04	17498.0	99.79	2.97	422.8 ± 7.0§
AW 9-9-03 8 / sheared margin of Early Paleozoic granite within Tethyan Haimanta Group						
Matrix	2.61E-02	9.78E-04	1602.6	97.71	2.66#	521.5 ± 19.3§
Matrix	2.53E-02	1.02E-03	2110.0	98.26	2.63#	505.6 ± 20.0§
AW 9-11-03 2 / sheared margin of Early Paleozoic granite within Tethyan Haimanta Group						
Matrix	2.55E-02	1.02E-03	1502.9	97.56	2.64#	509.6 ± 20.1§
AW 9-11-03 4 / Tethyan Haimanta Group garnet schist						
Included in garnet	1.87E-02	5.91E-04	452.1	91.88	2.86	375.4 ± 11.7§
Included in garnet	1.78E-02	3.53E-04	1912.4	98.08	2.95	357.3 ± 7.0§
Included in garnet	1.77E-02	3.69E-04	2507.4	98.54	3.11	355.2 ± 7.3§
Matrix	1.27E-02	1.24E-03	83.8	56.21	2.31	254.2 ± 24.8§
Included in garnet	1.08E-02	3.85E-04	163.8	77.60	3.42††	216.8 ± 7.7§
AW 9-11-03 6 / Tethyan Haimanta Group garnet schist						
Included in garnet	2.45E-02	1.07E-03	600.5	93.89	3.15	488.7 ± 21.1§
Included in garnet	2.24E-02	4.78E-04	456.1	91.95	3.29	448.5 ± 9.4§
Included in garnet	2.20E-02	6.69E-04	290.2	87.35	3.17	439.4 ± 13.2§
AW 9-13-03 3 / Tethyan Haimanta Group garnet schist						
Included in garnet	2.06E-03	3.59E-04	49.5	25.83	2.29#	41.5 ± 7.2§
Matrix	1.97E-03	3.23E-04	57.7	36.42	2.06#	39.9 ± 6.5§
Matrix	1.48E-03	1.44E-04	76.5	52.05	2.35#	29.9 ± 2.9§
Matrix	1.59E-03	2.29E-04	114.9	68.05	2.05#	32.2 ± 4.6§
Matrix	1.41E-03	1.12E-04	90.9	59.64	2.41#	28.4 ± 2.3§
AW 9-23-04 3 / Leucogranite within Greater Himalayan Crystalline complex						
Matrix	2.05E-02	1.28E-03	9128.0	99.58	2.15#	409.6 ± 25.3§
Matrix	1.90E-02	1.07E-03	13520.0	99.72	2.31	379.4 ± 21.1§
Matrix	1.52E-02	7.89E-04	8105.0	99.53	2.46	305.3 ± 15.7§
Matrix	1.24E-02	7.28E-04	855.9	95.52	2.25	249.3 ± 14.5§
Matrix	1.04E-02	9.84E-04	2432.0	98.42	1.79#	209.9 ± 19.7§
Matrix	6.11E-03	3.43E-04	1622.0	97.64	2.38	123.0 ± 6.9§
Matrix	1.33E-03	7.47E-05	748.6	94.88	2.45	26.8 ± 1.5§
Matrix	9.95E-04	4.69E-05	71.6	46.48	2.76	20.1 ± 0.9§
Matrix	9.82E-04	6.49E-05	82.8	53.70	2.29	19.9 ± 1.3§
AW 9-18-05 1C / Leucogranite cutting across foliation of Wangtu granitic gneiss						
Grain	3.26E-04	1.81E-05	121.9	68.54	2.22	6.59 ± 0.37§§
Grain	3.24E-04	1.67E-05	136.0	71.80	2.28	6.56 ± 0.34§§
Grain	3.16E-04	1.91E-05	129.1	70.30	2.20	6.39 ± 0.39§§
Grain	3.15E-04	1.60E-05	144.8	73.52	2.43	6.37 ± 0.32§§
Grain	3.11E-04	1.62E-05	158.6	75.83	2.17	6.29 ± 0.33§§
Grain	3.03E-04	1.78E-05	136.4	71.89	2.12	6.12 ± 0.36§§
Grain	3.02E-04	1.54E-05	134.3	71.44	2.13	6.10 ± 0.31§§
Grain	2.99E-04	1.73E-05	120.3	68.13	2.33	6.04 ± 0.35§§
Grain	2.95E-04	1.69E-05	130.5	70.62	2.40	5.96 ± 0.34§§
Grain	2.95E-04	1.57E-05	120.3	68.14	2.18	5.95 ± 0.32§§
Grain	2.93E-04	1.45E-05	127.1	69.82	2.54	5.92 ± 0.29§§
Grain	2.91E-04	1.83E-05	122.6	68.72	2.42	5.87 ± 0.37§§

Note: s.e. -- standard error.
*Radiogenic Pb corrected for common Pb.
†Calculated by assuming common $^{208}Pb/^{204}Pb$ = 36.7.
§Ages determined from calibration based on monazite standard 554.
#These ThO_2/Th ratios are less than the range of the calibration.
**Ages determined from calibration based on monazite standards 554 and 83-32.
††This ThO_2/Th ratio is at the upper limit of the range of the calibration.
§§Ages determined from calibration based on monazite standards 554 and Trebilcock.

9–18–05 1C). Greater Himalayan Crystalline complex sample AW 9–23–04 3 ages range from the Paleozoic to the Cenozoic; the Cenozoic dates are 26.8 ± 1.5, 20.1 ± 0.9, and 19.9 ± 1.3 Ma (1σ). AW 9–18–05 1C had a tight range of ages spanning from 6.59 ± 0.37 to 5.87 ± 0.37 Ma (1σ).

These results show that the MCT hanging-wall metasedimentary rocks southwest of the Kullu window underwent early Phanerozoic and mid-Cenozoic garnet-grade or greater metamorphism. Data for sample AW 9–13–03 3 show that the Tethyan Himalayan Sequence Haimanta Formation above the MCT underwent garnet-grade metamorphism ca. 41.5 Ma, and that this metamorphism may have persisted through ca. 28.5 Ma. The early Phanerozoic ages add to a growing body of evidence for Himalayan metamorphism at that time (e.g., Gehrels et al., 2003). We interpret the range of ages from the leucogranite sample (AW 9–23–04 3) to reflect inheritance; the youngest ages of ca. 27–20 Ma indicate the crystallization age. The ages of ca. 6.6–5.8 Ma obtained for the pegmatite intruding the Wangtu crystalline rocks (sample AW 9–18–05 1C) reflect either crystallization or cooling indicating early uplift along the Munsiari thrust and/or related thrusts.

THERMOCHRONOLOGY

We acquired $^{40}Ar/^{39}Ar$ thermochronologic data to constrain the cooling history of the MCT hanging wall to the southwest of the Kullu window; ~4–25 mg of biotite, muscovite, and potassium feldspar were separated, hand-picked, and irradiated along with sanidine from the 27.8 Ma Fish Canyon Tuff (Cebula et al., 1986: Renne et al., 1994) for 15–45 h at University of Michigan and McMaster University. The sanidine and the unknowns were step-heated in a double vacuum furnace and isotopic compositions of the released gas were measured using a VG 1200 mass spectrometer at UCLA. Data reduction was accomplished via the in-house program AGECAL.EXE, and uncertainties were calculated at the 1σ level. Results do not include uncertainties in J-factors or decay constants. Multidiffusion domain modeling (Lovera et al., 1989) of potassium feldspar data for four samples (AW 9–4-03 6A, AW 9–19–03 3, AW 9–24–03 5, and AW 9–27–03 1B) was conducted to extract thermal history information. Representative mica and feldspar results for a single sample are shown in Figure 14; age spectra, thermal history results, and data tables are in Supplemental File 6[6].

Excess argon affects these samples: only one muscovite spectra displays a plateau-type pattern, many biotite plateau ages are older than the range of the muscovite spectra for the same sample, and half of the individual analyses along K-feldspar spectra are older than mica ages for the same sample. Nonetheless, these data provide meaningful information on the cooling history of the MCT hanging wall.

Maximum Ar mica cooling ages for the MCT hanging-wall rocks above the Baragaon gneiss must be younger than ca. 40 Ma, because the age of a monazite included in garnet from sample AW 9–13–03 3, a garnet schist in these rocks, is ca. 41.5 Ma. Some mica cooling ages for these rocks are much older (AW 9–3-03 12, AW 9–7-03 5A), suggesting the presence of excess Ar, others are roughly equivalent to ca. 40 Ma (AY 9–3-03 12A, AW 9–4-03 6A), and the youngest mica age is 31.6 ± 0.6 Ma (muscovite

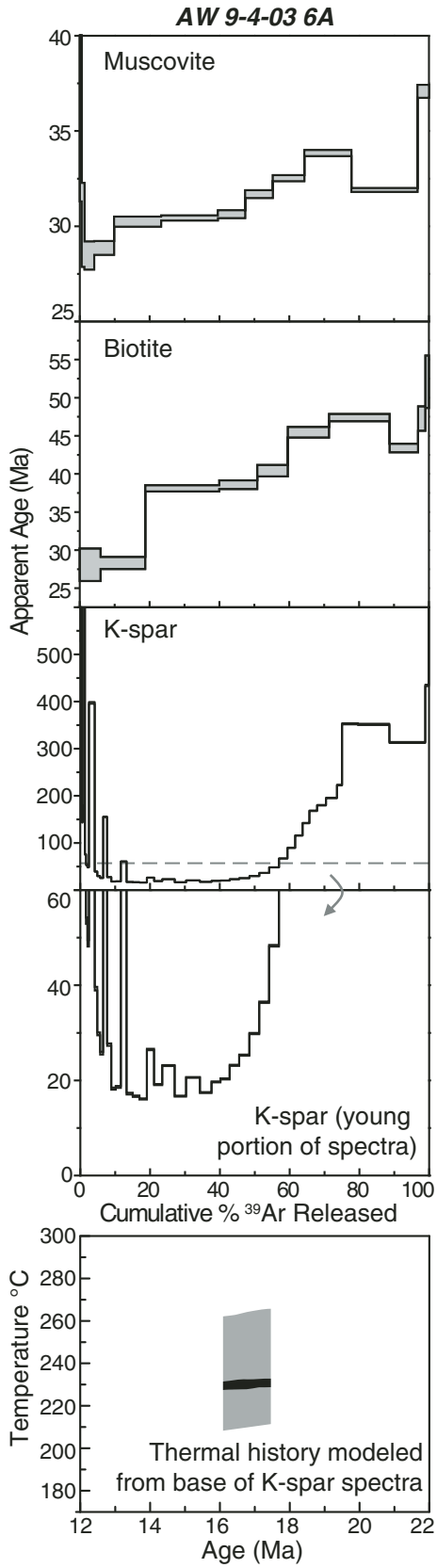

Figure 14. Representative $^{40}Ar/^{39}Ar$ thermochronology results for sample AW 9–4-03 6A. K-spar—K-feldspar.

[6]Supplemental File 6. PDF file of mica and K-feldspar $^{40}Ar/^{39}Ar$ thermochronology results for the Main Central thrust hanging wall to the southwest of the Kullu window. (A) Mica age spectra. (B) K-feldspar age spectra. (C) Thermal history results, from modeling of only that small (young) portion of the K-feldspar age spectra that may not be contaminated by excess Ar. (D) Mica data table. (E) K-feldspar data table. If you are viewing the PDF of this paper or reading it offline, please visit http://dx.doi.org/10.1130/GES00627.S7 or the full-text article on www.gsapubs.org to view Supplemental File 6.

from sample AW 9–4-03 6A). This suggests a maximum age of cooling below ~375 °C of ca. 30 Ma for the MCT hanging-wall rocks above the Baragaon gneiss. For the Baragaon gneisses, biotite cooling spectra for samples AW 9–4-03 3, AW 9–19–03 3, AW 9–26–03 1B, and AW 9–27–03 1B provide a maximum age for cooling below ~325 °C of ca. 50 Ma.

The K-feldspar age spectra, representing samples from the ca. 830 Ma gneiss, the Mandi granite, and the Baragaon gneiss, all show a single consistent pattern. With more than ~40% of the ^{39}Ar released, the individual analyses give ages much older than mica ages for these rocks and the ca. 41.5 Ma included monazite age, so the spectra after this point yield no interpretable age information. However, between 0% and ~40% gas release, all of the spectra form a roughly parabolic pattern, the minimum of which may be taken as a maximum age plateau. The minimum age along these parabolic age spectra is ca. 15–20 Ma or younger. We used the multi-domain diffusion model (Lovera et al., 1989) to model the minima of these age spectra parabolas, with resultant thermal histories that essentially represent a point in the cooling path. This point is consistently at ~220–230 °C at 13–19 Ma, representing the maximum time that these rocks were at these temperatures. The coherent cooling pattern in the Baragaon gneisses and the overlying Haimanta Group likely indicates that these rocks behaved as a single tectonic unit during Middle Miocene cooling.

DISCUSSION

Our mapping documents variations in structural style across thrust hanging walls in the Himachal Himalaya, showing large-magnitude internal shortening and penetrative deformation across almost all layers. U-Th-Pb geochronology of igneous and detrital zircon reveals layers that can be correlated across major structures including the MCT and STD, i.e., ca. 1.85 Ga orthogneiss and Neoproterozoic siliciclastic layers. Additional geochronologic and geochemical analyses show ca. 1.85 Ga, ca. 830 Ma, and ca. 470 Ma granitic rocks derived primarily from remelted continental crust, and reveal a previously unknown phase of granitic pegmatite intrusion ca. 8–6 Ma. These pegmatites are undeformed and crosscut Wangtu gneiss foliation, providing a minimum age for this fabric; a similar record of early Paleozoic granite crosscutting foliation in the STD hanging wall indicates fabric development here prior to the Cenozoic Himalayan orogeny. Combined *P-T* results and Th-Pb monazite geochronology show that garnet-producing metamorphism occurred in the early Phanerozoic and middle Cenozoic in the southern MCT hanging wall. We discuss the implications of these findings for the applicability of current Himalayan tectonic models to the Himachal region, the pre-Cenozoic stratigraphic framework, and the Cenozoic tectonic evolution.

Viability of Himalayan Tectonic Models in the Himachal Himalaya

Proposed Himalayan tectonic models make distinct predictions for the affinity of high-grade rocks, fault kinematics, exhumation history, along-strike changes in structural geometry and stratigraphy, and metamorphism (Fig. 2; Table 1; see review in the Introduction).

Most Himalayan tectonic models show the Greater Himalayan Crystalline complex as derived from the India plate, but in early channel flow models (Nelson et al., 1996; Hodges et al., 2001) these rocks represent Tibetan material that has tunneled southward into the Himalaya. Our detrital zircon results reveal similar age populations in the Greater Himalayan Crystalline complex, Haimanta Group of the lower Tethyan Himalayan Sequence, and the Outer Lesser Himalaya (Figs. 12 and 13). Because the Haimanta Group and Outer Lesser Himalaya are indisputably of India plate origin, these data support the interpretation that the Greater Himalayan Crystalline complex comprises Indian materials.

Wedge extrusion and early channel flow models show the STD as a solely top-to-the-north shear zone, whereas channel flow models that incorporate asymmetric thrust extrusion (e.g., Beaumont et al., 2004) and the tectonic wedging model show alternating top-to-the-north and top-to-the-south kinematics along this structure. Our results and previous investigations show alternating kinematics along the STD in the Himachal Himalaya (Choudhuri et al., 1992; Jain et al., 1999; Vannay et al., 2004; Webb et al., 2007).

The exhumation of the Greater Himalayan Crystalline complex occurs during STD activity (Early and Middle Miocene) in wedge extrusion and channel flow models, but after STD activity (post–Middle Miocene) in the tectonic wedging model. The overturning of the southernmost STD within the Phojal anticline requires deformation of the leading edge of the Greater Himalayan Crystalline complex after cessation of motion along the STD, so these frontal Greater Himalayan Crystalline complex rocks could not be eroded during STD activity. Furthermore, previous studies indicated that the leading edge of the Greater Himalayan Crystalline complex remains buried in parts of the Himachal Himalaya, an interpretation that has been repeatedly determined for the western Himachal geology (e.g., Thakur and Rawat, 1992; Frank et al., 1995; Fuchs and Linner, 1995; Thakur, 1998; DiPietro and Pogue, 2004; Yin, 2006).

The wedge extrusion and early channel flow models predict along-strike continuity of the three major Himalayan tectonic units (Lesser Himalayan Sequence, Greater Himalayan Crystalline complex, Tethyan Himalayan Sequence) and bounding faults (MCT, STD). In contrast, the tectonic wedging model shows a southern termination of the Greater Himalayan Crystalline complex where the MCT and STD merge, such that the southern MCT hanging wall is continuous with the STD hanging wall. The metamorphic pattern predicted by the models corresponds to their overall structural geometry: for the wedge extrusion and channel flow models, the MCT hanging wall consists of only Greater Himalayan Crystalline complex rocks and thus displays the famously inverted metamorphic field gradient of the Greater Himalayan Crystalline complex, whereas the tectonic wedging model predicts an MCT hanging wall with the inverted Greater Himalayan Crystalline complex metamorphic pattern in the north and the right-way-up Tethyan Himalayan Sequence metamorphic pattern to the south.

Critical tests of these predictions were provided by investigation of the southern MCT hanging wall and comparison with the northern MCT and STD hanging walls. Some results do not distinguish these three sheets. (1) Protolith lithologies are similar for all three hanging walls, and detrital zircon age populations from them show similar age spectra spanning from ca. 550 Ma to ca. 3500 Ma (Figs. 12 and 13). (2) U-Pb zircon and Th-Pb monazite geochronology confirm that early Paleozoic granites intrude the southern MCT hanging wall (Fig. 9; Table 4). Granitic rocks of this age intrude the STD hanging wall (e.g., Miller et al., 2001) and are also associated with the Greater Himalayan Crystalline complex where the original contacts are sheared (Frank et al., 1977). (3) *P-T* determinations of ~450–630 °C and ~7–9 kbar obtained for the southern MCT hanging wall (Table 3) are consistent with the metamorphic conditions of the structurally lowest levels of the Greater Himalayan Crystalline complex and the STD hanging wall (e.g., Vannay and Grasemann, 1998; Vannay et al., 1999; Chambers et al., 2009). (4) Th-Pb monazite dating and crosscutting relationships indicate the preservation of early Paleozoic metamorphic fabrics in the southern MCT hanging wall and STD hanging wall (Fig. 9E; Table 4; see also Marquer et al., 2000; Chambers et al., 2009), but records of metamorphism of this age are reported from the Greater Himalayan Crystalline complex in other parts of the Himalaya (e.g., Gehrels et al., 2003). Other results support the correlation of the southern MCT hanging wall with the STD hanging wall. (1) In contrast to the penetratively

deformed Greater Himalayan Crystalline complex, both the southern MCT and the STD hanging walls feature undeformed and weakly deformed granitic rocks (Figs. 8E and 9E). (2) Metamorphic grade increases upsection across the Greater Himalayan Crystalline complex along the well-studied Sutlej section at the east end of the Kullu window, matching the famous Greater Himalayan Crystalline complex inverted metamorphic field gradient observed across many Himalayan sections (Figs. 5 and 6C) (e.g., Vannay and Grasemann, 1998; Vannay et al., 1999). However, the southern MCT hanging wall only displays an inverted metamorphic field gradient within the ~2-km-thick MCT shear zone (our mapping; see also Grasemann et al., 1999; Gregory, 2004). Metamorphic grade decreases with increasing structural elevation across the rest of the southern MCT hanging wall from garnet grade to conditions below biotite grade, matching the STD hanging wall (Fig. 5) (Epard et al., 1995; Chambers et al., 2009; this study). (3) No fault separates the rocks of the southern MCT hanging wall from rocks of the Chamba syncline area to the northwest, where the same lithologies are overlain by Permian–Jurassic Tethyan sedimentary rocks along a depositional contact (Figs. 3, 6A and 6B) (e.g., Frank et al., 1995).

In summary, tectonic wedging is the only tectonic model that accommodates all of the following findings for the Himachal Himalaya: detrital zircon results that indicate Indian crustal affinity of the Greater Himalayan Crystalline complex, alternating top-to-the-north and top-to-the-south STD kinematics, Greater Himalayan Crystalline complex exhumation only after cessation of STD motion, and the connected southern MCT and STD hanging walls with shared Tethyan affinity and pattern of metamorphic isograds. An important further consideration is that previous workers have inferred Early–Middle Miocene exhumation of the Greater Himalayan Crystalline complex on the basis of the detrital record without consideration of the similar evolution of the lower Tethyan Himalayan Sequence and the Greater Himalayan Crystalline complex (e.g., DeCelles et al., 1998; White et al., 2002). Because the Greater Himalayan Crystalline complex and the lower Tethyan Himalayan Sequence (the Haimanta Group and associated granites) are similar in protolith lithologies, isotopic constraints, zircon age populations, and even metamorphic grade, these criteria cannot be used to distinguish between these two units at isolated bedrock exposures or in the detrital record. In the Himalayan mountains, high-grade metamorphism (kyanite, sillimanite, migmatite) and structural setting may distinguish these units. In the detrital record, only the high-grade mineral record is sufficient, but it cannot distinguish between high-grade minerals from Tso Morari in the northernmost Himalaya (e.g., Schlup et al., 2003) and those from the Greater Himalayan Crystalline complex.

Pre-Cenozoic Stratigraphic Framework of Northern India

A key task in unraveling the Cenozoic tectonic history of the northwest India Himalaya is the construction of a pre-Cenozoic stratigraphic framework. This task is commonly done by stacking younger units atop older units and including intrusive bodies. However, the magnitude of thrusting in the Himalaya, e.g., at least ~150 km along the combined distance of the Tons thrust and MCT, far exceeds the distance along which regular stratigraphy is maintained in the Indian craton (cf. Rao et al., 2000). Rather, ca. 2.5 Ga to Mesozoic bedrock is exposed over such distances. Since a high percentage of the deformed Himachal Himalaya rocks were Indian craton rocks (correlations discussed in the following), we made our pre-Cenozoic stratigraphic framework by first considering which fault-bound slices were at the surface as the India-Asia collision commenced and then determining the relative undeformed position of these slices from southwest to northeast.

Late Cretaceous and early Cenozoic rocks may be used as a proxy for the solid Earth's surface at the beginning of the collision, so sequences that are overlain by such rocks along sedimentary contacts are vertically constrained in the restored cross section. Three deformed sequences are thus constrained: (1) the Deoban and Damtha Groups, overlain by the latest Cretaceous–Middle Eocene Singtali-Subathu rocks; (2) the Outer Lesser Himalaya, also overlain by the latest Cretaceous–Middle Eocene Singtali-Subathu rocks; and (3) the Tethyan Himalayan Sequence, which contains Cretaceous strata (Figs. 3 and 4A). Of these three, the Deoban and Damtha Groups originated furthest to the southwest because (1) correlative Indian craton strata of the Vindhyan Supergroup underlie undeformed Sub-Himalayan stratigraphy beneath the Main Himalayan thrust (Powers et al., 1998); (2) Deoban rocks are deformed with Sub-Himalaya rocks in the frontal fold and thrust belt, e.g., Deoban rocks and depositionally overlying Subathu and Dharamsala rocks are thrust to the southwest along the Bilaspur thrust (e.g., Srikantia and Sharma, 1976); and (3) the Outer Lesser Himalaya moved southwest along the Tons thrust over Deoban and Damtha rocks locally capped by Singtali Formation and/or Subathu Formation rocks (e.g., West, 1939; Valdiya, 1980). Therefore the Tons thrust footwall rocks restore to the southwest relative to the hanging-wall rocks. Although the Outer Lesser Himalaya is thrust over the Sub-Himalaya, occupying the outer (i.e., farther south) portion of the Lesser Himalaya in much of the Himachal Himalaya, it represents a far-traveled thrust sheet relative to the Deoban and Damtha Groups. The Outer Lesser Himalaya originated to the southwest of the Tethyan Himalayan Sequence, as the northern Mesozoic sedimentary rocks of the latter represent the shelf and slope of the Indian Neotethys continental margin (e.g., Gaetani and Garzanti, 1991).

With the relative positions of the known surface fault slices thus constrained, we next correlate deformed rocks of matching age and lithology into single pre-deformation layers: First, our detrital zircon results and other data sets indicate that the Haimanta Group, Greater Himalayan Crystalline complex, and Lesser Himalayan Shimla Group represent deformed parts of a formerly continuous unit. These units share similar protoliths (Table 2), their Nd-Sr isotopic signatures match (see Supplemental File 2 [see footnote 2]), detrital zircon results from all three units show similar age spectra (Figs. 12 and 13), and the time window for deposition of all these units is narrow and equivalent, at the end of the Proterozoic. The older age limit is provided by the detrital zircon age data and ranges from ca. 550 to 800 Ma for different samples. The younger age limit is determined by the early Paleozoic intrusions and metamorphic events for both the Haimanta Group [our U-(Th)-Pb zircon and Th-Pb monazite geochronology] and the Greater Himalayan Crystalline complex (Walker et al., 1999; Miller et al., 2001), and overlying early Cambrian strata for both the Haimanta Group and the Shimla Group (e.g., Hughes and Jell, 1999; Myrow et al., 2006). Therefore a Neoproterozoic sedimentary sequence can be traced across both the MCT and STD. One significant distinction is that no evidence for early Paleozoic tectonism has been discovered in the Outer Lesser Himalaya, whereas both the Tethyan Himalayan Sequence Haimanta Group and the Greater Himalayan Crystalline complex record early Paleozoic granitic magmatism and garnet growth in metapelitic lithologies (our work; Frank et al., 1977; Miller et al., 2001; Gehrels et al., 2003). Since the Outer Lesser Himalayan rocks restore farther to the south than the other units, this difference may be accommodated if early Paleozoic tectonism was limited to the northernmost margin of India.

Second, we correlate the Baragaon granitic gneiss to the Wangtu granitic gneiss. The protolith of the discontinuous Baragaon granitic gneiss along the MCT shear zone crystallized ca. 1.85 Ga (Fig. 9). The Baragaon gneiss thus matches the Wangtu gneiss in age and lithology (Table 2; Fig. 9; Singh et al., 1994; Miller et al., 2000; Richards et al., 2005). This gives a second lithostratigraphic connection across the MCT. These rocks and the Jeori metasedimentary rocks are the oldest deformed units. We restore these to the base of the pre-collision stratigraphic framework.

Third, limited age constraints and lithologic similarities allow two additional tentative correlations: the Damtha Group may be laterally equivalent to the Berinag Group, and the upper, Neoproterozoic portion of the Deoban Group may be laterally equivalent to the Basantpur Formation of the Outer Lesser Himalaya (Figs. 12 and 13; Table 2).

The above considerations suggest a general model for a pre-deformation cross section involving a layer-cake stratigraphy gently tilted to the northeast, so that younger units progressively pinch out at the surface to the southwest (Fig. 15A). In a preferred model, we modify this layer-cake model such that the Deoban and Berinag-Damtha units pinch out to the northeast (Fig. 15B). The modifications are supported by the following considerations. (1) The Outer Lesser Himalaya is locally underlain by the quartzites and metavolcanics that may correlate with the Damtha-Berinag succession (the Darla volcanics, ~25 km to the northwest of Shimla). (2) The Outer Lesser Himalaya is locally underlain by ca. 1.85 Ga mylonitic granitic gneiss just to the southeast of the area shown in Figure 3 (Célérier et al., 2009a); this gneiss correlates with the ca. 1.85 Ga Wangtu-Baragaon gneiss. Further support for this model includes the juxtaposition of the Baragaon granitic gneiss directly below the Haimanta Group along the base of the southern MCT hanging wall (Figs. 3 and 4). The Baragaon appears to also underlie the Greater Himalayan Crystalline complex in the same fashion in Himachal along the Tons River (Figs. 3 and 6C) and to the northwest along the Kishtwar window (Stephenson et al., 2001). At the Nanga Parbat and Indus Syntaxes of the Pakistan Himalaya, rocks correlative to the Outer Lesser Himalaya–Haimanta Group–Greater Himalayan Crystalline complex overlie ca. 1.85 Ga granites and older rocks along an unconformity (e.g., DiPietro et al., 1999; DiPietro and Isachsen, 2001; DiPietro and Pogue, 2004).

This reconstruction of relative pre-Cenozoic structural positions explains the curious thrusting of younger rocks atop older rocks in the Himachal Himalaya. In most fold and thrust belts, older rocks are thrust over younger rocks because deep rocks are thrust over shallow rocks and older rocks commonly occur deeper than the younger rocks (e.g., Dahlstrom, 1969). However, in the Himachal Himalaya the opposite relationship is commonly observed in the Himachal Himalaya, e.g., the northern portions of both the Tons thrust and the MCT place Neoproterozoic rocks atop Mesoproterozoic and/or Paleoproterozoic rocks. The pre-Cenozoic relative positions of the Deoban and Damtha Groups, the Outer Lesser Himalaya, and the Tethyan Himalayan Sequence shows that younger rocks originated at equal and greater depth in the northeast compared with older rocks in the southwest. Therefore in general, from northeast to southwest young rocks thinned and pinched out such that progressively older rocks were exposed at the surface at the start of Cenozoic Himalayan shortening.

Structural Origin of the Kullu and Uttarkashi Windows

The elongated dome may represent a fault-propagation fold, with the Munsiari thrust as the propagating fault. We speculate that the tip line of the Munsiari thrust may cut upsection and perhaps locally offset the MCT (as shown in Fig. 3 along the southern margin of the Kullu window; see also Fig. 4). We further infer that the Chaura thrust is folded with this anticlinorium (Figs. 3 and 4). The thrust has been mapped within 10 km of the Sutlej River along its northeastern trace (Singh and Jain, 1993; Jain et al., 2000; Chambers et al., 2008; our observations); the steep to overturned southwestern trace shown in Figures 3 and 4 is inferred. Although the Munsiari thrust generally dips shallowly or moderately to the northeast, the fault is locally folded. For example, the fault is folded dips along the Tons River near Sankri, such that it dips to the southwest at ~1 km west of Sankri (Fig. 3) (Jain and Anand, 1988). The Munsiari fault is inactive, at least locally, as it is deformed by younger, deeper structures.

We interpret the structural package of deformed Munsiari Group rocks as an antiformal stack (Fig. 4). This interpretation is based upon our interpreted Chaura thrust geometry and the local deformation of the Munsiari thrust coupled with rapid, recent uplift of Munsiari Group rocks. The antiformal stack has six horses as drawn, the Jeori and Wangtu rocks representing two long horses. In this interpretation the Wangtu and Jeori rocks originate at the same structural level, and the total shortening across the stack would equal the length of all horses minus the deformed length, or ~150 km.

The geometric relationship of the Tons thrust to the Berinag thrust and their kinematic histories are key factors for determining the structural evolution of the Uttarkashi half-window, but these are poorly understood. The Tons and Berinag thrusts may represent a single thrust that cut upsection to the south, thus transporting progressively younger hanging-wall rocks to the south (Fig. 16). Alternatively, these may be distinct structures that were juxtaposed by successive footwall accretion or out-of-sequence thrusting.

Kinematic Reconstruction

We present a schematic Cenozoic tectonic history of the Himachal Himalaya by progressively deforming our preferred pre-Cenozoic stratigraphic framework (Fig. 17). Contraction and crustal thickening across

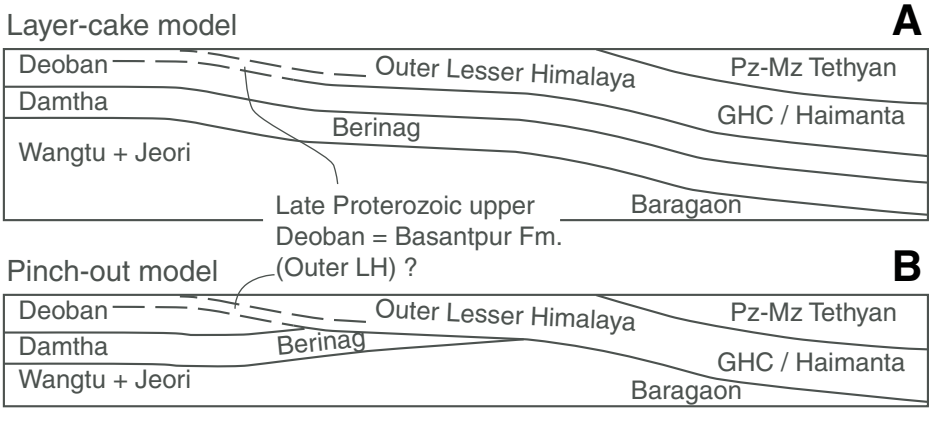

Figure 15. Schematic stratigraphic models of the Himachal Himalaya prior to the India-Asia collision. (A) Layer-cake model based on constraints on the surface geology and stratigraphic layering correlated by age and lithology. Pz-Mz—Paleozoic–Mesozoic; GHC—Greater Himalayan Crystalline complex. (B) Pinch-out (preferred) model, based on the above considerations and further interpretations of juxtaposed units (discussed in the text). Baragaon—Baragaon granitic gneiss, Berinag—Berinag Group, Damtha—Damtha Group, Deoban—Deoban Group, Haimanta—Haimanta Group and associated ca. 850 Ma and ca. 500 Ma granites, Jeori—Jeori metasedimentary rocks, Wangtu—Wangtu granitic gneiss.

the Tethyan Himalayan Sequence and the associated burial and metamorphism of the Tethyan Himalayan Sequence and Greater Himalayan Crystalline complex was underway by 45–40 Ma and persisted through the Oligocene (Wiesmayr and Grasemann, 2002; Catlos et al., 2007; Chambers et al., 2009; our results). Emplacement of the Greater Himalayan Crystalline complex between the MCT and STD was accomplished by the end of the Middle Miocene, as cessation of plastic deformation along the STD in this period is recorded by $^{40}Ar/^{39}Ar$ muscovite ages in the immediate STD hanging wall and footwall (Vannay et al., 2004; Thiede et al., 2005). We show a tectonic wedging kinematic evolution for Greater Himalayan Crystalline complex emplacement; the preceding discussion details why this is the only possibility among current proposed tectonic models. Top-to-the northeast slip along the STD likely surfaced to the north along the GCT (Fig. 2). Up until the Miocene, the Himalayan fold-and-thrust belt is thin-skinned, but by the Middle Miocene the Baragaon gneiss was accreted from the Indian basement into the MCT zone.

Continued accretion of basement slices in the Late Miocene resulted in stacking of the Wangtu and Jeori thrust horses. The folding of the Phojal anticline at the leading edge of the Greater Himalayan Crystalline complex must have occurred prior to this significant downcutting of the Himalayan sole thrust. We also show the accretion of supracrustal thrust horses of the Tons thrust sheet (the Outer Lesser Himalaya) and the Berinag thrust sheet into the growing thrust wedge in the Late Miocene. The accretion of the Tons thrust sheet at this time offers an alternative to our early interpretation of Tons thrust emplacement in the Eocene–Oligocene (see Célérier et al., 2009a). Some structures deforming the Himalayan foreland basin during this period are preserved in the Bilaspur thrust hanging wall. In the Pliocene–Quaternary, additional basement slices are incorporated into the growing thrust wedge. These horses have yet to be exposed at the surface. The combination of basement horse stacking and out-of-sequence faulting along the Munsiari thrust warped the MCT and created the Kullu window. Likewise, the duplexing of Damtha and Deoban Group rocks in the Bilaspur thrust hanging wall warped the overlying Tons thrust and MCT hanging walls into the Narkanda half-window and Shimla klippe. Forward propagation of the Himalayan thrust wedge incorporated additional sections of the foreland basin into fold and thrust belts.

CONCLUSIONS

This work examines the viability of models for the emplacement of the Himalayan crystalline core (i.e., the Greater Himalayan Crystalline complex) between two north-dipping faults (i.e., the MCT and STD). The differing predictions of the main models, i.e., wedge extrusion (e.g., Burchfiel and Royden, 1985), channel flow/focused denudation (e.g., Beaumont et al., 2001), and tectonic wedging (e.g., Webb et al., 2007) (Table 2), were examined in the Himachal Himalaya, where the rocks carried along the MCT change from Greater Himalayan Crystalline complex rocks in the east to Tethyan Himalayan Sequence rocks in the west (e.g., Thakur, 1998; DiPietro and Pogue, 2004; Yin, 2006). Recent field mapping (Webb et al., 2007) shows that the MCT and STD intersect in this region, bounding the leading edge of the Greater Himalayan Crystalline complex. Southwest of this branch line, the MCT carries Tethyan Himalayan Sequence rocks directly over Lesser Himalayan Sequence rocks, as confirmed in this work by metamorphic variations and detrital zircon geochronology. This tectonic framework is consistent with a tectonic wedging emplacement of the Greater Himalayan Crystalline complex.

We determined stratigraphic correlations across the MCT and STD, leading to a new model of the pre–India-Asia collision stratigraphic

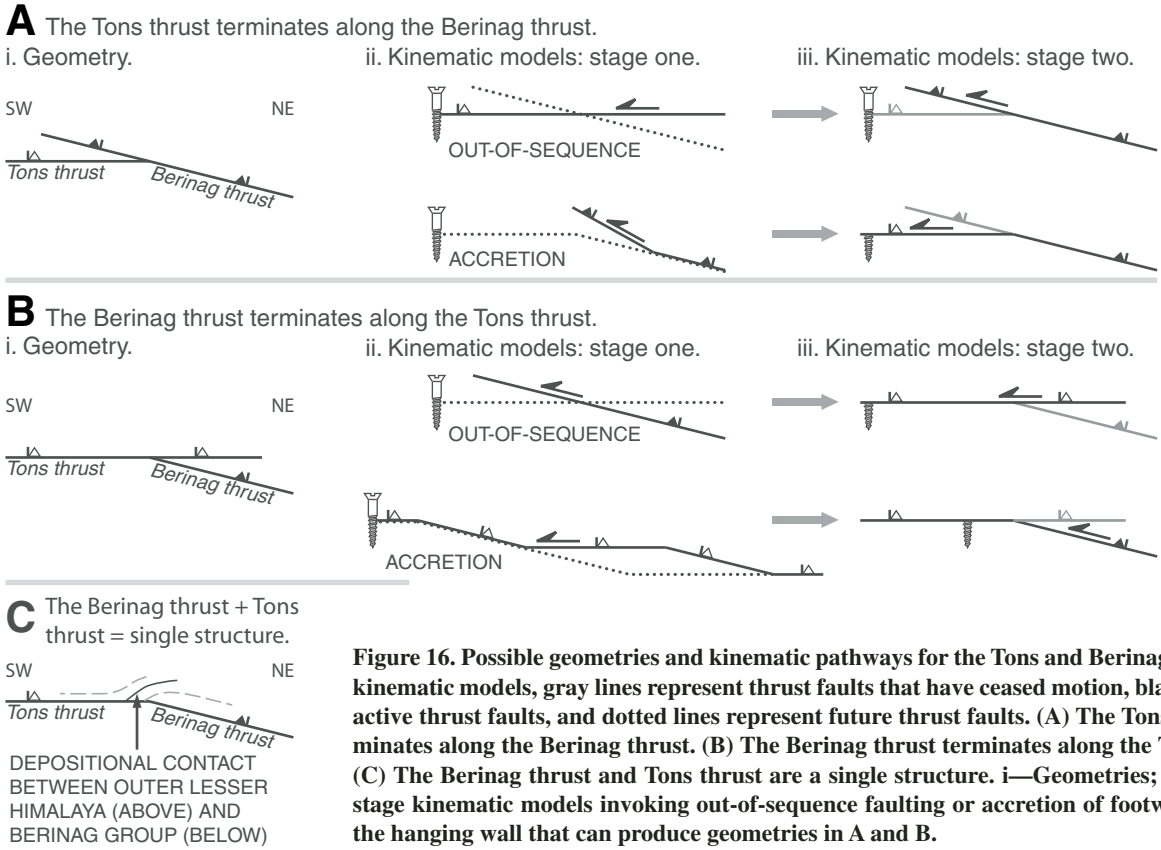

Figure 16. Possible geometries and kinematic pathways for the Tons and Berinag thrusts. In kinematic models, gray lines represent thrust faults that have ceased motion, black lines are active thrust faults, and dotted lines represent future thrust faults. (A) The Tons thrust terminates along the Berinag thrust. (B) The Berinag thrust terminates along the Tons thrust. (C) The Berinag thrust and Tons thrust are a single structure. i—Geometries; ii, iii—two-stage kinematic models invoking out-of-sequence faulting or accretion of footwall slices to the hanging wall that can produce geometries in A and B.

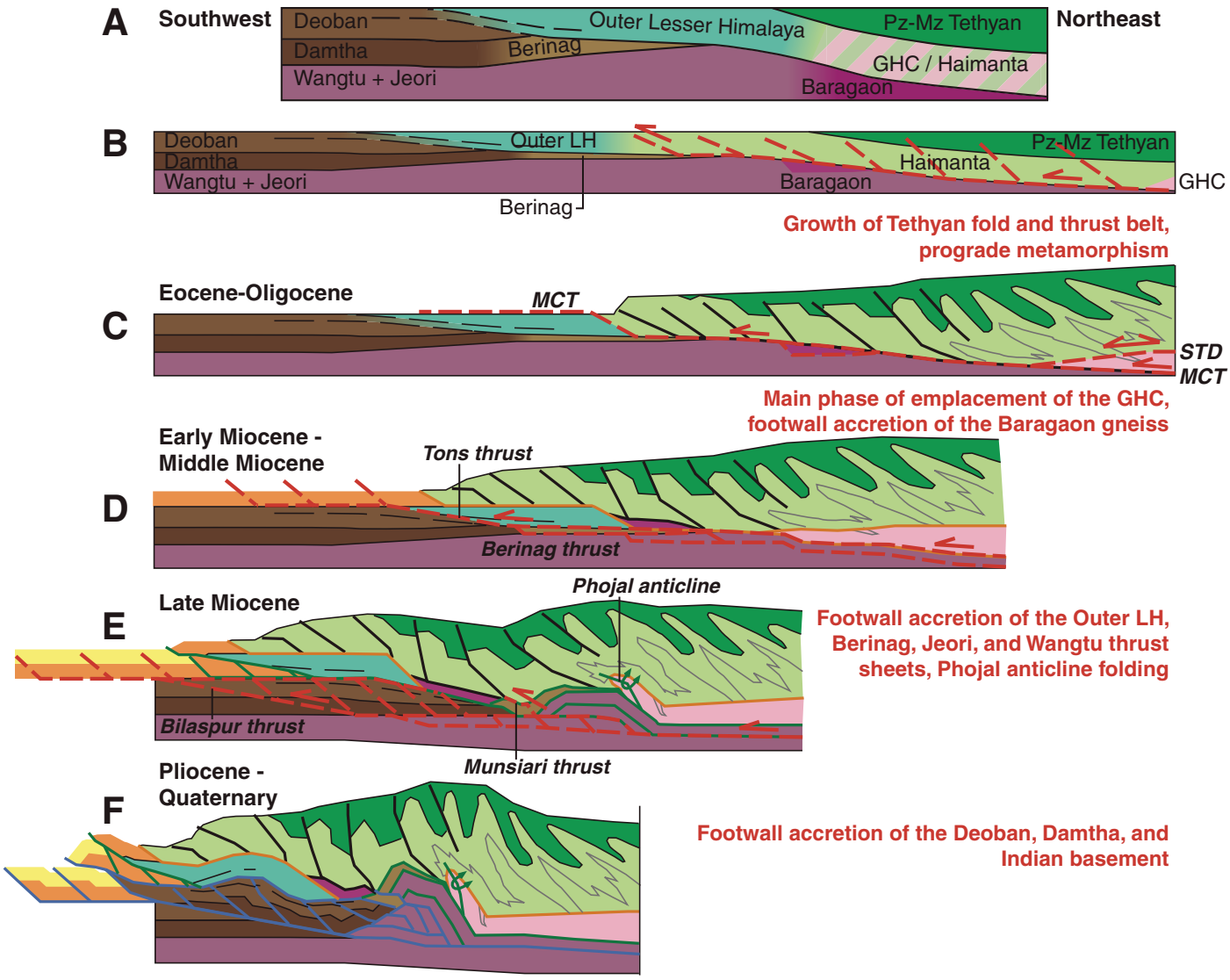

Fig. 17. Schematic reconstruction of the Himachal Himalaya based on the structural framework along the line A–A′ of Figure 3. (A) Preferred pre-deformation stratigraphic model, taken from Figure 15B. MCT—Main Central thrust; LH—Lesser Himalaya; STD—South Tibet detachment; other abbreviations as in Fig. 15. (B) Stretched version of part A diagram showing pre-deformation traces of Tethyan thrust faults. (C)–(F) Shortening stages, progressing to the present (F represents a schematic version of the cross section of Fig. 4A).

framework of this region. The restored positions of various stratigraphic levels vary from north to south, such that younger rocks to the north were commonly deeper than older rocks to the south. These geometries explain the thrusting of younger rocks over older rocks in the Himalaya. The protoliths and detrital zircon records of Neoproterozoic rocks in the Lesser Himalaya, Greater Himalayan Crystalline complex, and Tethyan Himalaya are similar, suggesting that these units formed a single stratigraphic horizon prior to Cenozoic tectonism. Our new tectonic model shows three main phases in the Cenozoic construction of the Himachal Himalaya: early contraction and crustal thickening, emplacement of the Greater Himalayan Crystalline complex as a tectonic wedge between the MCT and STD, and accretion of thrust slices from the subducting Indian plate to the growing orogenic wedge.

ACKNOWLEDGMENTS

We thank editors Dennis Henry and Michael Williams and two anonymous reviewers for their constructive feedback and guidance. Stephanie Briggs, George Jarzebinski, Frank Kyte, Oscar Lovera, Gilles Peltzer, Axel Schmitt, and Victor Valencia provided technical advice and fruitful discussions. Field support from C.S. Dubey, Ashok Kumar, Subhash Kumar, Sandeep Saod and his team, Braj Sharma, Manoj Tiwari, and especially Paul Burgess, Prashant Dubey, and Courtney Gregory, is gratefully acknowledged. Discussions with Om Bhargava, Peter Bird, Jen Chambers, Joe DiPietro, Darrell Henry, Brian Horton, Nigel Hughes, David Jacobs, Arvind Jain, Remy Leger, Ryan McKenzie, Bill Moore, Alex Robinson, Yongwei Sheng, Justin Simon, Birendra Singh, Sandeep Singh, and Mike Taylor all led to improvements in this work. This research was a grant from by the Tectonics Program, U.S. National Science Foundation, and a start-up fund from Louisiana State University.

APPENDIX 1. EXPANDED DESCRIPTION OF LITHOLOGIC UNITS

Major lithologic units in the study area are the Cretaceous and Cenozoic Sub-Himalayan Sequence, the Proterozoic and Cambrian Lesser Himalayan Sequence, the high-grade Greater Himalayan Crystalline complex, and the Neoproterozoic to Mesozoic Tethyan Himalayan Sequence (Figs. 3 and 4) (Table 2). These units were described briefly (see text discussion of Lithologic Units); expanded descriptions are provided here.

Sub-Himalayan Sequence

This sequence consists of lower shallow-marine strata and upper continental deposits; the two subunits are separated by an Oligocene unconformity (Table 2). The lower subunit is in depositional contact with the underlying Lesser Himalayan Sequence (see following) in the Main Central thrust (MCT) hanging wall ~15 km north and ~25 km west of Shimla (Pilgrim and West, 1928; West, 1939; Srikantia and Sharma, 1976) and in the footwall of the Tons thrust ~50 km north and ~20 km east-southeast of Dehra Dun (Jain, 1972; Bhargava, 1976; Valdiya, 1980) (Fig. 3). The relationships require that the MCT and Tons thrust have moved over the very top of the Proterozoic–Cambrian units of the Lesser Himalayan Sequence.

Lesser Himalayan Sequence

The Lesser Himalayan Sequence consists of (1) the Neoproterozoic–Cambrian Outer Lesser Himalayan Sequence in the hanging walls of the Krol and Tons thrusts, (2) the Paleoproterozoic to Neoproterozoic Damtha and Deoban Groups in the hanging wall of the Bilaspur thrust and the footwalls of the Tons and Berinag thrusts, (3) the Paleoproterozoic Berinag Group in the hanging wall of the Berinag thrust, and (4) the Paleoproterozoic Munsiari Group dominantly in the hanging wall of the Munsiari thrust (Table 2) (Figs. 3 and 4). Because these units are juxtaposed by faults, understanding the age relationships requires unraveling the history of the bounding faults. Here we describe the age and lithology of each unit.

Neoproterozoic–Cambrian Outer Himalayan Sequence

This 7.5-km-thick unit consists of, from bottom to top, the Darla volcanic unit, Basantpur Formation, Shimla Group, Krol Group, and Tal Formation (Table 2) (Valdiya, 1980; Kumar and Brookfield, 1987; Jiang et al., 2003). Its basement as observed in the Garhwal Himalaya southeast of our study area consists of 1.85 Ga augen gneiss (Célérier et al., 2009a) (Fig. 1). The Darla unit is only exposed near Shimla below the Basantpur Formation. The Basantpur Formation consists of limestone, siltstone, shale, and locally minor slate (Table 2). The Shimla Group comprises shale, siltstone, sandstone, minor graywacke, conglomerate, and tillite (Pilgrim and West, 1928; Valdiya, 1970; Srikantia and Sharma, 1976; Kumar and Brookfield, 1987). It has been correlated with the Paleoproterozoic Damtha Group in the MCT footwall (e.g., Valdiya, 1995) or alternatively with the Neoproterozoic Haimanta Formation in the MCT hanging wall (e.g., Kumar and Brookfield, 1987; Miller et al., 2001). As shown here, our U-Pb detrital-zircon dating supports correlation of the Shimla and Haimanta rocks. The Krol Group, dominated by dolostone and limestone, is below the Tal Formation; the latter comprises sandstone and siltstone and contains early Cambrian trilobites (Myrow et al., 2003).

Paleoproterozoic to Neoproterozoic Damtha and Deoban Groups

The Damtha Group comprises siliciclastic strata and the Deoban Group is dominated by carbonates with shale and siltstone in its uppermost section (Table 2). The latest Paleoproterozoic to Neoproterozoic age of the Deoban Group is constrained from fossils (mainly stromatolite); these rocks depositionally overlie the Damtha Group (Valdiya, 1995).

Paleoproterozoic Berinag Group

The Berinag Group consists dominantly of quartz arenite locally interbedded with metabasalt flows and minor slate and intruded by sills and dikes (e.g., V.P. Sharma, 1977; Valdiya, 1980; Miller et al., 2000). The metaigneous rocks underwent greenschist facies metamorphism (Miller et al., 2000).

Paleoproterozoic Munsiari Group

The unit consists of two subunits bounded by two thrusts at their bases: the upper Wangtu gneiss bounded by Chaura thrust and the lower Jeori gneiss bounded by the Munsiari thrust (e.g., Singh and Jain, 1993; Valdiya, 1995; Jain et al., 2000; Chambers et al., 2008). The Wangtu gneiss is dominated by orthogneiss with minor intercalated metasediments, whereas the Jeori gneiss is mostly paragneiss (Table 2). Undeformed pegmatitic felsic dikes with garnet and centimeter-scale muscovite books and feldspar locally crosscut the Wangtu gneissic foliation (Fig. 7B). Kyanite and sillimanite in metasediments are present in the Jeori and the lower part of the Wangtu gneisses (Fig. 5). The Munsiari rocks underwent Late Miocene prograde metamorphism and record an inverted temperature profile (~600–700 °C) with a normal pressure gradient (~9–7 kbar) (Vannay and Grasemann, 1998; Vannay et al., 1999, 2004; Caddick et al., 2007; Chambers et al., 2008). Apatite fission track ages as young as ca. 1 Ma and $^{40}Ar/^{39}Ar$ muscovite ages as young as ca. 5 Ma are recorded from the Munsiari rocks (Fig. 4A) (Jain et al., 2000; Thiede et al., 2004, 2005, 2009; Vannay et al., 2004), which are probably related to recent and possibly active development of a duplex system below the Kullu window.

Greater Himalayan Crystalline Complex

The Greater Himalayan Crystalline complex in the MCT hanging wall is ~7–9 km thick and consists of paragneiss, schist, and orthogneiss intruded by minor Tertiary leucogranites concentrated mostly in its upper 2–3 km. Metasediments in the complex are younger than 830 Ma, as constrained by U-Pb detrital-zircon dating (Richards et al., 2005; our observations, see following) and orthogneiss was crystallized in the early Paleozoic, based on Rb-Sr whole-rock isochron dates (Frank et al., 1977).

An inverted metamorphic field gradient is observed along the Sutlej River, which is expressed by garnet-staurolite-bearing rocks at the base, kyanite and sillimanite in the middle, and migmatitic rocks near the top across the Greater Himalayan Crystalline complex (Fig. 5) (Vannay and Grasemann, 1998). Oxygen isotope thermometry indicates that peak temperatures at the base of the Greater Himalayan Crystalline complex are ~600 °C and rise to ~750 °C in the uppermost section; calculated pressures from the garnet-muscovite-aluminosilicate-plagioclase barometer are constant across the Greater Himalayan Crystalline complex at ~8 kbar (Fig. 4A) (Vannay et al., 1999). Northwest of the Sutlej River near Tos, Manali, and Khoksar, the Greater Himalayan Crystalline complex rocks yield peak temperatures ranging from ~550 to ~700 °C and pressures ranging from ~6 to ~10 kbar (Epard et al., 1995; Jain et al., 1999; Walker et al., 1999; Wyss, 2000; Verma et al., 2005). The estimated temperatures from the northwestern area were calculated from garnet-hornblende and garnet-biotite pairs and may represent minimum values of the peak metamorphic conditions due to later retrograde metamorphism (Vannay and Grasemann, 1998).

The U-Pb dating of monazite grains from kyanite schist near Manali yields a discordia line on a concordia diagram with upper and lower intercepts of 498.6 ± 20.2 Ma and 30.1 ± 1.3 Ma, respectively (Walker et al., 1999). The older intercept age was likely induced by intrusion of Cambrian–Ordovician granites (Frank et al., 1977, 1995). Th-Pb spot ages for monazite grains from Greater Himalayan Crystalline complex metapelite along the Sutlej River range from 39.6 ± 2.8 Ma to 22.8 ± 0.4 Ma (E. Catlos, 2004, personal commun.); monazite Th-Pb spot ages of ca. 44–19.5 Ma were obtained from a similar section along the Bhagirathi River (Foster et al., 2000; Catlos et al., 2007). The Greater Himalayan Crystalline complex rocks in the study area were exhumed to below ~400 °C in the Early Miocene, as indicated by $^{40}Ar/^{39}Ar$ muscovite ages, but the metamorphic complex did not cool down below 110–60 °C until ca. 2–4 Ma, as indicated by the young zircon and apatite fission track ages (Jain et al., 2000; Schlup, 2003; Vannay et al., 2004; Thiede et al., 2004, 2005, 2009).

Tethyan Himalayan Sequence

This sequence consists of the Neoproterozoic–early Cambrian Haimanta Group, Cambrian Parahio Formation, and remaining Paleozoic–Mesozoic strata above. The Haimanta Group comprises metasedimentary rocks and is intruded by early Paleozoic granites (Table 2) (e.g., Jäger et al., 1971; Frank et al., 1995; Miller et al., 2001; Chambers et al., 2009). Its basement is likely the Paleoproterozoic Baragaon gneiss in the MCT shear zone directly below the unit (Bhanot et al., 1978; Miller et al., 2000; this study). South of the MCT–South Tibet detachment (STD) branch line, metamorphic grades of the Haimanta Group decrease upward in the MCT hanging wall, whereas north of the branch line the Haimanta rocks show a similar upward decrease in metamorphic grade in the STD hanging wall. In both cases, the decreasing metamorphic grade is expressed by the presence of garnet schist in the basal section and phyllite and slate in the upper section, as well as the regional pattern of metamorphic isograds (Fig. 5). Grade progression within the shear zones is distinct: an inverted metamorphic field gradient occurs in the 2-km-thick MCT shear zone (Grasemann et al., 1999; Gregory, 2004; Law et al., 2010), whereas metamorphic patterns are right-way-up across the STD (Vannay and Grasemann, 1998). Estimated *P-T* conditions in the basal Haimanta Group are 5–8 kbar and 450–660 °C (Epard et al., 1995; Vannay and Grasemann, 1998; Vannay et al., 1999; Jain et al., 1999; Wyss, 2000; Chambers et al., 2009; our observations, see following). In contrast, illite crystallinity indicates that the upper Haimanta Group

underwent metamorphism at temperatures of only 200–300 °C (Wiesmayr and Grasemann, 2002). Using Raman spectroscopy of carbonaceous material, Gregory (2004) obtained temperatures of 499 ± 5 °C near Mandi and 520 ± 4 °C and 529 ± 9 °C near Narkanda for garnet schist in the basal Haimanta Group.

The U-Pb monazite dating of Haimanta garnet schist suggests that it underwent prograde metamorphism at 34–27 Ma (Chambers et al., 2009). Sparse $^{40}Ar/^{39}Ar$ muscovite thermochronology yields Early to Middle Miocene ages in the basal portions of the Haimanta Group (Schlup, 2003; Vannay et al., 2004; Thiede et al., 2005; Chambers et al., 2009). Zircon fission track ages of the Haimanta Group rocks range from Late Triassic to Early Miocene, and apatite ages span the Middle Miocene to Pliocene (Schlup, 2003). Late Miocene to Pliocene apatite ages are dominantly from the lowermost part of the Haimanta Group (Lal et al., 1999; Schlup, 2003; Vannay et al., 2004; Thiede et al., 2009).

The Cambrian Parahio Formation is dominated by shale, siltstone, fine sandstone, and minor carbonates. It likely represents continuous sedimentation of the Haimanta Group (Myrow et al., 2006). The remaining Paleozoic and Mesozoic Tethyan Himalayan Sequence strata are above an Ordovician angular unconformity (e.g., Wiesmayr and Grasemann, 2002). In the Tandi-Chamba and Tso Morari areas (western and northeastern parts of our map area in Fig. 3), Cambrian–Carboniferous strata are missing, whereas Permian and younger strata directly overlie the Haimanta Group (Fig. 3) (e.g., Steck, 2003).

Nd and Sr Chemostratigraphy

Results from previous investigations of the Nd and Sr isotopic characteristics of pre-Cenozoic rocks from the Himachal Himalaya and other Himalayan regions show two largely distinct groups in Nd and Sr isotopic space (Table 2; Supplemental File 2 [see footnote 2]). These groups can be distinguished by age: Mesoproterozoic and older rocks yield $\varepsilon_{Nd}(500) <\sim -14$ and a broad range of $^{87}Sr/^{86}Sr$ (500) values, whereas Neoproterozoic and younger rocks yield $\varepsilon_{Nd}(500) >\sim -14$ and a narrow range of $^{87}Sr/^{86}Sr$ (500) values. The only exception is the Berinag Group metabasalts, which are consistent with the Neoproterozoic and younger group despite an age of ca. 1.8 Ga (Supplemental File 2 [see footnote 2]) (Bhat and Le Fort, 1992, 1993; Miller et al., 2000). Data for Berinag Group quartzites are consistent with the Mesoproterozoic and older group of Himalayan rocks (Ahmad et al., 2000; Richards et al., 2005).

APPENDIX 2. EXPANDED DESCRIPTION OF REGIONAL TECTONIC FRAMEWORK

The first-order structures in the Himachal Himalaya were described, with emphasis on the Main Central thrust (MCT) and South Tibet detachment (STD) (see text discussion, Regional Tectonic Framework). Here we offer some additional information on those two major structures and comprehensive discussion of other structures.

Sub-Himalayan Thrust Zone

The Sub-Himalayan thrust zone in the Himachal Himalaya is bounded by the Main Frontal thrust (MFT) below and the Krol and Mandi thrusts above. The bounding faults of the thrust zone are not parallel; the northern Krol-Mandi thrust system defines the Dehra Dun reentrant in the south and the larger Kangra reentrant in the north (Fig. 3). The MFT places Neogene–Quaternary strata over the modern Indo-Gangetic Plain deposits and has an estimated Quaternary slip rate of 10 ± 6 mm/yr (Fig. 3) (Kumar et al., 2006). The Krol thrust places Proterozoic–Cambrian strata of the Outer Lesser Himalayan Sequence over Paleogene–Quaternary strata of the Sub-Himalayan Sequence, whereas the Mandi thrust juxtaposes Proterozoic strata of the Lesser Himalayan Sequence (Berinag, Deoban, Damtha units) over Paleogene–Quaternary strata of the Sub-Himalayan Sequence (Srikantia and Sharma, 1976; Powers et al., 1998; Raiverman, 2000). The Sub-Himalayan thrust zone comprises a southwestern subzone exposing Middle Miocene and younger strata and a northeastern subzone dominated by Early Miocene and older strata (Fig. 3). These subzones are separated by the Bilaspur and Palampur thrusts. The Bilaspur thrust along its southern trace carries Paleogene–Early Miocene strata (Subathu, Lower Dharamsala units) over Middle Miocene–Quaternary strata (Upper Dharamsala, Siwaliks units). The thrust cuts downsection of the hanging wall northwestward, exposing the Proterozoic Deoban Group and the Paleogene Subathu Formation. The slip along the Bilaspur fault is partitioned between the Mandi thrust and fault-fold systems linked to the Palampur thrust. The Palampur thrust places Paleogene–Miocene strata (Subathu, Dharamsala, Lower Siwalik units) over Middle Miocene–Quaternary strata (Siwaliks).

Internal structures of the southwestern subzone are complicated, expressed by southwest-directed thrusts, northeast-directed backthrusts, and tight folds at which thrusts terminate (Figs. 3 and 4A; Supplemental File 1A [see footnote 1]). The presence of backthrusts suggests the development of several thrust wedges in the thrust zones. As thrusts tend die out into folds, fault-propagation folds must also be present in the area. A minimum amount of shortening from the Main Frontal thrust to the Palampur thrust in the Kangra Reentrant is ~23 km, which is equivalent to ~22% shortening strain (Powers et al., 1998).

The Bilaspur-Palampur thrust systems and the Krol-Mandi thrust systems join in the northwest and southeast in map view, bounding the northeastern Sub-Himalayan thrust belt between. This map pattern is of a typical forward-propagating thrust duplex, with the Krol-Mandi thrust zone as an apparent roof fault and the Mandi-Bilaspur thrust zone as an apparent floor fault. However, a closer examination of the Krol-Mandi thrust zone and its footwall strata suggests that the Krol-Mandi thrust zone is an out-of-sequence structure. This conclusion is derived from the map relationship, where the Krol-Mandi thrust zone truncates beds in its footwall and locally cuts downsection in the thrust transport direction; the latter is a typical relationship for an out-sequence thrust, but contradicts the forward-propagating duplex system in which beds directly below the root thrust are parallel to the fault above (Boyer and Elliott, 1982; cf. Morley, 1988; Yin and Kelty, 1991).

Tons Thrust

The Tons thrust exhibits antiformal geometry and places the Outer Lesser Himalayan Sequence over the Deoban and Damtha Groups of the Lesser Himalayan Sequence; the latter are locally overlain by Cretaceous–Eocene strata (Fig. 3) (e.g., West, 1939; Srikantia and Sharma, 1976; Valdiya, 1980; Célérier et al., 2009a). The fault merges with the MCT to the north and the Krol thrust to the south along the Sutlej River. It may also link with the Berinag thrust in the southern Uttakashi area, as shown in Figure 3.

Berinag Thrust System

The Berinag thrust is exposed in the Kullu window where it appears in both the hanging wall and footwall of the Munsiari thrust (Fig. 3) (V.P. Sharma, 1977; Tewari et al., 1978; Valdiya, 1980; Srivastava and Mitra, 1994; Vannay and Grasemann, 1998; Vannay et al., 2004; Célérier et al., 2009a). In the Munsiari hanging wall the Berinag thrust is antiformal and places the Berinag Group over the Wangtu gneiss, whereas in the Munsiari footwall, the same fault exhibits synformal geometry and places the Berinag Group over the Damtha Group. As implied by this relationship, the Berinag thrust is offset by the underlying Munsiari thrust bounding the base of the Wangtu gneiss (Fig. 3).

In the Uttarkashi half-window, the southern exposure of the thrust places the Berinag Group over the Damtha Group and the northern exposure of the thrust places the Berinag Group over the Wangtu gneiss. The Berinag thrust merges with the MCT, as observed in the Kullu window, and the thrust is truncated by the Munsiari thrust, based on reinterpretation of the existing map (Jain and Anand, 1988) and our field observations. The systematic change in juxtaposition relationship from north to south across the Berinag thrust in the Kullu window and Uttarkashi half-window areas requires the fault to climb upsection from a detachment horizon along the Berinag-Wangtu contact to a north-dipping footwall ramp across the Berinag and Damtha strata to link with a higher footwall flat on top of the Damtha Group.

The linking of the Tons and Berinag thrusts in the westernmost Uttarkashi half-window led to the correlation of the Nagthat Formation in the Shimla Group (Table 2) with the Berinag Group (e.g., Valdiya, 1980; Srivastava and Mitra, 1994). This correlation was considered not feasible due to their different ages and chemostratigraphic signatures (e.g., Ahmad et al., 2000; Miller et al., 2000, 2001; Richards et al., 2005). The Shimla Group may have been deposited on top of the Berinag Group, and the two units together form the hanging wall of the linked Tons-Berinag thrust (as drawn in Fig. 3).

Munsiari Thrust

The Munsiari thrust is marked by a mylonitic shear zone involving an ~1–2-km-thick section of Munsiari Group gneiss in the hanging wall and ~1-km-thick Berinag Group in the footwall (Jain and Anand, 1988; Singh and Jain, 1993; Vannay et al., 2004; our observations). All observed mylonitic fabrics are consistent with a top-to-the-southwest sense of shear (Jain and Anand, 1988; Vannay et al., 2004; our observations). Distributed deformation also occurs in the Munsiari hanging wall and footwall. Jain and Anand (1988) reported an ~1-km-thick ductile shear zone located ~2 km below the fault with a top-to-the-southwest sense of shear. The Wangtu gneiss in the hanging wall is also extensively mylonitized or isoclinally folded, consistent with top-to-the-southwest shear (see also Jain and Anand, 1988; Singh and Jain, 1993; Vannay et al., 2004). Brittle fabrics (e.g., Riedel shears,

cataclasite, and slickenfibers) overprinting the ductile fabrics in the Munsiari thrust zone also indicate a top-to-the-southwest sense of shear (Jain and Anand, 1988; Singh and Jain, 1993; Vannay et al., 2004; our observations).

Chaura Thrust

This fault divides the Munsiari Group in the eastern Kullu window and places the Wangtu gneiss over the Jeori gneiss. The fault merges with the Munsiari thrust in map view (Fig. 3). The Chaura thrust zone preserves S-C fabric and σ-type porphyroclasts that are consistent with top-to-the-southwest shear (Singh and Jain, 1993; Jain et al., 2000; Chambers et al., 2008; our observations).

Main Central Thrust

Surface Trace and Fault Kinematics

In the map area the MCT is folded and displays large full and half-windows and isolated klippes: major thrust windows include the Kullu window, and the Narkanda and Uttarkashi half-windows, and klippes include the Shimla, Lansdowne, and Almora klippes, and two small klippes ~15 km southeast of Mussoorie (Figs. 3 and 6B). As discussed herein, the MCT in this region is a top-to-the-southwest mylonitic shear zone as much as 2 km thick (e.g., Grasemann et al., 1999; Vannay et al., 2004). Brittle deformation is restricted to the region along the Sutlej River, where the base of the MCT zone is a top-to-the-southwest brittle thrust placing the mylonitic Baragaon gneiss and metasedimentary rocks of the Haimanta Group over Deoban carbonates (Grasemann et al., 1999; our observations). Grasemann et al. (1999) investigated the mylonitic fabrics of the MCT zone within the Baragaon gneiss here, using fringe folds and quartz c- and <a> axes patterns to infer a decelerating strain path (i.e., early high-temperature simple shear deformation progressing to general shear deformation due to an increase in pure shear component as the shear zone cooled).

Hanging-Wall and Footwall Cutoffs and MCT Geometry in Cross-Section View

As noted herein, cutoff relationships in the MCT footwall suggest that the thrust cuts upsection to the southwest in its transport direction. Along the northern rims of the Kullu window and Uttarkashi half-window, the thrust places the Greater Himalayan Crystalline complex rocks over the Wangtu gneiss, which is considered to the basement of the Lesser Himalayan Sequence strata. Farther south, the MCT cuts progressively the Berinag Group in the southern Kullu window and the central Uttarkashi half-window, the Damtha and Deoban Groups in the Narkanda half-window and southernmost Uttarkashi half-window, the youngest Outer Lesser Himalayan Sequence below the Shimla klippe, and an MCT protrusion south of Naura directly east of the Shimla klippe (Fig. 3). The southernmost trace of the MCT along the northern limb of the Kangra reentrant merges with the Mandi thrust and places the Tethyan Himalayan Sequence directly over the Himalayan foreland-basin strata; MCT klippes occur along the leading edge of the preserved thrust sheet (Figs. 3, 4, and 6B). These footwall cutoff relationships suggest that the MCT origination was at least as deep as along the contact between the basement and the cover sequence of the northern Indian passive margin. Throughout its evolution, the MCT climbed up the entire section of the passive margin sequence and cut across the foreland strata. As the Baragaon gneiss in the MCT hanging wall and the Wangtu gneisses in the MCT footwall both represent the basement of the Indian craton, the MCT must be a basement-involved thick-skinned thrust in the Himachal Himalaya. This fault characteristic is remarkably similar to the MCT fault in the eastern Himalaya, where it also involves and duplicates the Indian basement rocks (Yin et al., 2010a, 2010b).

As discussed herein, the large footwall ramp along the MCT is not entirely due to the MCT cutting upsection: because Cretaceous–Eocene beds overlie progressively older units to the north (Fig. 3), the Proterozoic–Cambrian sequence of the northern Indian passive margin must have been tilted to the south prior to the emplacement of the MCT hanging wall. Some apparent MCT ramping merely reflects this earlier tilting.

The MCT along the northern limb of the Kangra reentrants truncates an east-trending anticline involving 11–7 Ma Late Miocene Middle Siwalik strata (Fig. 3) (Table 2), suggesting that the MCT must have been locally reactivated since ca. 7 Ma.

South Tibet Detachment

Surface Trace and Fault Kinematics

The trace and kinematics of the STD are discussed within the main body of the text. Two further notes: (1) another possible STD exposure occurs at the Leo Pargil dome, where high-grade rocks were exhumed along northeast-trending normal faults that initiated ca. 16–14 Ma, but the southern transition to lower grade Haimanta metasedimentary rocks is uncertain (Thiede et al., 2006). We speculate that the STD may be exhumed along the southern and possibly northern flanks of the Leo Pargil dome, such that the dome is cored by Greater Himalayan Crystalline complex rocks. (2) Although the northwest-trending Sarchu normal fault has been interpreted to link the STD mapped in the Himachal Himalaya in the east to the Zanskar shear zone in the west (e.g., Wyss et al., 1999), it is a steep brittle structure with total slip <2 km, making it an impossible candidate as an extension of the STD (cross section in Supplemental File 1A [see footnote 1]; Epard and Steck, 2004).

Great Counter Thrust System and Hanging-Wall Structures

The southern limb of the Spiti Synclinorium comprises the top-to-the-southwest Tethyan Himalayan fold-thrust belt, whereas its northeastern limb consists of a southwest-verging tight to isoclinal fold system commonly referred to as the Mata nappe (Figs. 3 and 4B) (Steck et al., 1998). The Mata nappe is tilted to the southwest and thrust to the southwest along its synclinal axial plane; this fault may daylight as the Dutung-Thaktote thrust (Steck et al., 1998). The Tso Morari ultrahigh-pressure (UHP) rocks underlie the Mata nappe. Evidence of UHP metamorphism is scarce; both the base of the Mata nappe and the UHP rocks record dominantly amphibolite facies metamorphism (e.g., Epard and Steck, 2008). Top-to-the-southwest ductile shear fabrics are dominant across the upper levels of the Tso Morari rocks through the lower levels of the Mata nappe (Epard and Steck, 2008). Both the UHP rocks and the Mata nappe carapace are domed within open and north-verging folds (e.g., Stutz and Steck, 1986; Steck et al., 1998). The northwest-trending subvertical Ribil fault uplifted these rocks relative to India-Asia suture zone rocks dominated by the Nidar ophiolite (e.g., Schlup et al., 2003; de Sigoyer et al., 2004). Farther north, the suture zone rocks are thrust northeastward over the Indus molasse along a strand of the latest Oligocene–Miocene Great Counter thrust system (GCT) (e.g., Schlup et al., 2003; de Sigoyer et al., 2004). The youngest structures in the Tso Morari region are north-trending normal faults that may link with northwest-trending right-lateral strike-slip faults (e.g., Epard and Steck, 2008).

UHP metamorphism is loosely constrained as ca. 55 Ma (e.g., de Sigoyer et al., 2000; Leech et al., 2005, 2007; O'Brien, 2006; cf. Gouzu et al., 2006), followed by amphibolite facies metamorphism and deformation of both the UHP rocks and the Mata nappe and exhumation of these rocks to the middle crust by ca. 40 Ma (de Sigoyer et al., 2000, 2004; Epard and Steck, 2008). Apatite fission track ages decrease from ca. 35 Ma in the south at the base of the Mata nappe to ca. 8 Ma across the Ribil fault (Schlup et al., 2003). The tectonic evolution of the Tso Morari UHP rocks and surrounding units remain uncertain (cf. Schlup et al., 2003; de Sigoyer et al., 2004; Yin, 2006; Epard and Steck, 2008; Beaumont et al., 2009). Following Yin (2006), we show the doming of the UHP rocks and motion along the Ribil fault as deformation within the GCT (Figs. 3 and 4B). This fault system overprints the India-Asia suture zone, juxtaposing Tethyan Himalayan Sequence rocks, suture zone sedimentary and ophiolitic rocks, and the Indus molasse atop the Ladakh batholith of the Asian plate (Yin, 2006; Epard and Steck, 2008). The GCT likely represents the northern extension of the STD (e.g., Yin et al., 1994, 1999).

Definition of the Main Boundary Thrust

Following the definition of Heim and Gansser (1939) that the Main Boundary thrust (MBT) places pre-Tertiary strata over Tertiary strata, we may designate the northern portion of the Bilaspur thrust to be the MBT. However, this definition breaks down for the same fault to the south, as its hanging-wall strata change from Proterozoic to Tertiary. The MBT definition of Heim and Gansser (1939) is also locally applicable to the Mandi-Krol thrust system and even to the MCT along the northern limb of the Kangra reentrant (Fig. 3). Furthermore, the folded Tons thrust places Proterozoic Lesser Himalayan Sequence strata over slivers of Cretaceous and Paleogene strata in its footwall along the southern margins of the Narkanda and Uttarkashi half-windows and in the southeast corner of our map area, qualifying this fault locally as MBT. The above examples illustrate the limitation of the traditional definition of the MBT that can lead to miscorrelation of different structures along strike as the same fault (see discussion in Yin, 2006). For this reason, we do not use the term Main Boundary thrust in our structural description of the Himachal Himalaya in this paper.

APPENDIX 3. EXPANDED REPORT OF U-TH-PB GEOCHRONOLOGY OF ZIRCON FROM GRANITIC ROCKS

Results of U-(Th)-Pb spot dating of zircon from granitoid and leucogranite samples were summarized in the discussion U-Th-Pb Zircon Geochronology: Granitic Rocks. This appendix includes a description of our methods and an expanded report of our results.

Methods

Analytical procedures reported in Quidelleur et al. (1997) were followed to acquire spot dates using the Cameca 1270 ion microprobe at UCLA. This work was accomplished using an 8–15 nA O^- primary beam and an ~25-µm-diameter spot size. U-Pb ratios were determined using a calibration curve based on UO/U versus Pb/U from zircon standard AS3 (age 1099.1 Ma; Paces and Miller, 1993), and isotopic ratios were adjusted for common Pb with a ^{204}Pb correction from the model of Stacey and Kramers (1975). Data reduction was accomplished via the in-house program ZIPS 3.0.3 by Chris Coath.

Main Central Thrust Hanging Wall

We analyzed 53 spots on 38 zircon crystals from 5 samples to characterize the age and affinities of granitic rocks in the Main Central thrust (MCT) hanging wall. Sample AY 9–3-03 12A was collected from mylonitic augen gneiss of the Audi shear zone (Fig. 6B); 12 spot dates on 9 zircon crystals from this sample were obtained (Fig. 11; Supplemental File 5A [see footnote 5]). The analyses form a cluster ca. 830 Ma in concordia space (Fig. 11). Only two ages are reversely disconcordant within 1σ error ellipses, but all ellipse centers are reversely discordant. Consequently the weighted mean age calculated from $^{207}Pb/^{206}Pb$ dates is younger (809 ± 15 Ma, 2σ, mean square of weighted deviates, MSWD = 0.36) than the weighted mean age calculated from $^{238}U/^{206}Pb$ dates (853 ± 19 Ma, 2σ, MSWD = 6.8). We interpret these data to record the protolith crystallization age. It is likely that these data record the same crystallization event as the data of sample AW 9–18–04 1D, which has a well-determined age of ca. 830 Ma (see following).

Sample AW 9–4-03 6A was collected from mylonitic augen gneiss ~1 m structurally above a sheared top-to-the-southwest basal contact with Haimanta Group metasedimentary rocks (Fig. 6B). We acquired 18 spot analyses on 9 zircon crystals from this sample (Fig. 11; Supplemental File 5A [see footnote 5]). The results resemble typical detrital zircon results, with a range of dates spanning the Paleoproterozoic to the early Paleozoic and variable concordance and/or discordance. A Neoproterozoic cluster of 5 concordant and reversely discordant dates acquired from spots on 3 zircon crystals yields a weighted mean age calculated from $^{207}Pb/^{206}Pb$ dates of 842 ± 22 Ma (2σ, MSWD = 0.85). Two early Paleozoic dates were obtained: a reversely discordant datum with a $^{207}Pb/^{206}Pb$ date of 469.7 ± 10.3 Ma (1σ) and a concordant datum with a $^{207}Pb/^{206}Pb$ date of 514.0 ± 28.2 Ma (1σ). The early Paleozoic analyses are of spots from the outer rims of analyzed zircon crystals, and spots from the core of these two zircon crystals yield Mesoproterozoic and Paleoproterozoic $^{207}Pb/^{206}Pb$ ages. Th/U ratios of the two early Paleozoic analyses are very low (<0.009), characteristic of zircon crystallizing in equilibrium with an aqueous metamorphic fluid (Ding et al., 2001). We interpret the dates older than ca. 840 Ma to represent inherited zircon, and we interpret the early Paleozoic rim ages to represent metamorphic overgrowth of the inherited zircon. The ca. 840 Ma dates may represent the time of granite crystallization, or inherited zircon if the granite crystallized later. The lower limit on the crystallization age is represented by the early Paleozoic age of metamorphism.

Two granitic samples yield early Paleozoic dates: AW 9–7-03 5A, collected from granite with 5 cm feldspars ~5 km east of Mandi (Figs. 6B and 10F), and AW 9–3-04 7A, collected from an ~1-m-thick mylonitic granite sill ~20 km north of Kullu in the overturned limb of the Phojal anticline (Fig. 6A). We analyzed 14 spots on 11 zircon crystals from sample AW 9–7-03 5A (Fig. 11; Supplemental File 5A [see footnote 5]). Excepting one reversely discordant analysis, these data are concordant and yield a weighted mean age calculated from $^{238}U/^{206}Pb$ dates of 470.6 ± 5.3 Ma (2σ, MSWD = 1.9). Spot dates on 5 different zircon crystals from sample AW 9–3-04 7A have similar results: concordant data with a weighted mean age calculated from $^{238}U/^{206}Pb$ dates of 473 ± 26 Ma (2σ, MSWD = 0.73). For both samples, we interpret the weighted mean age as the granite crystallization age.

We analyzed four spots on different zircon crystals from sample AW 9–24–04 4C, which was collected from a tourmaline-bearing leucogranite that crosscuts bedding preserved in amphibolite-grade metasedimentary rocks of the Leo Pargil dome (Fig. 6C). The acquired dates are variable, discordant, and Precambrian–Tertiary (Fig. 11; Supplemental File 5A [see footnote 5]). The youngest ($^{238}U/^{206}Pb$) date is 50.4 ± 2.4 Ma (1σ). These data likely reflect the ages of inherited zircon prior to Tertiary leucogranite crystallization.

MCT Shear Zone

We analyzed 71 spots on 51 zircon crystals from 7 samples to characterize the age and affinities of deformed granitic rocks within the MCT shear zone. The southernmost sample, AW 9–18–04 1D, was collected from a 3-m-thick layer of mylonitic augen gneiss with 5 cm feldspars in the MCT zone on the western flank of the Uttarkashi half-window (Fig. 6B). Spot analyses on 7 different zircon crystals yield a $^{207}Pb/^{206}Pb$ weighted mean age of 831 ± 19 Ma (2σ, MSWD = 0.69), which we interpret as the protolith crystallization age.

Analyses of the remaining six samples are consistent with protolith crystallization ca. 1.85 Ga. Sample AW 9–24–03 5 was collected from a mylonitic augen gneiss along the northern margin of the Narkanda half-window (Fig. 6B). We analyzed 15 spots on 10 zircon crystals from this sample (Fig. 11; Supplemental File 5A [see footnote 5]), and obtained $^{207}Pb/^{206}Pb$ dates ranging from 1690 Ma to 1866 Ma. Older dates are concordant, and with decreasing age the analyses are increasingly discordant. We interpret the older ages to represent the crystallization age, which we estimate as 1847 ± 10 (2σ, MSWD = 1.2). This estimate is a weighted mean age of $^{207}Pb/^{206}Pb$ dates that excludes the dates younger than 1800 Ma (8 of 15 ages were used). The younger discordant analyses likely reflect the effect of subsequent thermal disturbance or disturbances of ca. 1.85 Ga zircon. Sample AW 9–27–03 1B was collected from mylonitic augen gneiss that is ~12 km north of Narkanda and ~1 m structurally below a concordant contact with Haimanta garnet mica schist (Figs. 6B and 7C). We analyzed 13 spots on 9 zircon crystals from this sample (Fig. 11; Supplemental File 5A [see footnote 5]). Excepting one concordant analysis with a ca. 2.2 Ga $^{207}Pb/^{206}Pb$ date, the remaining discordant, concordant, and reversely discordant analyses cluster near ca. 1.85 Ga on the concordia plot and describe a weak chord extending from this age to a lower intercept in the Phanerozoic. We used 11 of 13 $^{207}Pb/^{206}Pb$ dates (excluding the ca. 2.2 Ga age and the youngest, discordant analysis) to calculate a weighted mean age of 1835 ± 14 Ma (2σ, MSWD = 2.8). We interpret the ca. 2.2 Ga date to represent inherited zircon, the 1835 Ma age as the protolith crystallization age, and the chord trend to reflect thermal disturbance or disturbances.

Three of the analyzed samples are from the southwestern flank of the Kullu window of the MCT. Sample AW 9–29–03 6A was collected from a strongly mylonitic augen gneiss and/or ultramylonite ~5 km west of Larji, and samples AW 9–4-03 3 and AW 9–26–03 1B were collected from mylonitic augen gneiss ~15 km southwest and ~20 km west of Rampur, respectively (Fig. 6B). We analyzed 9 spots on 6 zircon crystals from AW 9–29–03 6A, 7 spots on 5 zircon crystals from AW 9–4-03 3, and 15 spots on 9 zircon crystals from AW 9–26–03 1B (Fig. 11; Supplemental File 5A [see footnote 5]). Data from AW 9–29–03 6A and AW 9–4-03 3 plot as concordant clusters of ca. 1.85 Ga, with $^{207}Pb/^{206}Pb$ weighted mean ages of 1843 ± 10 (2σ, MSWD = 0.47) and 1842.4 ± 9.3 (2σ, MSWD = 0.66), respectively. We interpret these dates as protolith crystallization ages. Analyses of AW 9–26–03 1B zircon crystals have $^{207}Pb/^{206}Pb$ dates ranging from 1550 to 1865 Ma. The older dates are concordant, and increasingly younger $^{207}Pb/^{206}Pb$ dates are increasingly discordant. As with sample AW 9–24–03 5, we interpret the older ages to represent the crystallization age, which we estimate as 1840 ± 14 (2σ, MSWD = 3.1). This estimate is a weighted mean age of $^{207}Pb/^{206}Pb$ dates that excludes dates younger than 1800 Ma (10 of 15 ages were used). The younger discordant analyses likely reflect subsequent thermal disturbance or disturbances.

Sample AW 9–17–05 2 was collected from mylonitic augen gneiss along the northeastern flank of the Kullu window of the MCT, ~10 km north-northeast of Wangtu (Fig. 6C). As mapped by Vannay and Grasemann (1998), the MCT zone here contains Wangtu gneiss at the base below a <100-m-thick discontinuous layer of recrystallized orthoquartzite commonly interpreted as Berinag quartzite, which in turn is succeeded by the Greater Himalayan Crystalline complex. Sample AW 9–17–05 2 likely represents discontinuous augen gneiss at the base of the Greater Himalayan Crystalline complex. However, we were unable to confirm the orthoquartzite exposure here and therefore allow that the sample could represent the top of the Wangtu gneiss. We analyzed 5 spots on different zircon crystals from this sample (Fig. 11; Supplemental File 5A [see footnote 5]); 4 analyses yield discordant to concordant data that plots near ca. 1.85 Ga on concordia; the $^{207}Pb/^{206}Pb$ dates of these analyses yield a weighted mean age of 1863 ± 17 (2σ, MSWD = 2.6). The fifth analysis is strongly discordant. A concordia line determined from all 5 analyses yields a 1897 ± 27 Ma upper intercept and a 470 ± 120 Ma lower intercept (2σ, MSWD = 0.49). We interpret the Paleoproterozoic dates to reflect ca. 1.85 Ga protolith crystallization, and the lower intercept to record younger thermal disturbance. The ca. 470 Ma date of the lower intercept matches the crystallization age of MCT hanging-wall granitic rocks (see following), so it is possible that this age records the same early Paleozoic tectonic episode.

The cumulative results from the MCT zone help define the age and spatial extent of the ca. 1.85 Ga Baragaon gneiss. Previous dating of the Baragaon gneiss yielded conflicting Rb-Sr dates of ca. 1.43 Ga and ca. 1.84 Ga (Bhanot et al., 1978; Miller et al., 2000); our results support the latter age. MCT zone granites to the south are distinct from this unit, as shown by the ca. 830 Ma age obtained for the southernmost sample AW 9–18–04 1D.

MCT Footwall

Samples AW 9–18–05 1B and AW 9–18–05 1C were collected from Wangtu gneiss and an undeformed pegmatitic felsic dike that crosscuts foliation of the Wangtu gneiss, respectively (Fig. 6C). Spot analyses on 3 different zircon crystals from sample AW 9–18–05 1B are strongly discordant, yielding a weak chord with intercepts at 123 ± 280 Ma and 1911 ± 390 Ma (2σ, MSWD = 6.6) (Fig. 11; Supplemental File 5A [see footnote 5]); 4 spot analyses on different zircon crystals from sample AW 9–18–05 1C yield Late Miocene $^{238}U/^{206}Pb$ ages, with a weighted mean age 7.4 ± 1.2 Ma (2σ, MSWD = 5.1) (Fig. 11; Supplemental File 5A [see footnote 5]). The AW 9–18–05 1B upper intercept age is consistent with previous dates of ca. 1.85 Ga for the crystallization of the granitic protolith of the Wangtu gneiss (Table 2), and the lower intercept age may record the Late Miocene metamorphism of the Munsiari Group. We interpret the Late Miocene dates from the undeformed dike as crystallization ages.

APPENDIX 4. U-TH-PB GEOCHRONOLOGY OF DETRITAL ZIRCON: METHODS

Results of U-(Th)-Pb spot dating of detrital zircon were summarized in the discussion U-Th-Pb Zircon Geochronology: Detrital Zircon. Data for 16 samples were obtained using the laser ablation–multicollector–inductively coupled plasma–mass spectrometry (LA-MC-ICP-MS) facility at the University of Arizona, Tucson, and the UCLA ion microprobe. Procedures for ion microprobe zircon geochronology follow description in Appendix 3 (Methods); the following discussion pertains to the LA-MC-ICPMS analyses. These involve ablation of zircon with a New Wave–Lambda Physik DUV193 Excimer laser (operating at a wavelength of 193 nm) using a spot diameter of 25–50 μm. The ablated material is carried in helium into the plasma source of a GV Instruments Isoprobe, which is equipped with a flight tube of sufficient width that U, Th, and Pb isotopes are measured simultaneously. All measurements are made in static mode, using 10^{11} Faraday detectors for ^{238}U, ^{232}Th, ^{208}Pb, and ^{206}Pb, a 10^{12} Faraday collector for ^{207}Pb, and an ion-counting channel for ^{204}Pb. Ion yields are ~1.0 mv/ppm. Each analysis consists of one 20 s integration on peaks with the laser off (for backgrounds), 20 1 s integrations with the laser firing, and a 30 s delay to purge the previous sample and prepare for the next analysis. The ablation pit is ~15 μm in depth.

For each analysis, the errors in determining $^{238}U/^{206}Pb$ and $^{206}Pb/^{204}Pb$ ratios result in a measurement error of ~1%–2% (2σ) in the $^{238}U/^{206}Pb$ age. The errors in measurement of $^{207}Pb/^{206}Pb$ and $^{206}Pb/^{204}Pb$ also result in ~1%–2% (2σ) uncertainty in age for grains that are older than 1.0 Ga, but are substantially larger for younger grains due to low intensity of the ^{207}Pb signal. For most analyses, the crossover in precision of $^{238}U/^{206}Pb$ and $^{207}Pb/^{206}Pb$ ages occurs at 0.8–1.0 Ga.

Common Pb correction is accomplished by using the measured ^{204}Pb and assuming an initial Pb composition from Stacey and Kramers (1975) (with uncertainties of 1.0 for $^{206}Pb/^{204}Pb$ and 0.3 for $^{207}Pb/^{204}Pb$). Our measurement of ^{204}Pb is unaffected by the presence of ^{204}Hg because backgrounds are measured on peaks (thereby subtracting any background ^{204}Hg and ^{204}Pb), and because very little Hg is present in the argon gas.

Interelement fractionation of Pb/U is generally ~20%, whereas fractionation of Pb isotopes is generally ~2%. In-run analysis of fragments of a large zircon crystal (generally every fifth measurement) with known age of 564 ± 4 Ma (2σ) is used to correct for this fractionation. The uncertainty resulting from the calibration correction is generally 1%–2% (2σ) for both $^{238}U/^{206}Pb$ and $^{207}Pb/^{206}Pb$ ages.

The LA-MC-ICPMS analytical data are tabulated in Supplemental File 5C (see footnote 5), and interpreted ages are shown on relative and cumulative age-probability diagrams (Figs. 12 and 13) (from Ludwig, 2003). Uncertainties shown in the table are at the 1σ level, and include only measurement errors. Interpreted ages for both LA-MC-ICPMS and ion microprobe analyses are based on $^{238}U/^{206}Pb$ for grains younger than 1000 Ma and on $^{207}Pb/^{206}Pb$ for grains older than 1000 Ma (with few exceptions noted in the Fig. 12 caption). This division at 1000 Ma results from the increasing uncertainty of $^{238}U/^{206}Pb$ ages and the decreasing uncertainty of $^{207}Pb/^{206}Pb$ ages as a function of age. Analyses that are >30% discordant (by comparison of $^{238}U/^{206}Pb$ and $^{207}Pb/^{206}Pb$ ages) or >5% reverse discordant are not considered. The relative age-probability diagrams show each age and its uncertainty (for measurement error only) as a normal distribution, and sum all ages from a sample into a single curve.

REFERENCES CITED

Academy of Geological Sciences of China, 1975, Yazhou di zhi tu (Geologic map of Asia): Beijing, Academy of Geological Sciences of China, scale 1:5,000,000.

Acharyya, S.K., 1997, Stratigraphy and tectonic history reconstruction of the Indo-Burma-Andaman mobile belt: Indian Journal of Geology, v. 69, p. 211–234.

Acharyya, S.K., Mitra, N.D., and Nandy, D.R., 1986, Regional geology and tectonic setting of northeast India and adjoining region: Geological Survey of India Memoirs, v. 119, p. 6–12.

Agarwal, N.C., and Kumar, G., 1973, Geology of the upper Upper Bhagirathi and Yamuna Valleys, Uttarkashi District, Kumaun Himalaya: Himalayan Geology, v. 3, p. 1–23.

Aharon, P., Schidlowski, M., and Singh, I.B., 1987, Chronostratigraphic markers in the end-Precambrian carbon isotope record of the Lesser Himalaya: Nature, v. 327, p. 699–702, doi: 10.1038/327699a0.

Ahmad, T., Mukherjee, P.K., and Trivedi, J.R., 1999, Geochemistry of Precambrian mafic magmatic rocks of the Western Himalaya: Petrogenetic and tectonic implications: Chemical Geology, v. 160, p. 103–119, doi: 10.1016/S0009-2541(99)00063-7.

Ahmad, T., Harris, N., Bickle, M., Chapman, H., Bunbury, J., and Prince, C., 2000, Isotopic constraints on the structural relationships between the Lesser Himalayan Series and the High Himalayan Crystalline Series, Garhwal Himalaya: Geological Society of America Bulletin, v. 112, p. 467–477, doi: 10.1130/0016-7606(2000)112<467:ICOTSR>2.0.CO;2.

Arita, K., 1981, Origin of the inverted metamorphism of the lower Himalayas, Central Nepal: Tectonophysics, v. 95, p. 43–60.

Argand, E., 1924, La Tectonique de l'Asie: Proceedings of the 13th International Geological Congress, v. 7, p. 171–372.

Argles, T., Foster, G., Whittington, A., Harris, N., and George, M., 2003, Isotope studies reveal a complete Himalayan section in the Nanga Parbat syntaxis: Geology, v. 31, p. 1109–1112.

Auden, J.B., 1934, The geology of the Krol Belt: Geological Survey of India Records, v. 67, p. 357–454.

Bassi, U.K., 1989, The stratigraphy of the Kinnaur Tethyan Basin–A reappraisal: Geological Society of India Journal, v. 34, p. 587–595.

Beaumont, C., Jamieson, R.A., Nguyen, M.H., and Lee, B., 2001, Himalayan tectonics explained by extrusion of a low-viscosity crustal channel coupled to focused surface denudation: Nature, v. 414, p. 738–742, doi: 10.1038/414738a.

Beaumont, C., Jamieson, R.A., Nguyen, M.H., and Medvedev, 2004, Crustal channel flows: 1. Numerical models with applications to the tectonics of the Himalayan-Tibertan orogen: Journal of Geophysical Research, v. 109, doi:10.1029/2003JB02809.

Beaumont, C., Jamieson, R.A., Butler, J.P., and Warren, C.J., 2009, Crustal structure: A key constraint on the mechanism of ultra-high-pressure rock exhumation: Earth Planet. Scie. Lett., v. 287, p. 116–129.

Bhanot, V.B., Kwatra, S.K., Kansal, A.K., and Pandey, B.K., 1978, Rb-Sr whole rock age for Chail Series of northwestern Himalaya: Geological Society of India Journal, v. 19, p. 224–225.

Bhargava, O.N., 1976, Geology of the Krol belt and associated formations: A reappraisal: Geological Survey of India Memoirs, v. 106, p. 167–234.

Bhargava, O.N., 1980, Outline of the stratigraphy of the Eastern Himachel Pradesh, with special reference to the Jutogh Group, *in* Valdiya, K.S., and Bhatia, S.B., eds., Stratigraphy and correlations of Lesser Himalayan Formations: Delhi, India, Hindustan Publishing, p. 117–125.

Bhargava, O.N., Bassi, U.K., and Sharma, R.K., 1991, The crystalline thrust sheets, age of metamorphism, evolution and mineralization of the Himachal Himalaya: Indian Minerals, v. 45, p. 1–18.

Bhat, M.I., and Le Fort, P., 1992, Sm-Nd age and petrogenesis of Rampur metavolcanic rocks, NW Himalayas: Late Archaean relics in the Himalayan belt: Precambrian Research, v. 56, p. 191–210, doi: 10.1016/0301-9268(92)90101-S.

Bhat, I.M., and Le Fort, P., 1993, Nd-isotopic study of the Late Archaean continental tholeiites, NW Lesser Himalayas: A case of ocean island basalt source for continental tholeiites: Journal of Himalayan Geology, v. 4, p. 1–13.

Bhattacharya, A.K., Bhatnagar, G.S., Narayan Das, G.R., Gupta, J.N., Chhabria, T., and Bhalla, N.S., 1982, Rb/Sr dating and geological interpretation of the sheared granite-gneisses of Brijranigad-Ingedinala, Bhilangana Valley, Tehri District, U.P.: Himalayan Geology, v. 12, p. 212–224.

Biju-Sekhar, S., Yokoyama, K., Pandit, M.K., Okudaira, T., Yoshida, M., and Santosh, M., 2003, Late Paleoproterozoic magmatism in Delhi Fold Belt, NW India and its implication: Evidence from EPMA chemical ages of zircons: Journal of Asian Earth Sciences, v. 22, p. 189–207, doi: 10.1016/S1367-9120(02)00188-8.

Bordet, P., Colchen, M., and Le Fort, P., 1972, Some features of the geology of the Annapurna range Nepal Himalaya: Himalayan Geology, v. 2, p. 537–563.

Boyer, S.E., and Elliot, D., 1982, Thrust systems: AAPG Bulletin, v. 66, p. 1196–1230.

Brown, R.L., and Nazarchuk, J.H., 1993, Annapurna detachment fault in the Greater Himalaya of central Nepal, *in* Treloar, P.J., and Searle, M.P., eds., Himalayan tectonics: Geological Society of London Special Publication 74, p. 461–473, doi: 10.1144/GSL.SP.1993.074.01.31.

Buick, I.S., Allen, C., Pandit, M., Rubatto, D., and Hermann, J., 2006, The Proterozoic magmatic and metamorphic history of the Banded Gneiss Complex, central Rajasthan, India: LA-ICP-MS U-Pb zircon constraints: Precambrian Research, v. 151, p. 119–142, doi: 10.1016/j.precamres.2006.08.006.

Burchfiel, B.C., and Royden, L.H., 1985, North-south extension within the convergent Himalayan region: Geology, v. 13, p. 679–682, doi: 10.1130/0091-7613(1985)13<679:NEWTCH>2.0.CO;2.

Burchfiel, B.C., Zhiliang, C., Hodges, K.V., Yuping, L., Royden, L.H., Changrong, D., and Jiene, X., 1992, The South Tibetan Detachment System, Himalayan Orogen: Extension contemporaneous with and parallel to shortening in a collisional mountain belt: Geological Society of America Special Paper 269, 41 p.

Burg, J.P., Brunel, M., Gapais, D., Chen, G.M., and Liu, G.H., 1984, Deformation of leucogranites of the crystalline Main Central Sheet in southern Tibet (China): Journal of Structural Geology, v. 6, p. 535–542, doi: 10.1016/0191-8141(84)90063-4.

Caddick, M.J., Bickle, M.J., Harris, N.B.W., Holland, T.J.B., Horstwood, M.S.A., Parrish, R.R., and Ahmad, T., 2007, Burial and exhumation history of a Lesser Himalayan schist: Recording the formation of an inverted metamorphic sequence in NW India: Earth and Planetary Science Letters, v. 264, p. 375–390, doi: 10.1016/j.epsl.2007.09.011.

Catlos, E.J., Harrison, T.M., Kohn, M.J., Grove, M., Ryerson, F.J., Manning, C.E., and Upreti, B.N., 2001, Geochronologic and thermobarometric constraints on the evolution of the Main Central Thrust, central Nepal Himalaya: Journal of Geophysical Research, v. 106, no. B8, p. 16177–16204, doi: 10.1029/2000JB900375.

Catlos, E.J., Dubey, C.S., Marston, R.A., and Harrison, T.M., 2007, Geochronologic constraints across the Main Central Thrust shear zone, Bhagirathi River (NW India): Implications for Himalayan tectonics, *in* Cloos, M., et al., eds., Convergent margin terranes and associated regions: A tribute to W.G. Ernst: Geological Society of America Special Paper 419, p. 135–151, doi: 10.1130/2006.2419(07).

Cebula, G.T., Kunk, M.J., Mehnert, H.H., Naeser, C.W., Obradovich, J.D., and Sutter, J.F., 1986, The Fish Canyon Tuff, a potential standard for the ^{40}Ar-^{39}Ar and fission-track dating methods: Terra Cognita, v. 6, p. 139–140.

Célérier, J., Harrison, T.M., Webb, A.A.G., and Yin, A., 2009a, The Kumaun and Garwhal Lesser Himalaya, India; Part 1., Structure and stratigraphy: Geological Society of America Bulletin, v. 121, p. 1262–1280, doi: 10.1130/B26344.1.

Célérier, J., Harrison, T.M., Beyssac, O., Herman, F., Dunlap, W.J., and Webb, A.A.G., 2009b, The Kumaun and Garwhal Lesser Himalaya, India; Part 2. Thermal and deformation histories: Geological Society of America Bulletin, v. 121, p. 1281–1297, doi: 10.1130/B26343.1.

Chambers, J.A., Argles, T.W., Horstwood, M.S.A., Harris, N.B.W., Parrish, R.R., and Ahmad, T., 2008, Tectonic implications of Palaeoproterozoic anatexis and Late Miocene metamorphism in the Lesser Himalayan Sequence, Sutlej Valley, NW India: Geological Society of London Journal, v. 165, p. 725–737, doi: 10.1144/0016-76492007/090.

Chambers, J., Caddick, M., Argles, T., Horstwood, M., Sherlock, S., Harris, N., Parrish, R., and Ahmad, T., 2009, Empirical constraints on extrusion mechanisms from the upper margin of an exhumed high-grade orogenic core, Sutlej valley, NW India: Tectonophysics, v. 477, p. 77–92, doi: 10.1016/j.tecto.2008.10.013.

Choudhuri, B.K., Bist, K.S., and Rawat, B.S., 1992, Evidence for thrusting between the Higher Himalayan Crystallines and Tethyan metasediments in Lahaul and Kullu Valleys, Himachal Pradesh: Journal of Himalayan Geology, v. 3, p. 191–194.

Dahlstrom, C.D.A., 1969, Balanced cross sections: Canadian Journal of Earth Sciences, v. 6, p. 743–757, doi: 10.1139/e69-069.

Das, B.K., and Rastogi, R.G., 1988, Petrology of Jutogh metapelites near Chaur, Himachal Himalaya, India: Geological Society of India Journal, v. 31, p. 251–266.

Deb, M., Thorpe, R.I., Krstic, D., Corfu, F., and Davis, D.M., 2001, Zircon U-Pb and galena Pb isotope evidence for an approximate 1.0 Ga terrane constituting the western margin of the Aravalli-Delhi orogenic belt, northwestern India: Precambrian Research, v. 108, p. 195–213, doi: 10.1016/S0301-9268(01)00134-6.

DeCelles, P.G., Gehrels, G.E., Quade, J., and Ojha, T.P., 1998, Eocene–early Miocene foreland basin development and the history of Himalayan thrusting, western and central Nepal: Tectonics, v. 17, p. 741–765, doi: 10.1029/98TC02598.

DeCelles, P.G., Gehrels, G.E., Quade, J., LaReau, B., and Spurlin, M., 2000, Tectonic implications of U-Pb zircon ages of the Himalayan Orogenic Belt in Nepal: Science, v. 288, p. 497–499, doi: 10.1126/science.288.5465.497.

DeCelles, P.G., Robinson, D.M., Quade, J., Ojha, T.P., Garzione, C.N., Copeland, P., and Upreti, B.N., 2001, Stratigraphy, structure, and tectonic evolution of the Himalayan fold-thrust belt in western Nepal: Tectonics, v. 20, p. 487–509, doi: 10.1029/2000TC001226.

DeCelles, P.G., Robinson, D.M., and Zandt, G., 2002, Implications of shortening in the Himalayan foldthrust belt for uplift of the Tibetan Plateau: Tectonics, v. 21, 1062, doi: 10.1029/2001TC001322.

Deniel, C., Vidal, P., Fernandez, A., Le Fort, P., and Peucat, J.-J., 1987, Isotopic study of the Manaslu granite (Himalaya, Nepal): Inferences on age and source of Himalayan leucogranites: Contributions to Mineralogy and Petrology, v. 96, p. 78–92, doi:10.1007/BF00375529.

de Sigoyer, J., Chavagnac, V., Blichert-Toft, J., Villa, I.M., Luais, B., Guillot, S., Cosca, M., and Mascle, G., 2000, Dating the Indian continental subduction and collisional thickening in the northwest Himalaya: Multichronology of the Tso Morari eclogites: Geology, v. 28, p. 487–490, doi: 10.1130/0091-7613(2000)28<487:DTICSA>2.0.CO;2.

de Sigoyer, J., Guillot, S., and Dick, P., 2004, Exhumation of the ultra-high pressure Tso Morari unit in eastern Ladakh (NW Himalaya): A case study: Tectonics, v. 23, doi:10.1029/2002TC001492.

Dèzes, P.J., 1999, Tectonic and metamorphic evolution of the Central Himalayan Domain in southeast Zanskar (Kashmir, India): Université de Lausanne Mémoires de Géologie 32, 149 p.

Dèzes, P.J., Vannay, J.C., Steck, A., Bussy, F., and Cosca, M., 1999, Synorogenic extension: Quantitative constraints on the age and displacement of the Zanskar shear zone (northwest Himalaya): Geological Society of America Bulletin, v. 111, p. 364–374, doi: 10.1130/0016-7606(1999)111<0364:SEQCOT>2.3.CO;2.

Ding, L., Zhong, D., Yin, A., Kapp, P., and Harrison, T.M., 2001, Cenozoic structural and metamorphic evolution of the eastern Himalayan syntaxis (Namche Barwa): Earth and Planetary Science Letters, v. 192, p. 423–438, doi: 10.1016/S0012-821X(01)00463-0.

DiPietro, J.A., and Isachsen, C.E., 2001, U-Pb zircon ages from the Indian plate in northwest Pakistan and their significance to Himalayan and pre-Himalayan geologic history: Tectonics, v. 20, p. 510–525, doi: 10.1029/2000TC001193.

DiPietro, J.A., and Pogue, K.R., 2004, Tectonostratigraphic subdivisions of the Himalaya: A view from the west: Tectonics, v. 23, TC5001, doi: 10.1029/2003TC001554.

DiPietro, J.A., Pogue, K.R., Hussain, A., and Ahmad, I., 1999, Geologic map of the Indus syntaxis and surrounding area, northwest Himalaya, Pakistan, *in* Macfarlane, A.R., et al., eds., Himalaya and Tibet: Mountain roots to mountain tops: Geological Society of America Special Paper 328, p. 159–178, doi: 10.1130/0-8137-2328-0.159.

Epard, J.L., and Steck, A., 2002, Structural development of the Tso Morari ultra-high pressure nappe of the Ladakh Himalaya: Tectonophysics, v. 451, p. 242–264.

Epard, J.L., and Steck, A., 2004, The Eastern prolongation of the Zanskar Shear Zone (Western Himalaya): Eclogae Geologicae Helvetiae, v. 97, p. 193–212, doi:10.1007/s00015-004-1116-7.

Epard, J.L., Steck, A., Vannay, J.C., and Hunziker, J., 1995, Tertiary Himalayan structures and metamorphism in the Kulu Valley (Mandi-Khoksar Transect of the Western Himalaya)—Shikar-Beh-Nappe and Crystalline Nappe: Schweizerische Mineralogische und Petrographische Mitteilungen, v. 75, p. 59–84.

Foster, G., Kinny, P., Vance, D., Prince, C., and Harris, N., 2000, The significance of monazite U-Th-Pb age data in metamorphic assemblages; a combined study of monazite and garnet chronometry: Earth and Planetary Science Letters, v. 181, p. 327–340, doi: 10.1016/S0012-821X(00)00212-0.

Foster, G., Vance, D., Argles, T., and Harris, N., 2002, The Tertiary collision-related thermal history of the northwest Himalaya: Journal of Metamorphic Geology, v. 20, p. 827–843.

France-Lanord, C., Derry, L., and Michard, A., 1993, Evolution of the Himalaya since Miocene time: Isotopic and sedimentological evidence from the Bengal fan, in Treloar, P.J., and Searle, M.P., eds., Himalayan tectonics: Geological Society [London] Special Publication 74, p. 603–621.

Frank, W., Hoinkes, G., Miller, C., Purtscheller, F., Richter, W., and Thoni, M., 1973, Relations between metamorphism and orogeny in a typical section of the Indian Himalayas: Tschermaks Mineralogische und Petrographische Mitteilungen, v. 20, p. 303–332, doi: 10.1007/BF01081339.

Frank, W., Thoni, M., and Purtscheller, F., 1977, Geology and petrography of Kullu–South Lahul area: Colloques Internationaux du CNRS, v. 286, p. 147–172.

Frank, W., Grasemann, B., Guntli, P., and Miller, C., 1995, Geological map of the Kishtwar-Chamba-Kulu region (NW Himalayas, India): Jahrbuch der Geologischen Bundesanstalt, v. 138, p. 299–308.

Fuchs, G., 1982, The geology of the Pin valley in Spiti, H.P., India: Jahrbuch der Geologischen Bundesanstalt Wien, v. 124, p. 325–359.

Fuchs, G., and Linner, M., 1995, Geological traverse across the western Himalaya; a contribution to the geology of eastern Ladakh, Lahul, and Chamba: Jahrbuch der Geologischen Bundesanstalt Wien, v. 138, p. 655–685.

Gaetani, M., and Garzanti, E., 1991, Multicyclic history of the northern India continental margin (northwestern Himalaya): American Association of Petroleum Geologists Bulletin, v. 75, p. 1427–1446.

Garzanti, E., Casnedi, R., and Jadoul, F., 1986, Sedimentary evidence of a Cambro-Ordovician orogenic event in the northwestern Himalaya: Sedimentary Geology, v. 48, p. 237–265, doi: 10.1016/0037-0738(86)90032-1.

Gehrels, G.E., DeCelles, P.G., Martin, A., Ojha, T.P., Pinhassi, G., and Upreti, B.N., 2003, Initiation of the Himalayan Orogen as an early Paleozoic thin-skinned thrust belt: GSA Today, v. 13, no. 9, p. 4–9, doi: 10.1130/1052-5173(2003)13<4:IOTHOA>2.0.CO;2.

George, M.T., Harris, N.B.W., and Butler, R.W.H., 1993, The tectonic implications of contrasting granite magmatism between the Kohistan island arc and the Nanga Parbat–Haramost massif Pakistan Himalaya, in Treloar, P.J., and Searle, M.P., eds., Himalayan tectonics: Geological Society [London] Special Publication 74, p. 173–191.

Ghent, E.D., and Stout, M.Z., 1981, Geobarometry and geothermometry of plagioclase-biotite-garnet-muscovite assemblages: Contributions to Mineralogy and Petrology, v. 76, p. 92–97, doi: 10.1007/BF00373688.

Gilley, L.D., Harrison, T.M., Leloup, P.H., Ryerson, F.J., Lovera, O.M., and Wang, J.-H., 2003, Direct dating of left-lateral deformation along the Red River shear zone: China and Vietnam: Journal of Geophysical Research, v. 108, 2127, doi: 10.1029/2001JB001726.

Gouzu, C., Itaya, T., Hyodo, H., and Ahmad, T., 2006, Cretaceous isochron ages from K-Ar and Ar-Ar dating of eclogitic rocks in the Tso Morari complex, western Himalaya, India: Gondwana Research, v. 9, p. 426–440.

Grasemann, B., Fritz, H., and Vannay, J.C., 1999, Quantitative kinematic flow analysis from the Main Central Thrust Zone (NW-Himalaya, India): Implications for a decelerating strain path and the extrusion of orogenic wedges: Journal of Structural Geology, v. 21, p. 837–853, doi: 10.1016/S0191-8141(99)00077-2.

Grazis, C.A., Blum, J.D., Chamberlain, C.P., and Poage, M., 1998, Isotope systematics of granites and gneisses of the Nanga Parbat massif, Pakistan Himalaya: American Journal of Science, v. 298, p. 673–698.

Gregory, C., 2004, Microstructural analysis of the Main Central Thrust, North West Himalaya (India) [thesis]: Canberra, Australia National University, 79 p.

Grujic, D., Casey, M., Davidson, C., Hollister, L.S., Kundig, R., Pavlis, T., and Schmid, S., 1996, Ductile extrusion of the Higher Himalayan Crystalline in Bhutan: Evidence from quartz microfabrics: Tectonophysics, v. 260, p. 21–43, doi: 10.1016/0040-1951(96)00074-1.

Grujic, D., Hollister, L.S., and Parrish, R.R., 2002, Himalayan metamorphic sequence as an orogenic channel: Insight from Bhutan: Earth and Planetary Science Letters, v. 198, p. 177–191, doi: 10.1016/S0012-821X(02)00482-X.

Gururajan, N.S., 1990, Deformation microstructures and geochemistry of the mylonitic augen gneisses in the Chail Thrust Zone in Satluj Valley of Himachal Pradesh: Geological Society of India Journal, v. 36, p. 290–306.

Gururajan, N.S., and Virdi, N.S., 1984, Superimposition of early Paleozoic contact metamorphism by Tertiary regional metamorphism around Dalash, District Kulu, Himachal Pradesh (India): Geological Society of India Journal, v. 25, p. 522–527.

Harrison, T.M., McKeegan, K.D., and LeFort, P., 1995, Detection of inherited monazite in the Manaslu leucogranite by $^{208}Pb/^{232}Th$ ion microprobe dating: Crystallization age and tectonic implications: Earth and Planetary Science Letters, v. 133, p. 271–282, doi: 10.1016/0012-821X(95)00091-P.

Harrison, T.M., Ryerson, F.J., LeFort, P., Yin, A., Lovera, O.M., and Catlos, E.J., 1997, A Late Miocene–Pliocene origin for the Central Himalayan inverted metamorphism: Earth and Planetary Science Letters, v. 146, p. E1–E7, doi: 10.1016/S0012-821X(96)00215-4.

Harrison, T.M., Grove, M., Lovera, O.M., and Catlos, E.J., 1998, A model for the oirign of Himalayan anatexis and inverted metamorphism: Journal of Geophysical Research, v. 103, p. 27017–27032.

Heim, A., and Gansser, A., 1939, Central Himalaya geological observations of the Swiss Expedition 1936: Zurich, Gebrüder Fretz, 246 p.

Herren, E., 1987, Zanskar shear zone: Northeast-southwest extension within the Higher Himalayas (Ladakh, India): Geology, v. 15, p. 409–413.

Hodges, K.V., 2000, Tectonics of the Himalaya and southern Tibet from two perspectives: Geological Society of America Bulletin, v. 112, p. 324–350, doi: 10.1130/0016-7606(2000)112<324:TOTHAS>2.0.CO;2.

Hodges, K.V., Parrish, R.R., Housh, T.B., Lux, D.R., Burchfiel, B.C., Royden, L.H., and Chen, Z., 1992, Simultaneous Miocene extension and shortening in the Himalayan Orogen: Science, v. 258, no. 5087, p. 1466–1470, doi: 10.1126/science.258.5087.1466.

Hodges, K.V., Parrish, R.R., and Searle, M.P., 1996, Tectonic evolution of the central Annapurna Range, Nepalese Himalayas: Tectonics, v. 15, p. 1264–1291, doi: 10.1029/96TC01791.

Hodges, K.V., Hurtado, J.M., and Whipple, K.X., 2001, Southward extrusion of Tibetan crust and its effect on Himalayan tectonics: Tectonics, v. 29, p. 799–809.

Holland, T.J.B., and Powell, R., 1998, An internally consistent thermodynamic data set for phases of petrological interest: Journal of Metamorphic Geology, v. 16, p. 309–343.

Hughes, N.C., and Droser, M.L., 1992, Trace fossils from the Phe Formation (Lower Cambrian), Zanskar Valley, northwestern India: Queensland Museum Memoirs, v. 32, p. 139–144.

Hughes, N.C., and Jell, P.A., 1999, Biostratigraphy and biogeography of Himalayan Cambrian trilobites, *in* Macfarlane, A.R., et al., eds., Himalaya and Tibet: Mountain roots to mountain tops: Geological Society of America Special Paper 328, p. 109–116, doi: 10.1130/0-8137-2328-0.109.

Hughes, N.C., Peng, S., Bhargava, O.N., Ahluwalia, A.D., Walia, S., Myrow, P.M., and Parcha, S.K., 2005, Cambrian biostratigraphy of the Tal Group, Lesser Himalaya, India, and early Tsanglangpuan (late Early Cambrian) trilobites from the Nigali Dhar syncline: Geological Magazine, v. 142, p. 57–80, doi: 10.1017/S0016756804000366.

Inger, S., and Harris, N., 1993, Geochemical constraints on leucogranite magmatism in the Langtang Valley, Nepal Himalaya: Journal of Petrology, v. 34, p. 345–368.

Jadoon, I.A.K., Lawrence, R.D., and Lillie, R.J., 1994, Seismic data, geometry, evolution, and shortening in the active Sulaiman fold-and-thrust belt of Pakistan, southwest of the Himalayas: American Association of Petroleum Geologists Bulletin, v. 78, p. 758–774.

Jäger, E., Bhandari, A.K., and Bhanot, V.B., 1971, Rb-Sr age determinations on biotites and whole rock samples from the Mandi and Chor granites, Himachal Pradesh, India: Eclogae Geologicae Helvetiae, v. 64, p. 521–527.

Jain, A.K., 1972, Structure of Bidhalna-Pharat windows and Garhwal thrust unit, Garhwal, U.P: Himalayan Geology, v. 2, p. 188–205.

Jain, A.K., and Anand, A., 1988, Deformational and strain patterns of an intracontinental collision ductile shear zone; an example from the Higher Garhwal Himalaya: Journal of Structural Geology, v. 10, p. 717–734, doi: 10.1016/0191-8141(88)90079-X.

Jain, A.K., Manickavasagam, R.M., and Singh, S., 1999, Collision tectonics in the NW Himalaya: Deformation, metamorphism, emplacement of leucogranite along Beas-Parbati Valleys, Himachal Pradesh, *in* Jain, A.K., and Manickavasagam, R.M., eds., Geodynamics of the NW Himalaya: Gondwana Research Group Memoir 6, p. 3–37.

Jain, A.K., Kumar, D., Singh, S., Kumar, A., and Lal, N., 2000, Timing, quantification and tectonic modelling of Pliocene-Quaternary movements in the NW Himalaya: Evidence from fission track dating: Earth and Planetary Science Letters, v. 179, p. 437–451, doi: 10.1016/S0012-821X(00)00133-3.

Jiang, G., Christie-Blick, N., Kaufman, A.J., Banerjee, D.M., and Rai, V., 2002, Sequence stratigraphy of the Neoproterozoic Infra Krol Formation and Krol Group, Lesser Himalaya, India: Journal of Sedimentary Research, v. 72, p. 524–542, doi: 10.1306/120301720524.

Jiang, G., Christie-Blick, N., Kaufman, A.J., Banerjee, D.M., and Rai, V., 2003, Carbonate platform growth and cyclicity at a terminal Proterozoic passive margin, Infra Krol Formation and Krol Group, Lesser Himalaya, India: Sedimentology, v. 50, p. 921–952, doi: 10.1046/j.1365-3091.2003.00589.x.

Johnson, M.R.W., Oliver, G.J.H., Parrish, R.R., and Johnson, S.P., 2001, Synthrusting metamorphism, cooling, and erosion of the Himalayan Kathmandu Complex, Nepal: Tectonics, v. 20, p. 394–415, doi: 10.1029/2001TC900005.

Kapp, P., Murphy, M.A., Yin, A., Harrison, T.M., Ding, L., and Guo, J., 2003, Mesozoic and Cenozoic tectonic evolution of the Shiquanhe area of western Tibet: Tectonics, v. 22, 1029, doi: 10.1029/2001TC001332.

Khan, S.D., Stern, R.J., Manton, M.I., Copeland, P., Kimura, J.I., and Khan, M.A., 2004, Age, geochemical and Sr-Nd-Pb isotopic constraints for mantle source characteristics and petrogenesis of Teru Volcanics, northern Kohistan terrane, Pakistan: Tectonophysics, v. 393, p. 263–280, doi: 10.1016/j.tecto.2004.07.038.

Kumar, R., and Brookfield, M.E., 1987, Sedimentary environments of the Simla Group (upper Precambrian), Lesser Himalaya, and their paleotectonic significance: Sedimentary Geology, v. 52, p. 27–43, doi: 10.1016/0037-0738(87)90015-7.

Kumar, S., Wesnousky, S.G., Rockwell, T.K., Briggs, R.W., Thakur, V.C., and Jayangondaperumal, R., 2006, Paleoseismic evidences of grate surface rupture earthquakes along the Indian Himalaya: Journal of Geophysical Research, v. 111, doi:10.1029/2004JB003309.

Kuno, H., 1968, Differentiation of basalt magmas, in Hess, H.H., and Plodervaart, A.A., eds., Basalts: The Poldervaart Treatise on Rocks of Basaltic Composition, 2: New York, Interscience, p. 623–688.

Lal, N., Mehta, Y.P., Kumar, D., Kumar, A., and Jain, A.K., 1999, Cooling and exhumation history of the Mandi granite and adjoining tectonic units, Himachal Pradesh, and estimation of closure temperature from external surface of zircon, *in* Jain, A.K., and Manickavasagam, R.M., eds., Geodynamics of the NW Himalaya: Gondwana Research Group Memoir 6, p. 207–216.

Law, R.D. Stahr III, D.W., Ahmad, T., and Kumar, S., 2010, Deformation Temperatures and Flow Vorticities Near the Base of the Greater Himalayan Crystalline Sequence, Sutlej Valley and Shimla Klippe, NW India, *in* Leech, M.L. et al., eds., Proceedings for the 25th Himalaya-Karakoram-Tibet Workshop: U.S. Geological Survey Open-File Report 2010-1099, 2 p. (http://pubs.usgs.gov/of/2010/1099/law/).

Leech, M.L., Sing, S., Jain, A.K., Klemperer, R.M., and Manickavasagam, R.M., 2005, The onset of India-Asia continental collision: Early, steep subduction required by the timing of UHP metamorphism in the western Himalaya: Earth and Planetary Science Letters, v. 234, p. 83–97.

Leech, M.L., Singh, S., and Jain, A.K., 2007, Continuous metamorphic zircon growth and interpretation of U-Pb SHRIMP dating: An example from the Western Himalaya: International Geology Review, v. 49, p. 313–328.

Le Fort, P., 1975, Himalaya: The collided range. Present knowledge of the continental arc: American Journal of Science, v. 275A, p. 1–44.

Le Fort, P., 1996, Evolution of the Himalaya, *in* Yin, A., and Harrison, T.M., eds., The tectonic evolution of Asia: New York, Cambridge University Press, p. 95–106.

Leloup, P.H., Lacassin, R., Tapponnier, P., Schärer, U., Zhong, D., Liu, X., Zhang, L., Ji, S., and Trinh, P.T., 1995, The Ailao Shan-Red River shear zone (Yunnan, China), Tertiary transform boundary of Indochina: Tectonophysics, v. 251, p. 3–84, doi: 10.1016/0040-1951(95)00070-4.

Linner, M., Fuchs, G., Koller, F., and Thoeni, M., 2001, The Nidar Ophiolite within the Indus suture zone in eastern Ladakh—A marginal basin ophiolite from the Jurassic-Cretaceous boundary: Journal of Asian Earth Sciences, v. 19, p. 39.

Lovera, O.M., Richter, F.M., and Harrison, T.M., 1989, The $^{40}Ar/^{39}Ar$ thermochronometry for slowly cooled samples having a distribution of diffusion domain sizes: Journal of Geophysical Research, v. 94, p. 17917–17935, doi: 10.1029/JB094iB12p17917.

Ludwig, K.R., 2003, Users manual for Isoplot 3.00: A geochronological toolkit for Microsoft Exel: Berkeley, California, Berkeley Geochronology Center Special Publication 4, 70 p.

Marquer, D., Chawla, H.S., and Challandes, N., 2000, Pre-alpine high-grade metamorphism in High Himalaya crystalline sequences: Evidence from lower Palaeozoic Kinnaur Kailas granite and surrounding rocks in the Sutlej Valley (Himachal Pradesh, India): Eclogae Geologicae Helvetiae, v. 93, p. 207–220.

Meigs, A.J., Burbank, D.W., and Beck, R.A., 1995, Middle-late Miocene (>10 Ma) formation of the Main Boundary thrust in the western Himalaya: Geology, v. 23, p. 423–426, doi: 10.1130/0091-7613(1995)023<0423:MLMMFO>2.3.CO;2.

Miller, C., Klotzli, U., Frank, W., Thoni, M., and Grasemann, B., 2000, Proterozoic crustal evolution in the NW Himalaya (India) as recorded by circa 1.80 Ga mafic and 1.84 Ga granitic magmatism: Precambrian Research, v. 103, p. 191–206, doi: 10.1016/S0301-9268(00)00091-7.

Miller, C., Thoni, M., Frank, W., Grasemann, B., Klotzli, U., Guntli, P., and Draganits, E., 2001, The early Palaeozoic magmatic event in the Northwest Himalaya, India: Source, tectonic setting and age of emplacement: Geological Magazine, v. 138, p. 237–251, doi: 10.1017/S0016756801005283.

Mitchell, A.H.G., 1993, Cretaceous-Cenozoic tectonic events in the western Myanmar (Burma)-Assam region: Geological Society of London Journal, v. 150, p. 1089–1102, doi: 10.1144/gsjgs.150.6.1089.

Mitchell, A.H.G., Htay, M.T., Htun, K.M., Win, M.N., Oo, T., and Hlaing, T., 2007, Rock relationships in the Mogok metamorphic belt, Tatkon to Mandalay, central Myanmar: Journal of Asian Earth Sciences, v. 29, p. 891–910, doi: 10.1016/j.jseaes.2006.05.009.

Morley, C.K., 1988, Our of sequence thrusts: Tectonics, v. 7, p. 539–561.

Murphy, M.A., and Copeland, P., 2005, Transtensional deformation in the central Himalaya and its role in accommodating growth of the Himalayan orogen: Tectonics, v. 24, TC4012, doi: 10.1029/2004TC001659.

Myrow, P.M., Hughes, N.C., Paulsen, T.S., Williams, I.S., Parcha, S.K., Thompson, K.R., Bowring, S.A., Peng, S.C., and Ahluwalia, A.D., 2003, Integrated tectonostratigraphic analysis of the Himalaya and implications for its tectonic reconstruction: Earth and Planetary Science Letters, v. 212, p. 433–441, doi: 10.1016/S0012-821X(03)00280-2.

Myrow, P.M., Thompson, K.R., Hughes, N.C., Paulsen, T.S., Sell, B.K., and Parcha, S.K., 2006, Cambrian stratigraphy and depositional history of the northern Indian Himalaya, Spiti Valley, north-central India: Geological Society of America Bulletin, v. 118, p. 491–510, doi: 10.1130/B25828.1.

Najman, Y., and Garzanti, E., 2000, Reconstructing early Himalayan tectonic evolution and paleogeography from Tertiary foreland basin sedimentary rocks, northern India: Geological Society of America Bulletin, v. 112, p. 435–449, doi: 10.1130/0016-7606(2000)112<435:REHTEA>2.0.CO;2.

Najman, Y., Clift, P., Johnson, M.R.W., and Robertson, A.H.F., 1993, Early stages of foreland basin evolution in the Lesser Himalaya, northern India, *in* Treloar, P.J., and Searle, M.P., eds., Himalayan tectonics: Geological Society of London Special Publication 74, p. 541–558, doi: 10.1144/GSL.SP.1993.074.01.36.

Najman, Y.M.R., Pringle, M.S., Johnson, M.R.W., Robertson, A.H.F., and Wijbrans, J.R., 1997, Laser Ar-40/Ar-39 dating of single detrital muscovite grains from early foreland-basin sedimentary deposits in India: Implications for early Himalayan evolution: Geology, v. 25, p. 535–538, doi: 10.1130/0091-7613(1997)025<0535:LAADOS>2.3.CO;2.

Nelson, K.D., and 27 others, 1996, Partially molten middle crust beneath southern Tibet: Synthesis of Project INDEPTH results: Science, v. 274, p. 1684–1688, doi: 10.1126/science.274.5293.1684.

O'Brien, P.J., 2006, The age of deep, steep continental subduction in the NW Himalaya: Relating zircon growth to metamorphic history (Comment on: Leech, M.L., Singh, S., Jain, A.K., Klemperer, S.L., and Manickavasagam, R.M., 2005, The onset of India-Asia continental collision: Early, steep subduction required by the timing of UHP metamorphism in the western Himalaya: Earth and Planetary Science Letters, v. 234, p. 83–97): Earth and Planetary Science Letters, v. 245, p. 814–816.

Paces, J.B., and Miller, J.D., 1993, Precise U-Pb age of the Duluth Complex and related mafic intrusions, northeastern Minnesota: Geochronological insights in physical,

petrogenetic, paleomagnetic, and tectonomagmatic processes associated with the 1.1 Ga midcontinent rift system: Journal of Geophysical Research, v. 98, p. 13997–14013, doi: 10.1029/93JB01159.

Pachauri, A.K., 1980, Structural characteristics of the area around Purola, Yamuna Valley region, Garhwal Himalaya, *in* Saklani, P.S., ed., Structural geology of the Himalaya: New Delhi, India, Today and Tomorrow's Printers and Publishers, p. 113–132.

Pandey, A.K., Virdi, N.S., and Gairola, V.K., 2003, Evolution of structural fabrics and deformation events in the Kulu-Rampur and Larji Window zones, NW Himalaya, India: Himalayan Geology, v. 24, p. 1–21.

Parrish, R.R., and K.V. Hodges, 1996, Isotopic constraints on the age and provenance of the Lesser and Greater Himalayan sequences, Nepalese Himalaya: Geological Society of America Bulletin, v. 108, p. 904–911, doi: 10.1130/0016-7606(1996)108<0904:ICOTAA>2.3.CO;2.

Patel, R.C., Singh, S., Asokan, A., Manickavasagam, R.M., and Jain, A.K., 1993, Extensional tectonics in the Himalayan orogen, Zanskar, NW India, *in* Treloar, P.J., and Searle, M.P., eds., Himalayan tectonics: Geological Society of London Special Publication 74, p. 445–459, doi: 10.1144/GSL.SP.1993.074.01.30.

Pearce, J.A., Harris, N.B.W., and Tindle, A.G., 1984, Trace element discrimination diagrams for the tectonic interpretation of granitic rocks: Journal of Petrology, v. 25, p. 956–983.

Pecher, P.A., and Scaillet, B., 1989, La structure du Haut-Himalaya au Garwhal (Indes): Eclogae Geologicae Helvetiae, v. 82, p. 655–668.

Peterman, E.M., Hacker, B.R., Grove, M., Gehrels, G.E., and Mattinson, J.M., 2006, A multi-method approach to improving monazite geochronology: TIMS, LA-ICP-MS, SIMS and EPMA: Eos (Transactions, American Geophysical Union), v. 87, abs. V21A-0551.

Pilgrim, G.E., and West, W.D., 1928, The structure and correlation of the of the Simla rocks: Geological Survey of India Memoirs, v. 53, p. 1–140.

Powell, C.M.A., and Conaghan, P.J., 1973, Polyphase deformation in Phanerozoic rocks of the Central Himalayan Gneiss, northwest India: Journal of Geology, v. 81, p. 127–143, doi: 10.1086/627830.

Powers, P.M., Lillie, R.J., and Yeats, R.S., 1998, Structure and shortening of the Kangra and Dehra Dun reentrants, sub-Himalaya, India: Geological Society of America Bulletin, v. 110, p. 1010–1027, doi: 10.1130/0016-7606(1998)110<1010:SASOTK>2.3.CO;2.

Prince, C.I., 1999, The timing of prograde metamorphism in the Garhwal Himalaya, India (PhD Thesis]: Milton Keynes, UK, Open University, 308 p.

Quidelleur, X., Grove, M., Lovera, O.M., Harrison, T.M., Yin, A., and Ryerson, F.J., 1997, Thermal evolution and slip history of the Renbu Zedong Thrust, southeastern Tibet: Journal of Geophysical Research, v. 102, no. B2, p. 2659–2679.

Raha, P.K., 1980, Stratigraphy and depositional environment of the Jammu Limestone, Udhampur District, Jammu, *in* Valdiya, K.S., and Bhatia, S.B., eds., Stratigraphy and correlations of Lesser Himalayan Formations: Delhi, India, Hindustan Publishing, p. 145–151.

Raha, P.K., and Sastry, M.V.A., 1982, Stromatolites and Precambrian stratigraphy in India: Precambrian Research, v. 18, p. 293–318, doi: 10.1016/0301-9268(82)90006-7.

Raina, B.N., 1981, Need for re-interpretation of the geology of the Simla area: Some suggestions: Contemporary Geoscientific Researches in Himalaya, v. 1, p. 101–108.

Raiverman, V., 2000, Foreland sedimentation in Himalayan tectonic regime: A relook at the orogenic processes: Dehra Dun, India, Bishen Singh Mahendra Pal Singh, 378 p.

Rao, P.N., and Pati, U.C., 1980, Geology and tectonics of Bhilangana Valley and its adjoining parts, Garhwal Himalaya, with special reference to the Main Central Thrust: Himalayan Geology, v. 10, p. 220–237.

Rao, V.V., Prasad, B.R., Reddy, P.R., and Tewari, H.C., 2000, Evolution of Proterozoic Aravalli Delhi fold belt in the northwestern Indian Shield from seismic studies: Tectonophysics, v. 327, p. 109–130, doi: 10.1016/S0040-1951(00)00156-6.

Rattan, S.S., 1973, Stratigraphy and sedimentation of the Chamba area, western Himachel Pradesh: Himalayan Geology, v. 3, p. 231–248.

Rautela, P., and Thakur, V.C., 1992, Structural analysis of the Panjal thrust zone, Himachal Himalaya, India: Journal of Himalayan Geology, v. 3, p. 195–207.

Renne, P.R., Deino, A.L., Walter, R.C., Turrin, B.D., Swisher, C.C., Becker, T.A., Curtis, G.H., Sharp, W.D., and Jaouni, A.R., 1994, Intercalibration of astronomical and radioisotopic time: Geology, v. 22, p. 783–786, doi: 10.1130/0091-7613(1994)022<0783:IOAART>2.3.CO;2.

Richards, A., Argles, T., Harris, N., Parrish, R.R., Ahmad, T., Darbyshire, F., and Draganits, E., 2005, Himalayan architecture constrained by isotopic tracers from clastic sediments: Earth and Planetary Science Letters, v. 236, p. 773–796, doi: 10.1016/j.epsl.2005.05.034.

Robinson, A.C., 2005, Tectonic evolution of the Kongur Shan extensional system, northeastern Pamir: Implications for the evolution of the western Himalayan-Tibetan orogen [Ph.D. thesis]: University of California Los Angeles, 333 p.

Robinson, A.C., Yin, A., Manning, C.E., Harrison, T.M., Zhang, S.-H., and Wang, X.-F., 2007, Cenozoic evolution of the eastern Pamir: Implications for strain-accommodation mechanisms at the western end of the Himalayan-Tibetan orogen: Geological Society of America Bulletin, v. 119, p. 882–896, doi: 10.1130/B25981.1.

Robinson, D.M., DeCelles, P.G., and Copeland, P., 2006, Tectonic evolution of the Himalayan thrust belt in western Nepal: Implications for channel flow models: Geological Society of America Bulletin, v. 118, p. 865–885, doi: 10.1130/B25911.1.

Robyr, M., Vannay, J.C., Epard, J.L., and Steck, A., 2002, Thrusting, extension, and doming during the polyphase tectonometamorphic evolution of the High Himalayan Crystalline Zone in NW India: Journal of Asian Earth Sciences, v. 21, p. 221–239, doi: 10.1016/S1367-9120(02)00039-1.

Rupke, J., 1974, Stratigraphic and structural evolution of the Kumaon Lesser Himalaya: Sedimentary Geology, v. 11, p. 81–265, doi: 10.1016/0037-0738(74)90027-X.

Schlup, M., 2003, Exhumation history of the western Himalaya: The Rupshu-Lahul-Kullu geochronological transect (NW history) [Ph.D. thesis]: Lausanne, Switzerland, University of Lausanne, 175 p.

Schlup, M., Carter, A., Cosca, M., and Steck, A., 2003, Exhumation history of eastern Ladakh revealed by $^{40}Ar/^{39}Ar$ and fission-track ages: the Indus River–Tso Morari transect, NW Himalaya: Geological Society of London Journal, v. 160, p. 385–399, doi: 10.1144/0016-764902-084.

Searle, 1986, Structural evolution and sequence of thrusting in the High Himalayan, Tibetan-Tethys and Indus suture zones of Zanskar and Ladakh, western Himalaya: Journal of Structural Geology, v. 8, p. 923–936.

Searle, M.P., Cooper, D.J.W., and Rex, A.J., 1988, Collision tectonics in the Ladakh-Zanskar Himalaya: Royal Society of London Philosophical Transactions, v. A326, p. 117–150.

Searle, M.P., Law, R.D., Godin, L., Larson, K.P., Struele, M.J., Cottle, J.M., and Jessup, M.J., 2008, Defining the Himalayan main central thrust in Nepal: Journal of the Geological Society, London, v. 165, p. 523–534.

Shanker, R., and Dua, K.J.S., 1978, On the existence of a tear fault along upper Beas valley, District Kulu, Himachel Pradesh, and its bearing on the thermal activity: Himalayan Geology, v. 8, p. 446–472.

Sharma, K.K., 1977, A contribution to the geology of the Sutluj Valley, Kinnaur, Himachal Pradesh, India: Colloques internationaux du CNRS, v. 268, p. 369–378.

Sharma, V.P., 1977, Geology of the Kulu-Rampur belt, Himachal Pradesh: Geological Survey of India Memoirs, v. 106, p. 235–407.

Singh, I.B., and Rai, V., 1983, Fauna and biogenic structures in Krol-Tal succession (Vendian–Early Cambrian), Lesser Himalaya: Their biostratigraphic and palaeoecological significance: Palaeontological Society of India Journal, v. 28, p. 67–90.

Singh, K., and Thakur, V.C., 2001, Microstructures and strain variation across the footwall of the Main Central Thrust Zone, Garwhal Himalaya, India: Journal of Asian Earth Sciences, v. 19, p. 17–29, doi: 10.1016/S1367-9120(00)00006-7.

Singh, S., and Jain, A.K., 1993, Deformational and strain patterns of the Jutogh nappe along the Sutlej Valley in Jeori-Wangtu region: Himachal Himalaya: Journal of Himalayan Geology, v. 4, p. 41–55.

Singh, S., Claesson, S., Jain, A.K., Sjoberg, H., Gee, D.G., Manickavasagam, R.M., and Andreasson, P.G., 1994, Geochemistry of the Proterozoic peraluminous granitoids from the Higher Himalayan Crystalline (HHC) and Jutogh Nappe, NW-Himalaya, Himachal Pradesh, India: Nepal Geological Society Journal, v. 10, p. 125.

Singh, S., Barley, M.E., Brown, S.J., Jain, A.K., and Manickavasagam, R.M., 2002, SHRIMP U-Pb in zircon geochronology of the Chor granitoid: Evidence for Neoproterozoic magmatism in the Lesser Himalayan granite belt of NW India: Precambrian Research, v. 118, p. 285–292, doi: 10.1016/S0301-9268(02)00107-9.

Singh, S., Claesson, S., Jain, A.K., Gee, D.G., Andreasson, P.G., and Manickavasagam, R.M., 2006, 2.0 Ga granite of the lower package of the Higher Himalayan Crystallines, Maglad Khad, Sutlej Valley, Himachal Pradesh: Geological Society of India Journal, v. 67, p. 295–300.

Singh, S.K., Trivedi, J.R., and Krishnaswami, S., 1999, Re-Os isotope systematics in black shales from the Lesser Himalaya: Their chronology and role in the Os-187/Os-188 evolution of seawater: Geochimica et Cosmochimica Acta, v. 63, p. 2381–2392, doi: 10.1016/S0016-7037(99)00201-X.

Sinha, A.K., 1975, Calcareous nammofossils from the Simla Hills, with a discussion of their age in the tectono-stratigraphic column: Jour. Geol. Soc. India, v. 16, p. 69–77.

Socquet, A., and Pubellier, M., 2005, Cenozoic deformation in western Yunnan (China-Myanmar border): Journal of Asian Earth Sciences, v. 24, p. 495–515, doi: 10.1016/j.jseaes.2004.03.006.

Spear, F.S., and Cheney, J.T., 1989, A petrogenetic grid for pelitic schists in the system SiO_2-Al_2O_3-Fe-MgO-K_2O-H_2O: Contributions to Mineralogy and Petrology, v. 101, p. 149–164.

Srikantia, S.V., and Bhargava, O.N., 1979, The Tandi Group of Lahaul; its geology and relationship with the Central Himalayan gneiss: Geological Society of India Journal, v. 20, p. 531–539.

Srikantia, S.V., and Bhargava, O.N., 1984, The Jutogh Klippe of the Simla area of the Himachal Himalaya; its geology and structural evolution: Geological Society of India Journal, v. 25, p. 220–230.

Srikantia, S.V., and Bhargava, O.N., 1988, The Jutogh Group of metasediments of the Himachal Himalaya; its lithostratigraphy: Geological Society of India Journal, v. 32, p. 279–294.

Srikantia, S.V., and Bhargava, O.N., 1998, Geology of Himachal Pradesh: Bangalore, Geological Society of India, 406 p.

Srikantia, S.V., and Sharma, R.P., 1976, Geology of the Shali Belt and the adjoining areas: Geological Survey of India Memoirs, v. 106, p. 31–166.

Srivastava, P., and Kumar, S., 1997, Possible evidences of animal life in Neoproterozoic Deoban microfossil assemblage, Garhwal Lesser Himalaya, Uttar Pradesh: Current Science, v. 72, p. 145–149.

Srivastava, P., and Kumar, S., 2003, New microfossils from the Meso-Neoproterozoic Deoban Limestone, Garhwal Lesser Himalaya, India: Palaeobotanist, v. 52, p. 13–47.

Srivastava, P., and Mitra, G., 1994, Thrust geometries and deep structure of the outer and lesser Himalaya, Kumaon and Garhwal (India): Implications for evolution of the Himalayan fold-and-thrust belt: Tectonics, v. 13, p. 89–109, doi: 10.1029/93TC01130.

Stacey, J.S., and Kramers, J.D., 1975, Approximation of terrestrial lead isotope evolution by a two-stage model: Earth and Planetary Science Letters, v. 26, p. 207–221, doi: 10.1016/0012-821X(75)90088-6.

Steck, A., 2003, Geology of the NW Indian Himalaya: Eclogae Geologicae Helvetiae, v. 96, p. 147–196.

Steck, A., Epard, J.-L., Vannay, J.-C., Hunziker, J., Girard, M., Morard, A., and Robyr, M., 1998, Geological transect across the Tso Morari and Spiti areas: The nappe structures of the Tethys Himalaya: Eclogae Geologicae Helvetiae, v. 91, p. 103–121.

Stephenson, B.J., Searle, M.P., Waters, D.J., and Rex, D.C., 2001, Structure of the Main Central Thrust zone and extrusion of the High Himalayan deep crustal wedge, Kishtwar-Zanskar Himalaya: Geological Society of London Journal, v. 158, p. 637–652, doi: 10.1144/jgs.158.4.637.

Stutz, E.A., and Steck, A., 1986, La terminaison occidentale de Cristallin du Tso Morari (Haut–Himalaya; Ladakh meridional, Inde): Eclogae gelogicae Helvetica, v. 79, p. 253–269.

Tewari, A.P., Gaur, R.K., and Ameta, S.S., 1978, A note on the geology of a part of Kinnaur District, Himachal Pradesh: Himalayan Geology, v. 8, p. 574–582.

Tewari, V.C., 2003, Correlation and palaeobiology of Vindhyan and Lesser Himalayan stratigraphic successions: Palaeontological Society of India Journal, v. 48, p. 155–165.

Thakur, V.C., 1998, Structure of the Chamba nappe and position of the Main Central thrust in Kashmir Himalaya: Journal of Asian Earth Sciences, v. 16, p. 269–282, doi: 10.1016/S0743-9547(98)00011-7.

Thakur, V.C., and Rawat, B.S., 1992, Geologic map of Western Himalaya: Dehra Dun, India, Wadia Institute of Himalayan Geology, scale 1:1,000,000.

Thiede, R.C., Bookhagen, B., Arrowsmith, J.R., Sobel, E.R., and Strecker, M.R., 2004, Climatic control on rapid exhumation along the Southern Himalayan Front: Earth and Planetary Science Letters, v. 222, p. 791–806, doi: 10.1016/j.epsl.2004.03.015.

Thiede, R.C., Arrowsmith, J.R., Bookhagen, B., McWilliams, M.O., Sobel, E.R., and Strecker, M.R., 2005, From tectonically to erosionally controlled development of the Himalayan fold-and-thrust belt: Geology, v. 33, p. 689–692, doi: 10.1130/G21483.1.

Thiede, R.C., Arrowsmith, J.R., Bookhagen, B., McWilliams, M., Sobel, E.R., and Strecker, M.R., 2006, Dome formation and extension in the Tethyan Himalaya, Leo Pargil, northwest India: Geological Society of America Bulletin, v. 118, p. 635–650, doi: 10.1130/B25872.1.

Thiede, R.C., Ehlers, T.A., Bookhagen, B., and Strecker, M.R., 2009, Erosional variability along the northwest Himalaya: Journal of Geophysical Research, v. 114, F01015, doi: 10.1029/2008JF001010.

Thöni, M., 1977, Geology, structural evolution and metamorphic zoning in the Kulu Valley (Himachal Himalayas, India) with special reference to the reversed metamorphism: Mitteilungen Gesellschaft Geologische Bergbaustudenien Österreich, v. 24, p. 125–187.

Trivedi, J.R., Gopalan, K., and Valdiya, K.S., 1984, Rb-Sr ages of granitic rocks within the Lesser Himalayan Nappes, Kumaun, India: Geological Society of India Journal, v. 25, p. 641–654.

Upreti, B.N., 1999, An overview of the stratigraphy and tectonics of the Nepal Himalaya: Journal of Asian Earth Sciences, v. 17, p. 577–606, doi: 10.1016/S1367-9120(99)00047-4.

Valdiya, K.S., 1969, Stromatolites of the Lesser Himalayan carbonate formations and the Vindhyans: Geological Society of India Journal, v. 10, p. 1–25.

Valdiya, K.S., 1970, Simla Slates: The Precambrian flysch of the Lesser Himalaya, its turbidites, sedimentary structures and paleocurrents: Geological Society of America Bulletin, v. 81, p. 451–468, doi: 10.1130/0016-7606(1970)81[451:SSTPFO]2.0.CO;2.

Valdiya, K.S., 1978, Extension and analogues of the Chail Nappe in the Kumaun Himalaya: Indian Journal of Earth Sciences, v. 5, p. 1–19.

Valdiya, K.S., 1980, Geology of Kumaun Lesser Himalaya: Dehra Dun, India, Wadia Institute of Himalayan Geology, 291 p.

Valdiya, K.S., 1995, Proterozoic sedimentation and Pan-African geodynamic development in the Himalaya: Precambrian Research, v. 74, p. 35–55, doi: 10.1016/0301-9268(95)00004-O.

Vannay, J.C., and Grasemann, B., 1998, Inverted metamorphism in the High Himalaya of Himachal Pradesh (NW India): Phase equilibria versus thermobarometry: Schweizerische Mineralogische und Petrographische Mitteilungen, v. 78, p. 107–132.

Vannay, J.C., and Steck, A., 1995, Tectonic evolution of the High Himalaya in Upper Lahul (NW Himalaya, India): Tectonics, v. 14, p. 253–263, doi: 10.1029/94TC02455.

Vannay, J.C., Sharp, Z.D., and Grasemann, B., 1999, Himalayan inverted metamorphism constrained by oxygen isotope thermometry: Contributions to Mineralogy and Petrology, v. 137, p. 90–101, doi: 10.1007/s004100050584.

Vannay, J.C., Grasemann, B., Rahn, M., Frank, W., Carter, A., Baudraz, V., and Cosca, M., 2004, Miocene to Holocene exhumation of metamorphic crustal wedges in the NW Himalaya: Evidence for tectonic extrusion coupled to fluvial erosion: Tectonics, v. 23, TC1014, doi: 10.1029/2002TC001429.

Venkatachala, B.S., and Kumar, A., 1998, Fossil microbiota from the Vaishnodevi Limestone, Himalayan Foothills, Jammu: Age and palaeoenvironmental implications: Geological Society of India Journal, v. 52, p. 529–536.

Verma, P., Sengupta, S., Chaddha, D.K., and Pant, N.C., 2005, Dehydration melting studies in a 'kyanite terrain,' Manali, NW Himalayas: Journal of Asian Earth Sciences, v. 25, p. 345–366, doi: 10.1016/j.jseaes.2004.03.005.

Virdi, N.S., 1979, Status of the Chail Formation vis-à-vis Jutogh-Chail relationship in the Himachal lesser Himalaya: Himalayan Geology, v. 9, p. 111–125.

Walker, J.D., Martin, M.W., Bowring, S.A., Searle, M.P., Waters, D.J., and Hodges, K.V., 1999, Metamorphism, melting, and extension: Age constraints from the High Himalayan slab of southeast Zanskar and northwest Lahaul: Journal of Geology, v. 107, p. 473–495, doi: 10.1086/314360.

Webb, A.A.G., Yin, A., Harrison, T.M., Célérier, J., and Burgess, W.P., 2007, The leading edge of the Greater Himalayan Crystallines revealed in the NW Indian Himalaya: Implications for the evolution of the Himalayan Orogen: Geology, v. 35, p. 955–958, doi: 10.1130/G23931A.1.

West, W.D., 1939, The structure of the Shali Window near Simla: Geological Survey of India Records, v. 74, p. 133–163.

White, N.M., Parrish, R.R., Bickle, M.J., Najman, Y.M.R., Burbank, D., and Maithani, A., 2001, Metamorphism and exhumation of the NW Himalaya constrained by U-Th-Pb analyses of detrital monazite grains from early foreland basin sediments: Geological Society of London Journal, v. 158, p. 625–635, doi: 10.1144/jgs.158.4.625.

White, N.M., Pringle, M., Garzanti, E., Bickle, M., Najman, Y., Chapman, H., and Friend, P., 2002, Constraints on the exhumation and erosion of the High Himalayan Slab, NW India, from foreland basin deposits: Earth and Planetary Science Letters, v. 195, p. 29–44, doi: 10.1016/S0012-821X(01)00565-9.

Whittington, A.G., Harris, N.B.W., Ayres, M.W., and Foster, G.L., 1999, Lithostratigraphic correlations in the western Himalaya—An isotopic approach: Geology, v. 27, p. 585–588.

Wiesmayr, G., and Grasemann, B., 2002, Eohimalayan fold and thrust belt: Implications for the geodynamic evolution of the NW-Himalaya (India): Tectonics, v. 21, 1058, 17 p., doi: 10.1029/2002TC001363.

Windley, B.F., 1988, Tectonic framework of the Himalaya, Karakoram and Tibet, and problems of their evolution: Royal Society of London Philosophical Transactions, ser. A, v. 326, p. 3–16, doi: 10.1098/rsta.1988.0078.

Wyss, M., 2000, Metamorphic evolution of the northern Himachal Himalaya: Phase equilibria constraints and thermobarometry: Schweizerische Mineralogische und Petrographische Mitteilungen, v. 80, p. 317–350.

Wyss, M., Hermann, J., and Steck, A., 1999, Structural and metamorphic evolution of the northern Himachal Himalaya, NW India (Spiti-eastern Lahul-Parvati valley traverse): Eclogae Geologicae Helvetiae, v. 92, p. 3–44.

Yeats, R.S., and Hussain, A., 1987, Timing of structural events in the Himalayan foothills of northwestern Pakistan: Geological Society of America Bulletin, v. 99, p. 161–176, doi: 10.1130/0016-7606(1987)99<161:TOSEIT>2.0.CO;2.

Yin, A., 1989, Origin of regional rooted low-angle normal faults: A mechanical model and its implications: Tectonics, v. 8, p. 469–482, doi: 10.1029/TC008i003p00469.

Yin, A., 2006, Cenozoic tectonic evolution of the Himalayan orogen as constrained by along-strike variation of structural geometry, exhumation history, and foreland sedimentation: Earth-Science Reviews, v. 76, p. 1–131, doi: 10.1016/j.earscirev.2005.05.004.

Yin, A., and Kelty, T.K., 1991, Structural evolution of the Lewis thrust system, southern Glacier National Park: Implications for the regional tectonic development: Geological Society of American Bulletin, v. 103, p. 1073–1089.

Yin, A., and Harrison, T.M., 2000, Geologic evolution of the Himalayan-Tibetan orogen: Annual Review of Earth and Planetary Sciences, v. 28, p. 211–280, doi: 10.1146/annurev.earth.28.1.211.

Yin, A., Harrison, T.M., Ryerson, F.J., Chen, W., Kidd, W.S.F., and Copeland, P., 1994, Tertiary structural evolution of the Gangdese thrust system, southeastern Tibet: Journal of Geophysical Research, v. 99, p. 18175–18201, doi: 10.1029/94JB00504.

Yin, A., Harrison, T.M., Murphy, M.A., Grove, M., Nie, S., Ryerson, F.J., Wang, X.F., and Chen, Z.L., 1999, Tertiary deformation history of southeastern and southwestern Tibet during the Indo-Asian collision: Geological Society of America Bulletin, v. 111, p. 1644–1664, doi: 10.1130/0016-7606(1999)111<1644:TDHOSA>2.3.CO;2.

Yin, A., Dubey, C.S., Webb, A.A.G., Kelty, T.K., Grove, M., Gehrels, G.E., and Burgess, W.P., 2010a, Geological correlation of the Himalayan orogen and Indian craton: Part 1: Structural geology, U-Pb zircon geochronology, and tectonic evolution of the Shillong Planteau and its neighboring regions in NE India: Geological Society of America Bulletin, v. 122, p. 336–359.

Yin, A., Dubey, C.S., Kelty, T.K., Webb, A.A.G., Harrison, T.M., Chou, C.Y., and Célérier, J., 2010b, Geological correlation of the Himalayan orogen and Indian craton: Part 2: Structural geology, geochronology, and tectonic evolution of the Eastern Himalaya: Geological Society of America Bulletin, v. 122, p. 360–395.

Manuscript Received 11 July 2010
Revised Manuscript Received 23 February 2011
Manuscript Accepted 16 March 2011